

**Structural and Physical Properties of Salts  
Containing Tetrahedral Anions with Group 13  
Metals  
(Aluminates and Halogenidogallates)**

Inaugural-Dissertation

zur

Erlangung des Doktorgrades

der Mathematisch-Naturwissenschaftlichen Fakultät

der Universität zu Köln

vorgelegt von

**Tudor Lucian Timofte**

aus Iași, Rumänien

**Köln 2008**



Die vorliegende Arbeit wurde im Zeitraum von Oktober 2005 bis September 2008 am Institut für Anorganische Chemie der Universität zu Köln und an der Fakultät für Chemie und Biochemie der Ruhr-Universität Bochum unter der Anleitung von Prof. Dr. Anja-Verena Mudring angefertigt.

Berichtersteller/in: **Prof. Dr. Anja-Verena Mudring**

**Prof. Dr. Gerd Meyer**

Tag der mündlichen Prüfung: 20.02.2009

## Acknowledgements

First, I would like to thank my supervisor, Professor Dr. Anja-Verena Mudring for her guidance, fruitful discussions and for providing an optimal environment to accomplish this thesis. I am grateful for having the chance to join her research group.

I am thankful to Professor Dr. Gerd Meyer and to Professor Dr. Alexandru Cecal (“Al. I. Cuza” University-Iasi, Rumänien); their support of all kind made this PhD project possible.

I want to thank also Dr. I. Pantenburg, Mrs. I. Müller, Dr. K. Merz and Mrs. M. Winter for single crystal XRD measurements. To Mr. H. Schuhmacher I thank for the powder XRD measurements. I send my gratitude to Dr. W. Tyrra for helping me measure and interpret the NMR spectra. I am grateful also to all the other collaborators who helped me run all the other necessary measurements.

Special thanks go to my colleagues/ex-colleagues Dr. Franziska Rieger, Dr. Arash Babai and Dipl. Chem. Anna Getsis – they never rejected a request for help, on contrary! I would like to thank to all other colleagues from Cologne and Bochum, for the nice working atmosphere and all the help they gave me. I enjoyed during my whole PhD a wonderful, optimistic and nice attitude from all the people I met; I am positively impressed, and I thank you all one more time for that!

Not at last, I want to thank my wife and my family. They showed me the whole sympathy and they gave me tremendous support.

## Abstract

The aim of this doctoral thesis is to investigate the chemistry of compounds with group 13 metals tetrahedral anions  $[MX_4]^-$  (where M = Al, Ga and X= Cl, Br, I). Since these anions are known to be weakly coordinating, a structural comparison between alkali metal and monovalent indium and/or thallium tetrahalogenidoaluminates and tetrahalogenidogallates, offers the possibility to study the structural influence of the  $5s^2$ , respectively  $6s^2$  lone pair.

This thesis presents structural investigations on indium(I) tetrachloridoaluminate, indium(I) tetraiodidoaluminate, thallium(I) tetrachloridoaluminate, thallium(I) tetrabromidoaluminate, thallium(I) tetraiodidoaluminate, thallium(I) tetrachloridogallate, thallium(I) tetrabromidogallate and thallium(I) tetraiodidogallate. In order to allow a better structural comparison of the above mentioned compounds with analogous alkali metal compounds, the so far unknown structures of caesium tetraiodidoaluminate and caesium tetraiodidogallate were determined. For the same reason ammonium tetrachloridogallate and ammonium tetraiodidoaluminate were investigated. Comparing the crystal structures of the above specified heavy metal tetrahalogenidometallates with the alkali metal analogues, leads to the conclusion that there are no obvious structural distortions to notice, which could be attributed to the lone-pair, and therefore In(I) and Tl(I) act as true “pseudo-alkali” metals in these compounds.

Apart from the tetrahalogenidometallates, the structure of indium(I) heptachloridogallate was investigated.  $InGa_2Cl_7$  crystallizes isotypically with  $Ga_3Cl_7$  and  $KGa_2Cl_7$ , in the acentric space group  $Pna2_1$  (No. 33).

Moreover, the known salts containing  $[MX_4]^-$  anions exhibit relatively low melting points (below  $400^\circ C$ ). Coupling of very weakly coordinating anions, of the above specified

type, with organic cations could lead to a further depression of the melting point.

The second aim of this thesis was to synthesize compounds containing very weakly coordinating anions (tetrahedral alkoxyaluminates) with drastically lowered melting points. Fluorinated alkoxyaluminates, such as tetrakis(hexafluoroisopropyl)aluminate and tetrakis(nonafluoro-tert-butyl)aluminate, have even lower coordinating capabilities, being one of the least coordinating anions. In combination with bulky organic cations, such as 1-butyl-3-methylimidazolium and 1-butyl-1-methylpyrrolidinium, two ionic liquids 1-butyl-3-methylimidazolium tetrakis(hexafluoroisopropyl)aluminate ( $T_m = 34.1^\circ\text{C}$ ) and 1-butyl-1-methylpyrrolidinium tetrakis(hexafluoroisopropyl)aluminate ( $T_m = 46.8^\circ\text{C}$ ), and the two molten salts 1-butyl-3-methylimidazolium tetrakis(nonafluoro-tert-butyl)aluminate ( $T_m = 149.1^\circ\text{C}$ ), and 1-butyl-1-methylpyrrolidinium tetrakis(nonafluoro-tert-butyl)aluminate ( $T_m = 201.7^\circ\text{C}$ ) could be obtained. Despite of the relatively high melting points, these compounds are suitable for electrochemical applications (*e.g.* as electrolytes), since they have very broad potential windows – approximately 9V. An additional advantage for the molten salts previously mentioned is that they are hydrolysis stable, whereas the two ionic liquids, also named above, are sensitive towards hydrolysis.

## Zusammenfassung

Ziel der Arbeit ist die kristallchemische Untersuchung von Verbindungen mit tetraedrischen Metallat-Anionen  $[MX_4]^-$  mit  $M = Al, Ga, X = Cl, Br, I$ . Da diese Anionen als schwachkoordinierend gelten, bietet der strukturelle Vergleich der Alkalimetall-Tetrahalogenidoaluminat und Tetrahalogenidogallate mit den entsprechenden Verbindungen des einwertigen Indiums und einwertigen Thalliums eine Möglichkeit, den Einfluss des freien  $5s^2$ - bzw. des  $6s^2$ -Elektronenpaares auf die Kristallstruktur zu untersuchen.

In dieser Arbeit wurden die Verbindungen Indium(I)tetrachloridoaluminat, Indium(I)tetraiodidoaluminat, Thallium(I)tetrachloridoaluminat, Thallium(I)tetrabromidoaluminat, Thallium(I)tetraiodidoaluminat, Thallium(I)tetrachloridogallat, Thallium(I)tetrabromidogallat und Thallium(I)tetraiodidogallat strukturell untersucht. Um bessere Vergleichsmöglichkeiten für diese Verbindungen mit den entsprechenden Alkalimetallverbindungen zu schaffen, wurden die bis dahin unbekanntes Kristallstrukturen der Verbindungen Cäsiumtetraiodidoaluminat, Cäsiumtetraiodidogallat, Ammoniumtetrachloridogallat sowie Ammoniumtetraiodidoaluminat bestimmt. Der Vergleich der genannten Tetrahalogenidometallate der schweren Elemente der 3. Hauptgruppe zeigt, dass offensichtlich keine strukturellen Verzerrungen auftreten, die sich auf die Wirkung der freien Elektronenpaare zurückführen lassen. Daher verhalten sich In(I) und Tl(I) in diesen Verbindungen als echte „Pseudoalkalimetall“-Kationen.

Außerdem wurde die Kristallstruktur von Indium(I)heptachloridogallat bestimmt.  $InGa_2Cl_7$  kristallisiert isotyp zu  $Ga_3Cl_7$  und  $KGa_2Cl_7$  in der azentrischen Raumgruppe  $Pn\bar{a}2_1$  (Nr. 33).

Da die  $[MX_4]^-$ -Einheiten enthaltenden Salze relativ niedrige Schmelzpunkte von unter  $400^\circ C$  aufweisen, sollte die Kombination von sehr schwach koordinierenden Anionen des

oben beschriebenen Typs mit organischen Kationen zu einer weiteren Verringerung des Schmelzpunktes führen.

Ein weiteres Ziel dieser Arbeit bestand daher darin, Verbindungen mit sehr schwach koordinierenden Anionen (tetraedrische Alkoxyaluminat-Anionen) mit deutlich erniedrigten Schmelzpunkten zu synthetisieren. Fluorierte Alkoxyaluminat, wie Tetrakis(hexafluoroisopropyl)aluminat und Tetrakis(nonafluoro-tert-butyl)aluminat, haben eine noch schwächere Koordinationsfähigkeit und gehören zu den am schwächsten koordinierenden Anionen. In Kombination mit sperrigen organischen Kationen, wie 1-Butyl-3-methylimidazolium und 1-Butyl-1-methylpyrrolidinium, wurden die beiden ionischen Flüssigkeiten 1-Butyl-3-methylimidazolium-tetrakis(hexafluoroisopropyl)aluminat ( $T_m = 34,1^\circ\text{C}$ ) und 1-Butyl-1-methylpyrrolidinium-tetrakis(hexafluoroisopropyl)aluminat ( $T_m = 46,8^\circ\text{C}$ ) sowie die beiden geschmolzenen Salze 1-Butyl-3-methylimidazolium-tetrakis(nonafluoro-tert-butyl)aluminat ( $T_m = 149,1^\circ\text{C}$ ), und 1-Butyl-1-methylpyrrolidinium-tetrakis(nonafluoro-tert-butyl)aluminat ( $T_m = 201,7^\circ\text{C}$ ) erhalten. Trotz der relativ hohen Schmelzpunkte der letzten beiden Verbindungen sind sie für elektrochemische Anwendungen (z. B. als Elektrolyte) geeignet, da sie sehr breite Potentialfenster (etwa 9V) aufweisen. Ein weiterer Vorteil dieser geschmolzenen Salze ist deren Stabilität gegen Hydrolyse, wohingegen die beiden synthetisierten ionischen Flüssigkeiten hydrolyseempfindlich sind.

## Index

1. Introduction .....	12
1.1 Aim of research .....	12
1.2 The $M^I X-M^{III} X_3$ system.....	14
1.2.1 The reported $M^I M^{III} X_4$ compounds .....	15
1.2.2 Structural information.....	18
1.3 Ionic liquids and molten salts containing weakly coordinating anions .....	22
1.3.1 Ionic liquids and molten salts .....	22
1.3.2 Weakly coordinating anions .....	24
1.4 Literature .....	26
2. Tetrahalogenidoaluminates and tetrahalogenidogallates .....	31
2.1 The baryte type $M^I M^{III} X_4$ class of salts .....	31
2.1.1. Preparation .....	31
2.1.2 Structural aspects.....	33
2.1.2.1 Crystal structure of $TlAlCl_4$ , $TlGaCl_4$ , $InAlCl_4$ and $[NH_4]GaCl_4$ .....	33
2.1.2.1.1 $TlAlCl_4$ .....	33
2.1.2.1.2 $TlGaCl_4$ .....	36
2.1.2.1.3 $InAlCl_4$ .....	38
2.1.2.1.4 $[NH_4]GaCl_4$ .....	39
2.1.2.2 XRD-powder diffraction.....	41
2.2 $M^I M^{III} X_4$ salts crystallizing in the $P 2_1 / c$ space group.....	43
2.2.1 Preparation .....	43
2.2.2 Structural aspects.....	44
2.2.2.1 Crystal structure of $TlAlI_4$ , $TlGaI_4$ , $CsAlI_4$ , $CsGaI_4$ and $TlGaBr_4$ .....	44
2.2.2.1.1 $TlAlI_4$ and $TlGaI_4$ .....	45
2.2.2.1.2 $CsAlI_4$ and $CsGaI_4$ .....	49
2.2.2.1.3 $TlGaBr_4$ .....	52
2.2.2.2 XRD-powder diffraction.....	57
2.3 $InAlI_4$ .....	58
2.3.1 Preparation .....	58
2.3.2 Structural aspects.....	58
2.3.2.1 Crystal structure of $InAlI_4$ .....	58
2.4 $TlAlBr_4$ .....	62
2.4.1 Preparation .....	62
2.4.2 Structural aspects.....	62
2.4.2.1 Crystal structure of $TlAlBr_4$ .....	62

2.5 Summary .....	66
2.6 Literature .....	68
3. Indium heptachloridodigallate - $\text{InGa}_2\text{Cl}_7$ .....	70
3.1 Preparation .....	70
3.2 Structural aspects .....	71
3.2.1 Crystal structure of $\text{InGa}_2\text{Cl}_7$ .....	71
3.3 Summary .....	76
3.4 Literature .....	77
4. Ionic liquids with weakly coordinating anions .....	78
4.1 General preparation .....	78
4.2 1-butyl-3-methylimidazolium tetrakis(hexafluoroisopropyl)aluminate .....	80
4.2.1 Preparation .....	80
4.2.2 Structural aspects .....	81
4.2.2.1 $^{27}\text{Al}$ -, $^{19}\text{F}$ -, $^1\text{H}$ -NMR .....	81
4.2.2.2 Crystal structure .....	83
4.2.2.3 IR/Raman spectroscopy .....	88
4.2.3 Physico-chemical properties .....	90
4.2.3.1 Differential scanning calorimetry .....	90
4.2.3.2 Cyclic voltammetry .....	91
4.2.3.3 Viscosity .....	91
4.3 1-butyl-1-methylpyrrolidinium tetrakis(hexafluoroisopropyl)aluminate .....	92
4.3.1 Preparation .....	92
4.3.2 Structural aspects .....	93
4.3.2.1 $^{27}\text{Al}$ -, $^{19}\text{F}$ - and $^1\text{H}$ - NMR .....	93
4.3.2.2 IR/Raman spectroscopy .....	95
4.3.3 Physico-chemical properties .....	97
4.3.3.1 Differential scanning calorimetry .....	97
4.3.3.2 Cyclic voltammetry .....	98
4.3.3.3 Viscosity .....	98
4.4 Summary .....	99
4.5 Literature .....	101
5. Molten salts with weakly coordinating anions .....	103
5.1 General preparation .....	103
5.2 1-butyl-3-methylimidazolium tetrakis(nonafluoro-tert-butyl)aluminate .....	104
5.2.1 Preparation .....	104
5.2.2 Structural aspects .....	105
5.2.2.1 $^{27}\text{Al}$ - and $^{19}\text{F}$ - NMR .....	105

5.2.2.2 IR/Raman spectroscopy .....	106
5.2.3 Physico-chemical properties.....	108
5.2.3.1 Differential scanning calorimetry .....	108
5.3 1-butyl-1-methylpyrrolidinium tetrakis(nonafluoro-tert-butyl)aluminate.....	108
5.3.1 Preparation .....	108
5.3.2 Structural aspects.....	109
5.3.2.1 <sup>27</sup> Al- and <sup>19</sup> F- NMR.....	109
5.3.2.2 IR/Raman spectroscopy.....	110
5.3.3 Physico-chemical properties.....	112
5.3.3.1 Differential scanning calorimetry .....	112
5.4 Summary .....	112
5.5 Literature .....	114
6. Appendix.....	115
6.1 General methods.....	115
6.1.1 Synthesis techniques.....	115
6.1.2 XRD powder analysis.....	115
6.1.3 XRD single crystal analysis .....	116
6.1.4 Nuclear magnetic resonance.....	117
6.1.5 IR/Raman spectroscopy .....	117
6.1.6 Differential scanning calorimetry .....	118
6.1.7 Cyclic voltammetry .....	118
6.1.8 Combustion analysis (CHNS).....	119
6.1.9 Viscosity .....	119
6.1.10 Literature .....	120
6.2 Software .....	121
6.3 Chemicals .....	123
6.4 Abbreviation list .....	124
6.5 Publication list .....	125
Curriculum Vitae.....	126

## 1. Introduction

### 1.1 Aim of research

The aim of this work is to investigate complex aluminate and gallate anions with ammonium, group 1 and group 13 metal and organic counter cations.  $\text{MX}_3/\text{MR}_3$  ( $\text{M}=\text{Al, Ga}$ ;  $\text{R}=\text{organic rest}$ ) are known to be strong Lewis acids, and as expected, upon adding a Lewis base, such as a halide atom or alkoxide rests, they will form  $[\text{MX}_4]^-$ , respectively  $[\text{MR}_4]^-$  anions, which have an approximately  $T_d$  tetrahedral symmetry. Even though the first reports on tetrahalogenidoaluminates/ tetrahalogenidogallates date back in the 50's [1], until today there is no full structural characterization of such compounds. Mainly urged to study processes and potential applications in metallurgy, chemists explored phase diagrams of the  $\text{M}^{\text{I}}\text{X}-\text{MX}_3$  systems. Aluminum chloride is today the industrially most important group 13 halide, its applications range from antiperspirants over catalytic processes like acylation, alkylation (*e.g.* Friedel-Crafts), condensation, polymerization and cyclisation [2], to its use as a battery electrolyte [3] and the introduction of it in ionic liquids/molten salts from the very beginning [4]. Monovalent indium has an ionic radius similar to potassium ion; the ionic radius of monovalent thallium is related in size to the radius of rubidium ion. By comparing  $\text{In}^{+1}$  and  $\text{Tl}^{+1}$  compounds with the analogous  $\text{K}^+$  and  $\text{Rb}^+$  compounds, it is possible to investigate eventual structural distortions, caused by the lone-pair (especially for the case of thallium) [5]. The aim was to get a better understanding on how and if the lone-pair of electrons influences the structure of  $\text{In}^{+1}$  and  $\text{Tl}^{+1}$  compounds.

A practical issue in different chemical processes is the melting point of the applied chemicals. A strategy to lower the melting point of the  $\text{M}^{\text{I}}[\text{M}^{\text{III}}\text{X}_4]$  class of compounds is to change the monovalent inorganic cation with an organic cation (which will restrain packing in the crystal lattice, and where also the localization/delocalization of the positive charge play a

role through coulombic interactions), and by changing the  $[\text{M}^{\text{III}}\text{X}_4]^-$  anionic unit with  $[\text{M}^{\text{III}}\text{R}_4]^-$ , which is a more weakly coordinating anion [6].

## 1.2 The $M^I X-M^{III} X_3$ system

First investigations on  $M^I X-M^{III} X_3$  systems (where  $M^I$ = monovalent cation, and  $M^{III}$ = trivalent metallic cation) date back to the beginning of the 20<sup>th</sup> century. One of the first systematic studies was published in 1923. Kendall *et al.* reported the existence of a compound with the formula " $RX_3 \cdot R'X$ " in almost all of the investigated phase diagrams, although its structural identity was unknown [7]. No wonder, since Gilbert N. Lewis developed his theory about valence and structure in chemical bonding at that time, and only few years later his concepts about acids and bases were commonly accepted [8]. Indeed, later publications already describe these compounds as  $[M^{III} X_4]^-$  salts [9].

The monovalent cations focused on in this work are indium and thallium. As these two heavy metals belong to the group 13 of the periodic table, it is somehow unusual to observe a stable oxidation state +I. Electron shell structure and the relativistic effects are the reason for the poor shielding capacity of d-, respectively f-orbitals, which make the effective nuclear charge to increase and pull the s and p electrons closer to nucleus [10][11]. Two immediate consequences of this are the so-called "inert-pair effect" (manifested by increased 2<sup>nd</sup> and 3<sup>rd</sup> ionization energies) and the decreased ionic radius (which render  $In^{+1}$  and  $Tl^{+1}$  similar to the alkali metallic cations,  $K^+$  and  $Rb^+$ ). The stability of the oxidation state +I grows by descending the group 13 [12]. As thallium is stronger influenced by the relativistic effects than indium, monovalent thallium compounds are more stable, in contrast to monovalent indium compounds, which have a tendency to oxidize to  $In^{+3}$  [2].

### 1.2.1 The reported $M^I M^{III} X_4$ compounds

Mainly phase diagrams (but also in some cases crystal structure reports) reveal the existence of tetrachloridoaluminates of Li [2], K [2], Na [13], Cs [14], Tl [14], Rb [15],  $NH_4$  [15] and In [16]; tetrabromidoaluminates of Li [15], Na [15], K [15],  $NH_4$  [15], In [17], Rb [17] and Cs [18]; tetraiodidoaluminates of Li [15], Rb [15], Cs [15],  $NH_4$  [15], Na [19] and In [20]. The same holds true for the tetrachloridogallates of Li [9], K [9], Cs [9],  $NH_4$  [9], Tl [21], Na [22], Rb [22], In [22]; tetrabromidogallates of Na [17], K [17], Rb [17], In [17], Tl [23], Cs [24], Li [25]; and tetraiodidogallates of K [26], Na [26], Tl [26], Li [27], Rb [28]. It must be emphasized that although the salts specified above are mentioned in literature, a complete, or at least satisfactory structural characterization fails to be found in many cases.

Because of the Lewis acidic character of the group 13 metals, but also because of the Lewis basicity of the halogens, “dimerisation” and “trimerisation” of the  $[MX_4]^-$  may occur, leading to the formation of  $[M_2X_7]^-$  [15][29][30][31] and  $[M_3X_{10}]^-$  [32][33] species.

Full structural information for  $CsAlI_4$ ,  $CsGaI_4$ ,  $InAlCl_4$ ,  $InAlI_4$ ,  $InGa_2Cl_7$ ,  $TlAlCl_4$ ,  $TlAlBr_4$ ,  $TlAlI_4$ ,  $TlGaCl_4$ ,  $TlGaBr_4$ ,  $TlGaI_4$  and  $NH_4GaCl_4$  could be obtained in this work. These products were earlier predicted from phase diagrams and, in some cases, from XRD powder analysis:  $CsGaI_4$  [34],  $InAlI_4$  [35],  $TlGaBr_4$  [36]. It must be specified that the phase diagrams play rather a qualitative role, than quantitative, since the purity of the chemicals and the accuracy of the devices used at the time these systems were measured was quite poor (comparing to nowadays techniques). Nevertheless they give an idea about the thermal behavior of these salts. Figures 1 to 10 show the reported phase diagrams for the  $M^I M^{III} X_4$  compounds presented in this thesis.

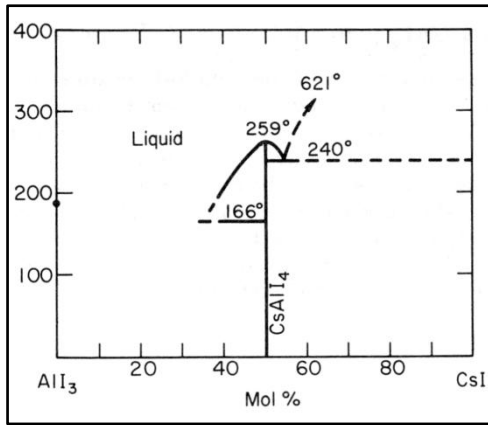


**Fig.1** Phase diagram of CsI-AlI<sub>3</sub> system [37]

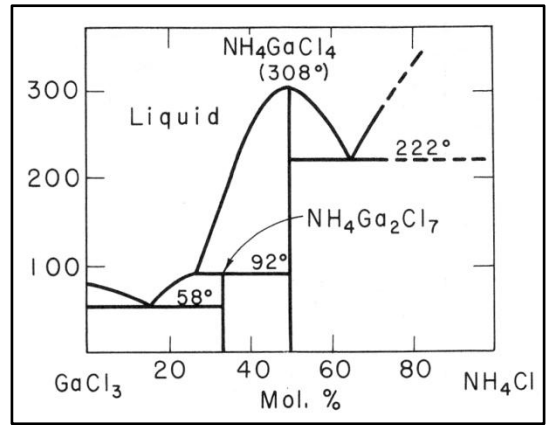


**Fig.2** Phase diagram of NH<sub>4</sub>Cl-GaCl<sub>3</sub> system [38]

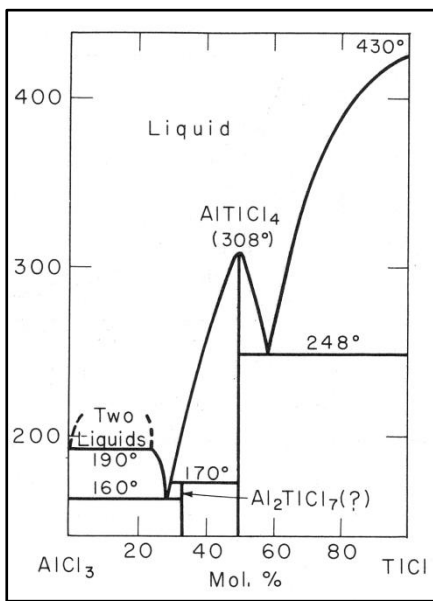


**Fig.3** Phase diagram of TlCl-AlCl<sub>3</sub> system [38]

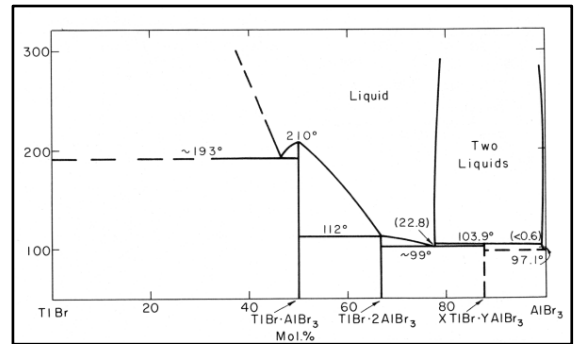


**Fig.4** Phase diagram of TlBr-AlBr<sub>3</sub> system [38]

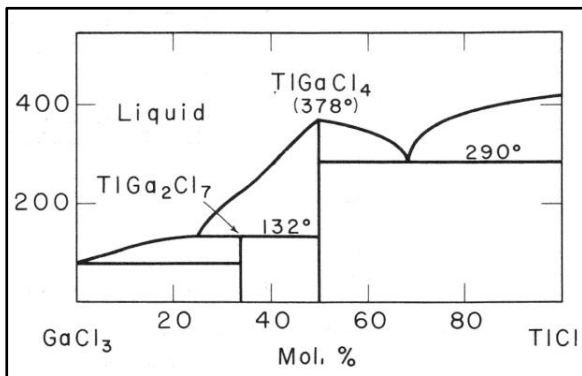


**Fig.5** Phase diagram of TlCl-GaCl<sub>3</sub> system [38]

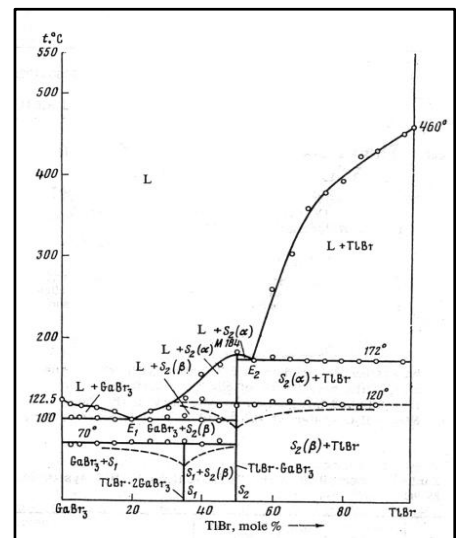


**Fig.6** Phase diagram of TlBr-GaBr<sub>3</sub> system [23]

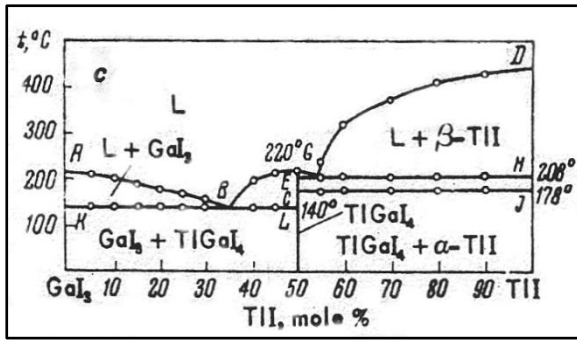


Fig.7 Phase diagram of TlI-GaI<sub>3</sub> system [26]

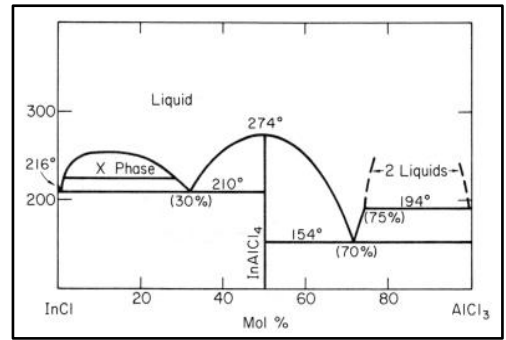


Fig.8 Phase diagram of InCl-AlCl<sub>3</sub> system [37]

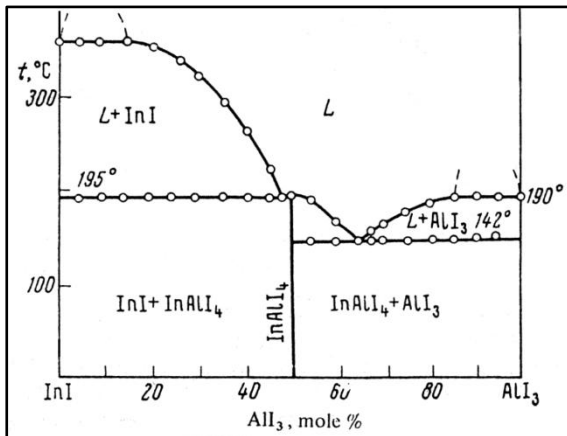


Fig.9 Phase diagram of InI-AlI<sub>3</sub> system [39]

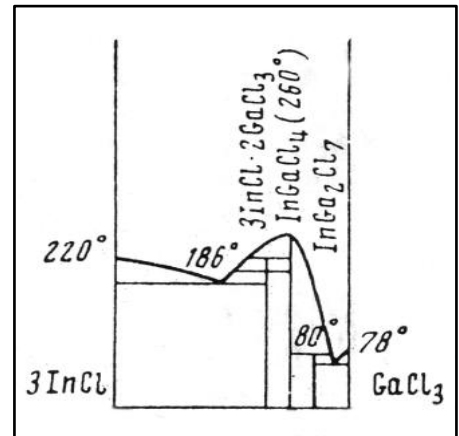


Fig.10 Phase diagram of InCl-GaCl<sub>3</sub> system [40]

### 1.2.2 Structural information

Research of the last decades provides a considerable number of crystal structures of  $M^I M^{III} X_4$  salts which helps predicting the structures of similar compounds, also their physicochemical properties, and allows for a structural classification [22][17][41]. The following tables (tab.1 and tab.2) show the known to date structure types of the alkali/pseudo-alkali tetrahalogenidometallates (written in red are the  $[MX_4]^-$  salts with no reported single crystal structures, written in blue are the compounds presented in this work).

**Tab.1** Space group of tetrahalogenidoaluminates with alkali/ pseudo-alkali metallic (and ammonium) cations

	$[AlCl_4]^-$	$[AlBr_4]^-$	$[AlI_4]^-$
<b>Li<sup>+</sup></b>	LiAlCl <sub>4</sub> <b>P 1 2<sub>1</sub>/c 1</b> [42]	LiAlBr <sub>4</sub>	LiAlI <sub>4</sub>
<b>Na<sup>+</sup></b>	NaAlCl <sub>4</sub> <b>P 2<sub>1</sub>2<sub>1</sub>2<sub>1</sub></b> [43]	NaAlBr <sub>4</sub> <b>P n m a</b> [17]	NaAlI <sub>4</sub> <b>P n m a</b> [44]
<b>K<sup>+</sup></b>	KAlCl <sub>4</sub> <b>P 1 2<sub>1</sub> 1</b> [45] <b>P n m a</b> (at $t > +114^\circ\text{C}$ ) [22] Unknown S.G.* (at $t < -77^\circ\text{C}$ ) [22]	KAlBr <sub>4</sub> <b>P 1 2/ a 1</b> [17]	KAlI <sub>4</sub>
<b>Rb<sup>+</sup></b>	RbAlCl <sub>4</sub> <b>P n m a</b> [41]	RbAlBr <sub>4</sub>	RbAlI <sub>4</sub>
<b>Cs<sup>+</sup></b>	CsAlCl <sub>4</sub> <b>P n m a</b> [41]	CsAlBr <sub>4</sub> <b>P n m a</b> [18]	CsAlI <sub>4</sub> <b>P 1 2<sub>1</sub>/ c 1</b>
<b>In<sup>+</sup></b>	InAlCl <sub>4</sub> <b>P n m a</b> [46]	InAlBr <sub>4</sub> <b>P 1 2/ a 1</b> [17]	InAlI <sub>4</sub> <b>P 1 2<sub>1</sub>/ m 1</b> [47]
<b>Tl<sup>+</sup></b>	TlAlCl <sub>4</sub> <b>P n m a</b> [22]	TlAlBr <sub>4</sub> <b>P 1 2/ a 1</b>	TlAlI <sub>4</sub> <b>P 1 2<sub>1</sub>/ c 1</b>
<b>[NH<sub>4</sub>]<sup>+</sup></b>	[NH <sub>4</sub> ]AlCl <sub>4</sub> <b>P n m a</b> [48]	[NH <sub>4</sub> ]AlBr <sub>4</sub>	[NH <sub>4</sub> ]AlI <sub>4</sub>

\*S.G. = Space Group

**Tab.2** Space group of tetrahalogenidogallates with alkali/ pseudo-alkali metallic (and ammonium) cations

	$[\text{GaCl}_4]^-$	$[\text{GaBr}_4]^-$	$[\text{GaI}_4]^-$
$\text{Li}^+$	$\text{LiGaCl}_4$ $P 1 2_1/ a 1$ [27]	$\text{LiGaBr}_4$ $P 1 2_1/ a 1$ [25]	$\text{LiGaI}_4$ $P 1 2_1/ a 1$ [27]
$\text{Na}^+$	$\text{NaGaCl}_4$ $P 1 2_1/ c 1$ [22]	$\text{NaGaBr}_4$ $P n m a$ [17]	$\text{NaGaI}_4$
$\text{K}^+$	$\text{KGaCl}_4$ $P 1 2_1/ n 1$ or $P 1 2_1 1$ (~ from $-25^\circ\text{C}$ to $130^\circ\text{C}$ ) [49] [50] $P n n a$ (at $t < -25^\circ\text{C}$ ) [50] $P n m a$ (at $t > +130^\circ\text{C}$ ) [50]	$\text{KGaBr}_4$ $R 3 c$ [17]	$\text{KGaI}_4$ $P 1 2_1/ c 1$ [51]
$\text{Rb}^+$	$\text{RbGaCl}_4$ $P n m a$ [22][52]	$\text{RbGaBr}_4$ $P n m a$ [17]	$\text{RbGaI}_4$
$\text{Cs}^+$	$\text{CsGaCl}_4$ $P n m a$ [24]	$\text{CsGaBr}_4$ $P n m a$ [24]	$\text{CsGaI}_4$ $P 1 2_1/ c 1$
$\text{In}^+$	$\text{InGaCl}_4$ $P n m a$ [22]	$\text{InGaBr}_4$ $P 1 2/ a 1$ [17]	$\text{InGaI}_4$
$\text{Tl}^+$	$\text{TlGaCl}_4$ $P n m a$ [22]	$\text{TlGaBr}_4$ $P 1 2_1/ c 1$	$\text{TlGaI}_4$ $P 1 2_1/ c 1$
$[\text{NH}_4]^+$	$[\text{NH}_4]\text{GaCl}_4$ $P n m a$	$[\text{NH}_4]\text{GaBr}_4$	$[\text{NH}_4]\text{GaI}_4$

For the  $\text{M}^{\text{I}}\text{M}^{\text{III}}\text{X}_4$  compounds presented in this thesis, several structure types are found, namely:

- 1) "Lithium tetrachloridoaluminate" –  $P 1 2_1/ c 1$  (No. 14);
- 2) "Natrium tetrachloridoaluminate" –  $P 2_1 2_1 2_1$  (No. 19);
- 3) "Barium sulphate (Baryte)" –  $P n m a$  (No. 62);
- 4) "Potassium tetrabromidoaluminate" –  $P 1 2/ a 1$  (No. 13);
- 5) "Indium tetraiodidoaluminate" –  $P 1 2_1/ m 1$  (No. 11);
- 6) "Potassium tetrachloridoaluminate" –  $P 1 2_1 1$  (No. 4);

7) “ $\beta$ -Gallium tetrabromidogallate” –  $R\ 3\ c$  (No. 161).

The preferred crystallographic structural type for the tetrahalogenidometallates of lithium is the “lithium tetrachloridoaluminate” type. The situation changes from sodium downwards, where no simple classification can be made. The “baryte” type is by far the most encountered (almost half of the compounds crystallize in this structure type). Polymorphism is observed for potassium tetrachloridoaluminate and potassium tetrachloridogallate, and found also in the case of similar compounds ( $\text{Ga}_2\text{Cl}_4$  [50] and  $\text{Ga}_2\text{Br}_4$  [17]), and it is likely that many other compounds from the analyzed systems exhibit polymorphic behavior, by comparing pseudo-alkali metal cations with their alkali metal analogues (considering  $M^{+1}$  ionic radii [3],  $\text{K}^+$  can be correlated with  $\text{In}^{+1}$  and  $\text{Tl}^{+1}$  with  $\text{Rb}^+$ ).

The tetrachloridoaluminates and tetrabromidoaluminates of indium and potassium respect the trend, and crystallize indeed in same space groups (the high temperature modification for the case of  $\text{KAlCl}_4$ ); as the crystal structure of potassium tetraiodidoaluminate is not determined, it can only be speculated that this one will crystallize like indium tetraiodidoaluminate in the  $P\ 1\ 2_1/m\ 1$  space group, or probably in the  $P\ 1\ 2_1/c\ 1$  space group, like  $\text{CsAlI}_4$  or  $\text{TlAlI}_4$ .

For thallium and rubidium can be said that only tetrachloridoaluminates of these two metals crystallize in the same space group; the crystal structure of tetrabromidoaluminates and tetraiodidoaluminates of rubidium are to date unknown. Rubidium tetrabromidoaluminate could crystallize in the “baryte” type or “potassium tetrabromidoaluminate” type, whereas rubidium tetraiodidoaluminate could show “baryte” type or “lithium tetrachloridoaluminate” type, as potential space group “candidates”.

For the class of tetrahalogenidogallates an exception must be mentioned: it is potassium tetrabromidogallate, which crystallize in an unusual for this family of compounds highly symmetric space group ( $R\ 3\ c$ ), while his analogue ( $\text{InGaBr}_4$ ) crystallize in the “potassium tetrabromidoaluminate” type ( $P\ 1\ 2/a\ 1$ ).

Tetrachloridogallates show a preference for “baryte” type; the high temperature form of  $\text{KGaCl}_4$  and the structure of  $\text{InGaCl}_4$  match this space group ( $P n m a$ ).

Rubidium and thallium tetrachloridogallates crystallize also in the “baryte” type.

The tetrabromidogallates of thallium and rubidium reveal different space groups (like in the case of tetrabromidogallates of indium and potassium).

Deliberately, the tetraiodidogallates of potassium, indium, rubidium and thallium were left for the end, since the crystal structures of  $\text{InGaI}_4$  and  $\text{RbGaI}_4$  are unknown. It is a high probability that these two salts crystallize in “lithium tetrachloridoaluminate” type, because all known tetraiodidogallates of these alkali metal and pseudo-alkali metal cations crystallize in this structural type.

### 1.3 Ionic liquids and molten salts containing weakly coordinating anions

#### 1.3.1 Ionic liquids and molten salts

The interest for ionic liquids expanded fast in the last decades. Over time a definition of ionic liquids has been contoured: these are compounds which consist completely of anions and cations and melt below 100°C [53]. The interest in this new class of solvents was to develop new electrolytes with as low melting points as possible for batteries [54]. Soon it was realized that these compound are also good replacements in many situations for the conventional organic solvents, because of a few key characteristics: relatively low toxicity (compared to organic solvents), wide liquid range (the thermal window between melting and the boiling/ decomposition point of a compound), very low vapor pressure, and not at last, the possibility to tune them depending on the desired solvent properties.

The ionic liquids are made generally from an organic cation and an inorganic/organic anion.

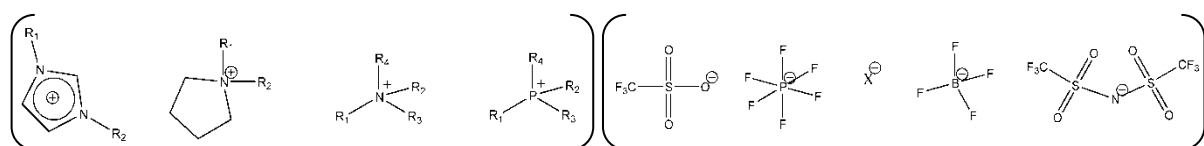


**Fig.11** Common cations and anions for ionic liquids

As ionic liquids melt by definition under 100°C, salts that melt above 100°C are called *molten salts*. The versatility of both ionic liquids and molten salts is that that their physicochemical properties can be modified by changing the cation or/and the anion [54][55]. From all the cations, the most widely used is by far the 1-alkyl-3-alkylimidazolium one [56]. Anyhow, in the last years ammonium and phosphonium ionic liquids have gained more and more interest, mainly due to their better thermal stability. Anions like bis(trifluoromethanesulphonyl)imide [Tf<sub>2</sub>N]<sup>-</sup>, tetrafluoroborate [BF<sub>4</sub>]<sup>-</sup>, hexafluorophosphate [PF<sub>6</sub>]<sup>-</sup>, or trifluoromethanesulfonate [TfO]<sup>-</sup> are frequently implemented in ionic liquids. Many

organic and metal-organic processes can be carried out in ionic liquids as alternative solvents [57]. High product yields and good selectivity have been reported by Heck reactions [58], Friedel-Crafts reactions [59], Diels-Alder cycloaddition [60] and biochemical reactions and processes [61]. Also interesting is the method proposed by Rogers *et al.* [62] for the recycling of cellulose. The ionic liquids chemistry is a relatively young research field, and therefore the applicability of this new “green” generation of solvents in industry [63] is rather in the incipient phase at the moment; nevertheless the potential within is highly promising. One example in this case is the **BASIL<sup>TM</sup>** Process (**B**iphasic **A**cid **S**cavenging utilizing **I**onic **L**iquids) [64], owned by BASF (Germany). Also secondary battery trials including ILs as electrolyte were reported [65].

Chloridometallate (aluminate and gallate) ionic liquids have been and are intensively studied. Changing from a  $M^I X-M^{III} X_3$  ( $M^I$ = alkali metal, X= halide atom, and  $M^{III}$ =Al, Ga) to a  $RX-M^{III} X_3$  system (R= organic cation) [66], have as a direct consequence a dramatic drop of the melting point of these salts (in many cases below 25°C, in which case a **R**oom **T**emperature **I**onic **L**iquid-**RTIL** is formed). In the last decades structural information and physicochemical properties of ionic liquids (mainly chloridoaluminates, but not only these) were gathered [54][67][68].

### 1.3.2 Weakly coordinating anions

The ionic liquids and molten salts presented in this work contain “weakly coordinating anions”. As a general definition **WCAs** (**Weakly Coordinating Anion**) are conjugated bases of superacids ( $\text{HClO}_4$ ,  $\text{HSbF}_6$ ,  $\text{HSO}_3\text{F}$ ,  $\text{CH}_3\text{SO}_3\text{H}$ ) [69]. Generally they find their origin in a strong Lewis acid, as this one binds so strongly a ligand, that the whole anion shows weak interactions with the counter ions. It was shown that the “non-coordinating” nature of  $[\text{ClO}_4]^-$ ,  $[\text{SO}_3\text{CF}_3]^-$ ,  $[\text{BF}_4]^-$ ,  $[\text{PF}_6]^-$ ,  $[\text{AsF}_6]^-$  was falsely presumed, and it was also shown that there are anions which coordinate weaker than the ones above mentioned [6]. *Strauss* proposed the replacement of “non-coordinating anion” term with the “weakly coordinating anion” one, which is more appropriate [6]. He presented also an ideal profile of an WCA: charge as low as possible (preferred -1); high symmetry, and an as large as possible volume, for a better delocalization of charge (the larger the delocalization, the weaker the coordination ability of the anion); the presence of nucleophilic sites should be avoided at the periphery of the anion (hydrogen or fluorine are preferred over oxygen or chlorine) [6]. Respecting the above specified criteria,  $[\text{B}(\text{OTeF}_5)_4]^-$  [70],  $[\text{Nb}(\text{OCH}(\text{CF}_3)_2)_6]^-$  [71],  $[\text{Al}(\text{OR}_F)_4]^-$  [72] and  $[\text{B}(\text{Ar}_F)_4]^-$  [73] WCAs were developed, as a second generation of weakly coordinating anions (together for example with carborane and borane anionic clusters). As it can be observed, the increase in volume of the anion is accompanied by high symmetry (often almost undistorted  $T_d$  symmetry), and “shielding” with fluorinated groups.

The importance of WCAs is attributed to the fact that they can stabilize highly electrophilic centers (enhancing this way some homogenous catalysis mechanisms), weak Lewis acid-base adducts, like  $[\text{Au}(\text{Xe})_4]^{2+}$  [74], but also cationic species like  $[\text{C}(\text{CH}_3)_3]^+$  [75]; beside of that, they can also be used as electrolytes, due to their electrochemical stability [76]. Figures 12 and 13 present several weakly coordinating anions as above classified, by separating them with respect to the coordination capabilities in two groups: first and second generation of weakly coordinating anions [6].

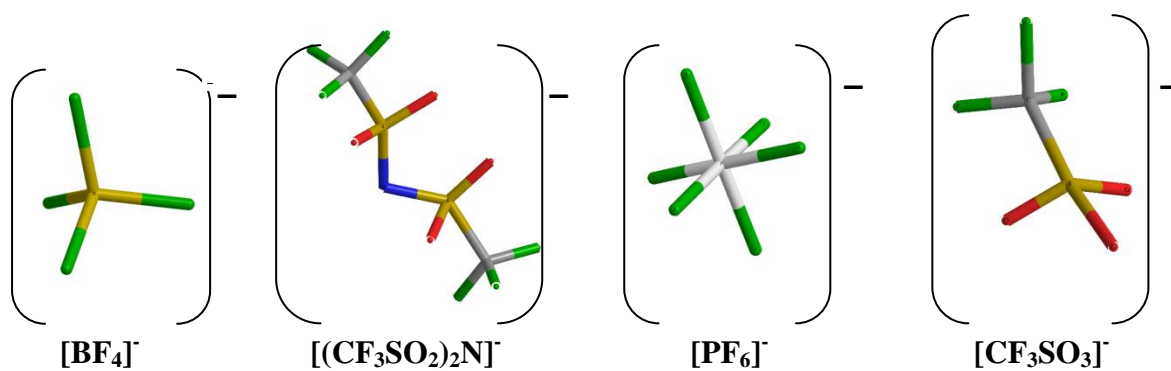


**Fig.12** “First generation” of weakly coordinating anions

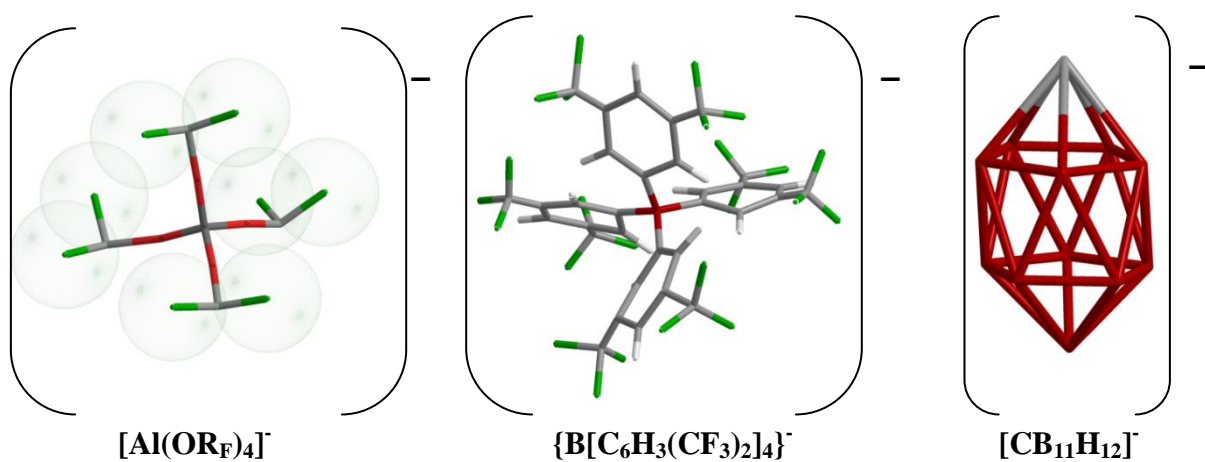


**Fig.13** “Second generation” of weakly coordinating anions

In this project two fluorinated alkoxyaluminates were considered: lithium tetrakis(hexafluoroisopropyl)aluminate and lithium tetrakis(nonafluoro-tert-butyl)aluminate (abbreviation  $\text{LiAl}(\text{hfip})_4$  and  $\text{LiAl}(\text{nftb})_4$ ). These anions were taken into consideration because they are one of the least coordinating anions known to date.

#### 1.4 Literature

- [1] H. L. Friedman, H. Taube, *J. Am. Chem. Soc.* **1950**, 72, 2236-2243.
- [2] N. N. Greenwood, A. Earnshaw, *Chemie der Elemente*, VCH, Weinheim, **1988**.
- [3] H. A. Hjuler, S. Von Winbush, R. W. Berg, N. J. Bjerrum, *J. Electrochem. Soc.* **1989**, 136 (4), 901-906.
- [4] F. H. Hurley, T. P. Wier, *J. Electrochem. Soc.* **1951**, 98, 203-206; 207-212.
- [5] P. Pyykkö, J.-P. Desclaux, *Acc. Chem. Res.* **1979**, 12, 276-281.
- [6] S. H. Strauss, *Chem. Rev.* **1993**, 93, 927-942.
- [7] J. Kendall, E. D. Crittenden, H. K. Miller, *J. Am. Chem. Soc.* **1923**, 45, 963-996.
- [8] G. N. Lewis, G. T. Seaborg, *J. Am. Chem. Soc.* **1939**, 61(7), 1886-1894.
- [9] H. L. Friedman, H. Taube, *J. Am. Chem. Soc.* **1950**, 72, 2236-2243.
- [10] P. Pyykkö, *Chem. Rev.* **1988**, 88, 563-594.
- [11] S. P. Kenneth, *Acc. Chem. Res.* **1979**, 12, 271-276.
- [12] C. E. Housecroft, A.G. Sharpe, *Anorganische Chemie*, Pearson Studium, München, **2006**.
- [13] W. Fischer, A.-L. Simon, *Z. Anorg. Allg. Chem.* **1960**, 306, 1-12.
- [14] S. Morozov, A. T. Simonich, *Zh. Neorg. Khim.* **1957**, 2, 1907-1914.
- [15] G. Boef, H. B. Slot, R. A. W. van Leeuwen, H. Wessels, J. W. van Spronsen, *Z. Anorg. Allg. Chem.* **1967**, 353, 93-102.
- [16] R. J. Clark, E. Griswold, J. Kleinberg, *J. Am. Chem. Soc.* **1958**, 80, 4764-4767.
- [17] T. Staffel, G. Meyer, *Z. Anorg. Allg. Chem.* **1990**, 585, 38-48.
- [18] R. W. Berg, *Acta Chemica Scandinavica* **1997**, 51, 455-461.
- [19] R. Burnus, D. J. Hinz, G. Meyer, *Z. Kristallogr.* **1994**, 209, 544.
- [20] P. I. Fedorov, N. S. Malova, Y. N. Denisov, *Zh. Neorg. Khim.* **1971**, 16(12), 3347-3349.
- [21] P. I. Fedorov, V. V. Tsimbalist, *Zh. Neorg. Khim.* **1964**, 9(7), 1676-1680.

- [22] G. Meyer, E. Schwan, *Z. Naturforsch., B: Chem. Sci.* **1980**, 35b(1), 117-118.
- [23] A. K. Molodkin, M. Rabbani, A. G. Dudareva, A. I. Ezhov, *Zh. Neorg. Khim.* **1980**, 25(8), 2245-2247.
- [24] R. C. Gearhart, J. D. Beck, R. H. Wood, *Inorg. Chem.*, **1975**, 14(10), 2413-2416.
- [25] W. Höhle, A. Simon, *Z. Naturforsch., B: Chem. Sci.* **1986**, 41B(11), 1391-1398.
- [26] P. I. Fedorov, G. A. Kot, *Zh. Neorg. Khim.* **1967**, 12(9), 2313-2316.
- [27] W. Höhle, B. Hettich, A. Simon, *Z. Naturforsch., B: Chem. Sci.* **1987**, 42(2), 248-250.
- [28] P. I. Fedorov, N. S. Malova, I. Y. Rodimtseva, *Zh. Neorg. Khim.* **1982**, 27(9), 2392-2394.
- [29] D. Mascherpa-Corral, P. Vitse, A. Potier, *Acta Crystallogr., Sect. B: Struct. Sci.* **1976**, 32(1), 247-250.
- [30] M. E. Peach, V. L. Tracy, T. C. Waddington, *J. Chem. Soc., Sect. A: Inorganic, Physical, Theoretical* **1969**, 3, 366-367.
- [31] W. Frank, W. Höhle, A. Simon, *Z. Naturforsch., B: Chem. Sci.* **1990**, 45(1), 1-7.
- [32] D. Mascherpa-Corral, A. Potier, *Journal of Inorganic and Nuclear Chemistry* **1977**, 39(9), 1519-1522.
- [33] Ala'a K. Abdul-Sada, A. M. Greenway, K. R. Seddon, T. Welton, *Organic Mass Spectrometry* **1989**, 24, 917-918.
- [34] E. M. Levin, H. F. McMurdie, *Phase diagrams for ceramists-Supplement*, The American Ceramic Society, Columbus-Ohio, **1975**.
- [35] ICDD PDF-2 database, *Sets 1-88*, [44-1112].
- [36] ICDD PDF-2 database, *Sets 1-88*, [28-460].
- [37] ICDD PDF-2 database, *Sets 1-88*, [30-1323].
- [38] E. M. Levin, C. R. Robbins, H. F. McMurdie, *Phase diagrams for ceramists-Supplement*, The American Ceramic Society, Columbus-Ohio, **1969**.
- [39] Y. N. Denisov, N. S. Malova, P. I. Fedorov, *Zh. Neorg. Khim.* **1976**, 21(1), 222-226.
- [40] Y. P. Afinogenov, V. A. Dantseva, *Zh. Neorg. Khim.* **1975**, 20(2), 516-518.

- [41] G. Mairesse, P. Barbier, J. P. Wignacourt, *Acta Crystallogr., Sect. B: Struct. Sci.* **1979**, 35, 1573-1580.
- [42] G. Mairesse, P. Barbier, J. P. Wignacourt, *Crystal Struct. Commun.* **1977**, 6(1), 15-18.
- [43] N. C. Baenziger, *Acta Crystallogr.* **1951**, 4, 216-219.
- [44] R. Burnus, D. J. Hinz, G. Meyer, *Z. Kristallogr.* **1994**, 209(6), 544.
- [45] G. Mairesse, P. Barbier, J. P. Wignacourt, *Acta Crystallogr., Sect. B: Struct. Sci.* **1978**, 34(4), 1328-1330.
- [46] T. Timofte, A.-V. Mudring, *Acta Crystallogr., Sect. E: Struct. Rep. Online* **2005**, 61, i199-i200.
- [47] T. Timofte, A.-V. Mudring, *Z. Anorg. Allg. Chem.* **2008**, 634(4), 622-623.
- [48] G. Mairesse, P. Barbier, J. P. Wignacourt, A. Rubbens, F. Wallart, *Can. J. Chem.* **1978**, 56, 764-771.
- [49] M. Gorlov, A. Fischer, L. Kloo, *Acta Crystallogr., Sect. E: Struct. Rep. Online* **2003**, 59, i70-i71.
- [50] G. Meyer, T. Staffel, M. Irmeler, *Thermochim. Acta* **1990**, 160, 63-70.
- [51] R. Burnus, A. Zajonc, G. Meyer, *Z. Kristallogr.* **1995**, 210(1), 61.
- [52] J.-X. Mi, H. Zhang, J.-F. Deng, S.-Y. Mao, J.-T. Zhao, *Z. Kristallogr.-New Cryst. Struct.* **2002**, 217, 479-480.
- [53] P. Wasserscheid, W. Keim, *Angew. Chem.* **2000**, 112, 3926-3945.
- [54] P. Wasserscheid, T. Welton, *Ionic Liquids in Synthesis*, 2<sup>nd</sup> Edition, Wiley-VCH, Weinheim, **2008**.
- [55] L. Crowhurst, P. R. Mawdsley, J. M. Perez-Arlandis, P. A. Salter, T. Welton, *Phys. Chem. Chem. Phys.* **2003**, 5, 2790-2794.
- [56] J. G. Huddleston, A. E. Visser, W. M. Reichert, H. D. Willauer, G. A. Broker, R. D. Rogers, *Green Chem.* **2001**, 3, 156-164.
- [57] T. Welton, *Chem. Rev. (Washington, DC, U. S.)* **1999**, 99, 2071-2083.

- [58] A. J. Carmichael, M. Earle, J. Holbrey, P. B. McCormac, K. R. Seddon, *Org. Lett.* **1999**, *1*(7), 997-1000.
- [59] C. J. Adams, M. Earle, G. Roberts, K. R. Seddon, *Chem. Comm. (Cambridge, U. K.)* **1998**, *19*, 2097-2098.
- [60] M. J. Earle, P. B. McCormac, K. R. Seddon, *Green Chem.* **1999**, *1*, 23-25.
- [61] S. G. Cull, J. D. Holbrey, V. Vargas-Mora, K. R. Seddon, G. J. Lye, *Biotechnol. Bioeng.* **2000**, *69*(2), 227-233.
- [62] R. P. Swatloski, S. K. Spear, J. D. Holbrey, R. D. Rogers, *J. Am. Chem. Soc.* **2002**, *124*, 4974-4975.
- [63] N. V. Plechkova, K. R. Seddon, *Chem. Soc. Rev.* **2008**, *37*, 123-150.
- [64] M. Maase, K. Massonne, K. Halbritter, R. Noe, M. Bartsch, W. Siegel, V. Stegmann, M. Flores, O. Huttenloch, M. Becker, *Int. Patent* **2003**, *WO 2003062171*.
- [65] S. Seki, Y. Kobayashi, H. Miyashiro, Y. Ohno *et al.*, *Chem. Commun. (Cambridge, U. K.)* **2006**, 544-545.
- [66] J. P. Schoebrechts, B. P. Gilbert, *J. Electrochem. Soc.* **1981**, *128*(12), 2679-2684.
- [67] M. J. Zaworotko, S. T. Cameron, A. Linden, K. C. Sturge, *Acta Crystallogr., Sect. C: Cryst. Struct. Commun.* **1989**, *45*, 996-1002.
- [68] P. C. Trulove, R. A. Osteryoung, *Inorg. Chem. (Washington, DC, U. S.)* **1992**, *31*, 3980-3985.
- [69] E. Riedel, *Moderne Anorganische Chemie*, Walter de Gruyter, Berlin, **2003**.
- [70] M. D. Noirod, O. P. Anderson, S. H. Strauss, *Inorg. Chem. (Washington, DC, U. S.)* **1987**, *26*, 2216-2223.
- [71] J. J. Rockwell, G. M. Kloster, W. J. DuBay, P. A. Grieco *et al.*, *Inorg. Chim. Acta* **1997**, *263*, 195-200.
- [72] I. Krossing, H. Brands, R. Feuerhake, S. Koenig, *J. Fluorine Chem.* **2001**, *112*, 83-90.
- [73] H. Kobayashi, *J. Fluorine Chem.*, **2000**, *105*, 201-203.

- [74] A. Bihlmeier, M. Gonsior, I. Raabe, N. Trapp, I. Krossing, *Chem.--Eur. J.* **2004**, *10*, 5041-5051.
- [75] T. Kato, C. A. Reed, *Angew. Chem., Int. Ed.* **2004**, *43*, 2908-2911.
- [76] F. Kita, H. Sakata, S. Sinomoto, A. Kawakami *et al.*, *J. Power Sources* **2000**, *90(1)*, 27-32.

## 2. Tetrahalogenidoaluminates and tetrahalogenidogallates

$M^I X-M^{III} X_3$ -type salts are known since 1923 [1]. The general synthesis procedure of these tetrahalogenidometallates, takes place by combining the  $M^I X$  salt with the  $M^{III} X_3$  salt in a 1:1 molar ratio under inert conditions, and heating to 200-300°C. In order to obtain crystals of suitable quality for XRD single crystal analysis, the solvent free melts were cooled to room temperature very slowly.

The synthesized compounds were grouped, into two major classes: *the barium sulphate type (baryte) class* and a second class formed by compounds crystallizing into *the  $P2_1/c$  space group*.

### 2.1 The baryte type $M^I M^{III} X_4$ class of salts

Thallium(I) tetrachloridoaluminate, thallium(I) tetrachloridogallate and indium(I) tetrachloridoaluminate belong to this category. Ammonium tetrachloridogallate is also presented here, since it crystallizes also in the “baryte” type. Ammonium tetrachloridoaluminate also crystallize in the “baryte” type [2]. The preference for the  $P n m a$  space group is also showed by the larger alkali metal tetrachloridoaluminates and tetrachloridogallates (Rb, Cs and K, by high temperatures). It has to be mentioned that In(I) and Tl(I) tetrachloridometallates crystallize in the  $P n m a$  space group, but  $Ga[AlCl_4]$  [3] and  $Ga[GaCl_4]$  [4] do not crystallize in this space group.

#### 2.1.1. Preparation

All preparations were carried out in an argon atmosphere glove box (MBraun, Germany). The educts were stored in the glove box and used as purchased. Borosilicate glass-ampoules were used as reaction containers (Schott Duran™ glass tubes).

TlAlCl<sub>4</sub> was prepared as follows: TlCl and AlCl<sub>3</sub> were mixed in a 1:1 molar ratio (0.733 mmol), introduced and sealed in a glass ampoule, and then heated by a rate of 10°C/h to 150°C and annealing 48 hours; the cooling took place slowly with a rate of 2°C/h to 25°C.

TlGaCl<sub>4</sub> was obtained from a mixture of TlCl and GaCl<sub>3</sub> in 1:1 molar ratio (0.733 mmol), which was introduced in a glass ampoule, and then sealed under vacuum, heated to 150°C and annealed for 48 hours. The heating rate was 10°C/h, and the cooling rate to room temperature was at 2°C/h.

In order to obtain InAlCl<sub>4</sub>, elemental In (1.219 mmol), InCl<sub>3</sub> (0.610 mmol) and AlCl<sub>3</sub> (1.829 mmol) (molar ratio In:InCl<sub>3</sub>:AlCl<sub>3</sub> = 2:1:3) were sealed under vacuum in a glass ampoule, then heated to 250°C with 10°C/h, and kept at this temperature for 7 days. Cooling to room temperature was achieved at a rate of 5 °C/h. Synthesis procedure was performed according to [5].

NH<sub>4</sub>GaCl<sub>4</sub> was obtained by mixing NH<sub>4</sub>Cl and GaCl<sub>3</sub> in a 1:1 (1.308 mmol) molar ratio; the mixture was introduced in a glass ampoule, sealed under vacuum; then heated and hold at 120°C for 96 hours. The heating rate was 10°C/h, and the cooling ran with 2°C/h to 25°C.

The reactions took place almost quantitatively in all the above specified cases, and as a general feature it can be said that the reacted mixtures consisted of a crystalline fraction and a glass-phase fraction.

In the case of the compounds TlAlCl<sub>4</sub>, TlGaCl<sub>4</sub> and NH<sub>4</sub>GaCl<sub>4</sub> colourless, transparent, prismatic crystals could be observed under the microscope; in the case of InAlCl<sub>4</sub> the crystals have a needle-like shape, are transparent with a light yellow nuance. Crystals were isolated in the glove box, sealed in glass capillaries, and then investigated by X-ray diffraction at room temperature.

## 2.1.2 Structural aspects

### 2.1.2.1 Crystal structure of TlAlCl<sub>4</sub>, TlGaCl<sub>4</sub>, InAlCl<sub>4</sub> and [NH<sub>4</sub>]GaCl<sub>4</sub>

TlAlCl<sub>4</sub> and TlGaCl<sub>4</sub> crystallize isotypic with the BaSO<sub>4</sub> type of structure, in the orthorhombic space group  $P n m a$  (no. 62), with four formula units in the unit cell ( $a = 1092.1(4)$  pm,  $b = 703.1(3)$  pm,  $c = 922.6(4)$  pm;  $V = 708.4(5) \cdot 10^6$  pm<sup>3</sup> for TlAlCl<sub>4</sub>, and  $a = 1091.0(5)$  pm,  $b = 706.2(3)$  pm,  $c = 926.6(4)$  pm;  $V = 713.9(6) \cdot 10^6$  pm<sup>3</sup> for TlGaCl<sub>4</sub>). The asymmetric unit of TlAlCl<sub>4</sub> and TlGaCl<sub>4</sub> contains one crystallographically independent Tl(I) cation, one M(III) cation (M = Al, Ga) and three chlorine anions. InAlCl<sub>4</sub> [6] and NH<sub>4</sub>GaCl<sub>4</sub> crystallize also isotypic with BaSO<sub>4</sub> type of structure ( $a = 1093.70$  pm,  $b = 705.19$  pm,  $c = 926.71$  pm;  $V = 714.74 \cdot 10^6$  pm<sup>3</sup> for InAlCl<sub>4</sub>, and  $a = 1098.0(3)$  pm,  $b = 701.0(2)$  pm,  $c = 931.0(2)$  pm,  $V = 716.59(322) \cdot 10^6$  pm<sup>3</sup> for NH<sub>4</sub>GaCl<sub>4</sub>), and as in the previous case, the unit cell contains four formula units. For indium tetrachloridoaluminate the crystallographically independent ions per asymmetric unit are one In<sup>1+</sup>, one Al<sup>3+</sup> and three Cl<sup>1-</sup>. Also with respect to the crystallographically independent ions, ammonium tetrachloridogallate has one N<sup>3-</sup>, one Ga<sup>3+</sup>, and three Cl<sup>1-</sup> crystallographically independent ions in the asymmetric unit. In all the cases the dominant structural feature is the anionic tetrahedron formed by the tetrachloridoaluminate, respectively tetrachloridogallate units. Table 3 present the crystallographic data for TlAlCl<sub>4</sub>, TlGaCl<sub>4</sub> and InAlCl<sub>4</sub>.

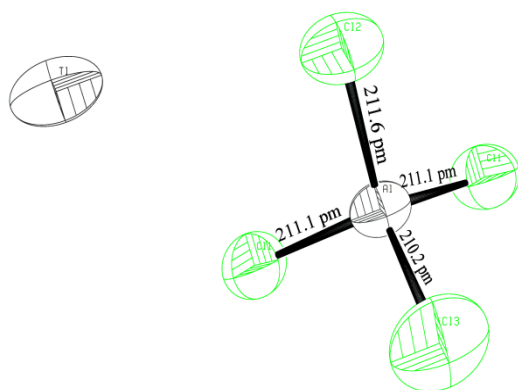
#### 2.1.2.1.1 TlAlCl<sub>4</sub>

In TlAlCl<sub>4</sub> the tetrachloridoaluminate tetrahedron is almost undistorted, since the Al-Cl bonds vary in length only in the 0.9-1.4 pm range. Considering the crystallographic packing arrangement, thallium(I) (C.N.=6+4) features a strongly distorted octahedral environment (fig.15); four extra chlorine atoms cap the octahedron at a slightly longer distance than the chlorine atoms which form the octahedron. These statements are in conformity with the reported van der Waals radii [7] and ionic radii [8][9].

**Tab.3** Crystallographic and refinement data for TlAlCl<sub>4</sub>, TlGaCl<sub>4</sub> and InAlCl<sub>4</sub>

Empirical formula	TlAlCl <sub>4</sub>	TlGaCl <sub>4</sub>	InAlCl <sub>4</sub>
Formula weight /amu	373.15	518.70	283.60
Crystal system	orthorhombic	orthorhombic	orthorhombic
Space group (no.)	<i>Pnma</i> (no. 62)	<i>Pnma</i> (no. 62)	<i>Pnma</i> (no. 62)
Unit cell dimensions /pm	<i>a</i> = 1092.1(4) <i>b</i> = 703.1(3) <i>c</i> = 922.6(4)	<i>a</i> = 1091.(5) <i>b</i> = 706.2(3) <i>c</i> = 926.6(4)	<i>a</i> = 1093.7 <i>b</i> = 705.19 <i>c</i> = 926.71
<i>V</i> /Å <sup>3</sup>	708.4(5)	713.9(6)	714.7(2)
$\rho_{xray} / g \cdot cm^{-3}$	3.499	3.869	2.636
<i>Z</i>	4	4	4
Theta range	2.89° ≤ $\theta$ ≤ 25.08°	2.88° ≤ $\theta$ ≤ 25.0°	2.76° ≤ $\theta$ ≤ 28.31°
Temperature	T = 293.(2) K	T = 293.(2) K	T = 298.(2) K
F(000)	1296	1776	520
Absorption correction	numerical Bruker SADABS	numerical Bruker SADABS	numerical Stoe X-SHAPE/X-RED
Absorption coefficient /mm <sup>-1</sup>	48.605	75.281	4.797
Structure solution /refinement	Direct methods, SIR-92, SHELXL-97	Direct methods, SIR-92, SHELXL-97	Direct methods, SHELXS/XL-97
Data/restraints/parameters	667 / 0 / 35	668 / 0 / 35	1353 / 0 / 35
N( <i>hkl</i> )	1774	3493	1353
N'( <i>hkl</i> ) unique with I > 2σ(I)	667	668	720
R <sub>int</sub>	0.0707	0.0899	0.0366
R <sub>1</sub> (I > 2σ); wR <sub>2</sub> (I > 2σ)	0.0775; 0.1933	0.0909; 0.2163	0.0508; 0.1543
R <sub>1</sub> (all); wR <sub>2</sub> (all)	0.1349; 0.2346	0.1224; 0.2402	0.0966; 0.1738
Goof	1.061	1.121	1.089
Extinction coefficient	0.043(6)	0.036(5)	0.017(2)
$\Delta F_{max}; \Delta F_{min} / e \cdot \text{Å}^{-3}$	2.472; -1.022	2.842; -1.211	1.014; -0.953
XRD measuring unit	Bruker AXS Smart CCD 1000	Bruker AXS Smart CCD 1000	Stoe IPDS

In figure 14 the almost undistorted tetrachloridoaluminate unit of the TlAlCl<sub>4</sub> crystal structure is shown. The coordination octahedra around thallium are oriented along parallel rows by which the octahedra are connected through one common edge (fig.16). The four chlorine atoms on opposite sides of thallium, at the edges which connect the octahedra in

**Fig.14** Structural unit of TlAlCl<sub>4</sub>

rows, reveal two different Tl-Cl distances; these two Tl-Cl distances alternate along the octahedra rows. The capping chlorines are positioned either on the top, or the bottom side of the each octahedron, but not symmetrically oriented over the four faces of one half of the octahedron.

The four capping chlorine atoms are distributed over three faces of one half of the octahedron: two capping chlorine atoms are each positioned over one faces (Cl2 capping chlorine atoms in fig.15); the other two capping chlorine atoms cap the face of the octahedron situated between the other two capped faces. The two chlorine atoms which share the face of the octahedron are situated at a distance of 340.7 pm from each other, and they are relatively near to the edges of the capped face (Cl1 capping chlorine atoms in fig.15). The coordinating environment around thallium is presented in figure 15, whereas in table 4 are registered the

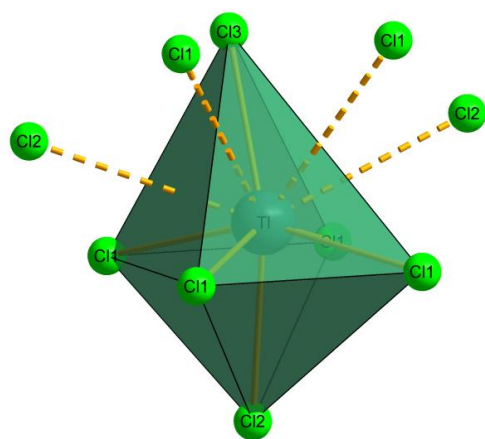


**Fig.15** Coordination environment around  $Tl^I$  in  $TlAlCl_4$

observed thallium-chlorine distances.

**Tab.4** Selected interatomic Tl-Cl distances

Tl-Cl	d/pm	Equivalent distances
Tl(1)-Cl(3)	332.0(12)	1x
Tl(1)-Cl(1)	337.2(7)	2x
Tl(1)-Cl(2)	342.2(9)	1x
Tl(1)-Cl(1)′	344.6(7)	2x
Tl(1)-Cl(2)′	386.4(4)	2x
Tl(1)-Cl(1)′	389.3(6)	2x

Along the rows formed by the edge-linked octahedra, the capping chlorines are alternating the side (top or bottom of the row), as it can be seen in the figure 16.

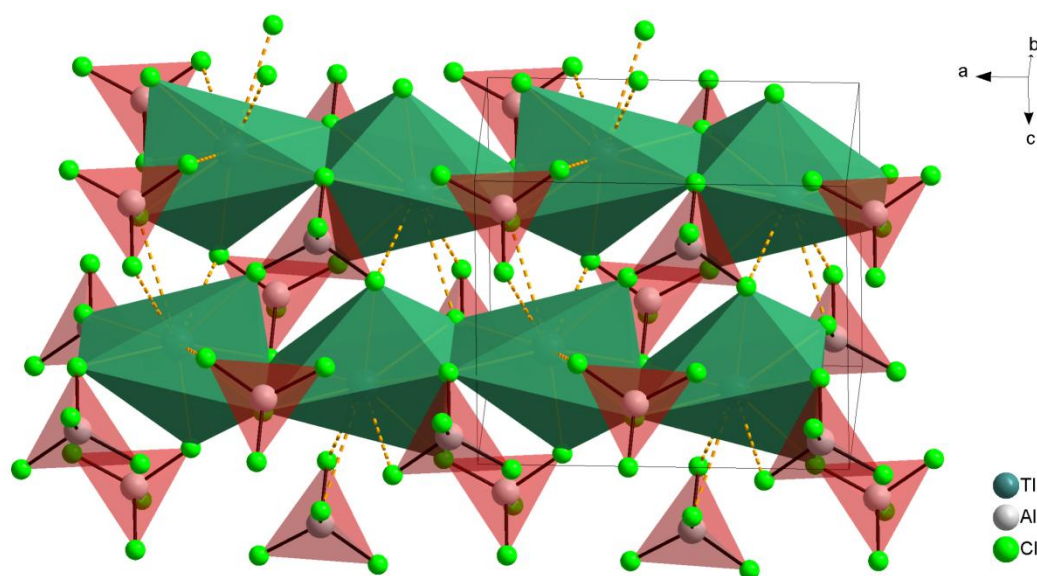


**Fig.16** Crystal structure of  $TlAlCl_4$ —approximate projection along crystallographic axis b

**Tab.5** Atomic coordinates and equivalent isotropic displacement parameters ( $\text{\AA}^2$ ) for  $\text{TlAlCl}_4$ 

Atom	x/a	y/b	z/c	S.O.F.	$U_{eq}$
Tl(1)	0.18455	$1/4$	0.31970	0.50000	0.10850
Al(1)	0.43444	$1/4$	0.31113	0.50000	0.05578
Cl(1)	0.42422	0.00767	0.17662	1.00000	0.08638
Cl(2)	0.28090	$1/4$	0.45105	0.50000	0.09664
Cl(3)	0.60092	$1/4$	0.42544	0.50000	0.13008

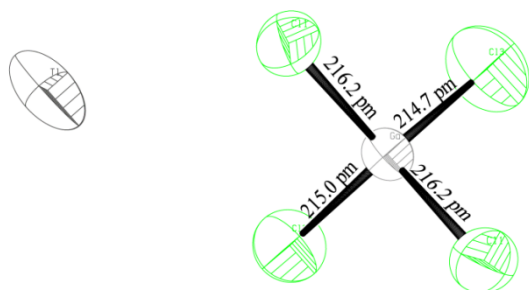
**Tab.6** Selected distances and angles for the tetrachloridoaluminate tetrahedron of  $\text{TlAlCl}_4$ 

Distance	d/pm		Angle	$l^\circ$	
Al(1)-Cl(3)	210.2(12)	1x	Cl(3)-Al(1)-Cl(1)	109.9(4)	2x
Al(1)-Cl(1)	211.1(8)	2x	Cl(1)-Al(1)-Cl(1)	107.6(5)	1x
Al(1)-Cl(2)	211.6(11)	1x	Cl(3)-Al(1)-Cl(2)	112.3(6)	1x
			Cl(1)-Al(1)-Cl(2)	108.5(4)	2x

### 2.1.2.1.2 $\text{TlGaCl}_4$

Since  $\text{TlGaCl}_4$  shows the same structure like  $\text{TlAlCl}_4$ , only the tetrachloridogallate

unit is shown (fig.17), the atomic coordinates and distances between atoms in the octahedral environment being very similar with previous.

**Fig.17** Structural unit of  $\text{TlGaCl}_4$ 

The tetrachloridogallate tetrahedron in  $\text{TlGaCl}_4$  is only slightly distorted, by comparing it with its analogous

tetrachloridoaluminate tetrahedron, the difference between Ga-Cl bond lengths being in 0.4-1.5 pm range. By comparing the Tl-Cl lengths in the structure of  $\text{TlGaCl}_4$  with the Rb-Cl lengths in the crystal structure of  $\text{RbGaCl}_4$  [10], the average distances between thallium and chlorine atoms in the coordination octahedron  $\{\text{TlCl}_6\}$  are slightly smaller than in the case of  $\{\text{RbCl}_6\}$  coordination environment (considering that rubidium larger in the same

coordination environment as thallium(I) is).

**Tab.7** Distances and angles in the tetrachloridoaluminate tetrahedral anion of TlGaCl<sub>4</sub>

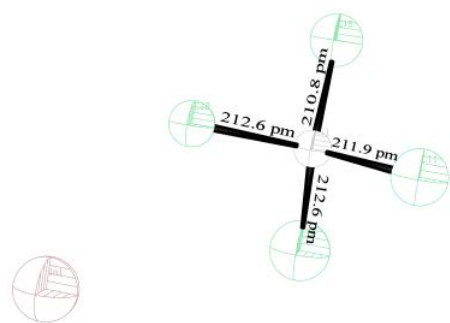
Distance	d/pm		Angle	/°	
Ga(1)-Cl(3)	214.7(13)	1x	Cl(3)-Ga(1)-Cl(2)	113.4(6)	1x
Ga(1)-Cl(2)	215.1(10)	1x	Cl(3)-Ga(1)-Cl(1)	109.3(4)	2x
Ga(1)-Cl(1)	216.2(6)	2x	Cl(2)-Ga(1)-Cl(1)	108.7(3)	2x
			Cl(1)-Ga(1)-Cl(1)	107.2(4)	1x

**Tab.8** Atomic coordinates and equivalent isotropic displacement parameters (Å<sup>2</sup>) for TlGaCl<sub>4</sub>

Atom	x/a	y/b	z/c	S.O.F.	U(eq)
Tl(1)	0.1847(2)	-1/4	0.3176(2)	0.5000	0.108(1)
Ga(1)	0.4329(3)	1/4	0.3112(4)	0.5000	0.048(1)
Cl(1)	0.4251(6)	0.0036(10)	0.1730(7)	1.0000	0.077(2)
Cl(2)	0.2745(12)	1/4	0.4493(12)	0.5000	0.094(4)
Cl(3)	0.6032(14)	1/4	0.4273(18)	0.5000	0.129(6)

**Tab.9** Selected interatomic Tl-Cl distances for the coordination environment of Tl(I)

Tl- Cl	d/pm	Equivalent distances
Tl(1)-Cl(3)	330.8(16)	1x
Tl(1)-Cl(1)	335.2(7)	2x
Tl(1)-Cl(2)	344.2(11)	1x
Tl(1)-Cl(1)'	344.7(7)	2x
Tl(1)-Cl(2)'	386.2(5)	2x
Tl(1)-Cl(1)'	391.3(7)	2x

2.1.2.1.3 InAlCl<sub>4</sub>**Fig.18** Structural unit of InAlCl<sub>4</sub>

The analogy continues in the distorted “baryte” type with InAlCl<sub>4</sub>. Indium tetrachloridoaluminate crystallizes isotypic with TlAlCl<sub>4</sub>, and the symmetry of the tetrachloridoaluminate tetrahedron (fig.18) is

confirmed by the interatomic bond lengths and angles presented in the tables below.

**Tab.10** Selected distances and angles in the tetrachloridoaluminate tetrahedron of InAlCl<sub>4</sub>

Distance	d/pm		Angle	/°	
Al(1)-Cl(1)	211.9(3)	1x	Cl(3)-Al(1)-Cl(1)	112.59(16)	1x
Al(1)-Cl(2)	212.56(17)	2x	Cl(3)-Al(1)-Cl(2)	109.58(10)	2x
Al(1)-Cl(3)	210.8(3)	1x	Cl(1)-Al(1)-Cl(2)	108.58(9)	2x
			Cl(2)-Al(1)-Cl(2)′	107.81(12)	1x

**Tab.11** Atomic coordinates and equivalent isotropic displacement parameters(Å<sup>2</sup>) for InAlCl<sub>4</sub>

Atom	x/a	y/b	z/c	S.O.F.	U(eq)
In(1)	0.3145(1)	1/4	0.6858(1)	1.0000	0.120(1)
Al(1)	0.5673(2)	0.7500	0.8111(2)	1.0000	0.048(1)
Cl(1)	0.7228(3)	0.7500	0.9474(3)	1.0000	0.095(1)
Cl(2)	0.5750(2)	0.9936(2)	0.6763(2)	1.0000	0.078(1)
Cl(3)	0.4017(3)	0.7500	0.9276(4)	1.0000	0.123(1)

**Tab.12** Selected interatomic In-Cl distances in the coordination environment of In(I)

In-Cl	d/pm	Equivalent distances
In(1)-Cl(2)	337.6(2)	2x
In(1)-Cl(2)′	343.0(2)	2x
In(1)-Cl(1)	342.4(3)	1x
In(1)-Cl(1)′	386.8(1)	2x
In(1)-Cl(3)	336.4(4)	1x
In(1)-Cl(2)′′	395.8(2)	2x

### 2.1.2.1.4 [NH<sub>4</sub>]GaCl<sub>4</sub>

[NH<sub>4</sub>]GaCl<sub>4</sub> crystallizes in the *P n m a* (no.62) space group, isotypic with the other three compounds presented above (TlAlCl<sub>4</sub>, TlGaCl<sub>4</sub> and InAlCl<sub>4</sub>).

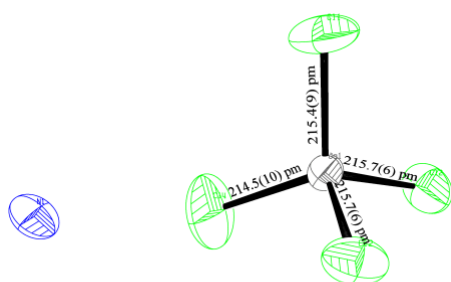


**Fig.19** Structural unit of NH<sub>4</sub>GaCl<sub>4</sub>

The tetrachloridogallate tetrahedron does not make exception from the other described compounds of this structural class, showing a slightly distorted symmetry. The mean Ga-Cl distance amounts to 215 pm, and the deviations

are in the 0.9-1.2 pm range; the tetrahedral angles vary from 107° to 113° (for selected interatomic distances and angles see table 14).

**Tab.13** Crystallographic and refinement data for [NH<sub>4</sub>]GaCl<sub>4</sub>

Empirical formula	<b>NH<sub>4</sub>GaCl<sub>4</sub></b>
Formula weight /amu	228.55
Crystal system	orthorhombic
Space group(no.)	<i>Pnma</i> (no.62)
Unit cell dimensions /pm	<i>a</i> = 1098.(3) <i>b</i> = 701.(2) <i>c</i> = 931.(2)
<i>V</i> /Å <sup>3</sup>	717(3) 2.118
$\rho_{xray}$ /g·cm <sup>-3</sup>	2.128
<i>Z</i>	4
Theta range	2.87° ≤ $\theta$ ≤ 24.99°
Temperature	293.(2) K
F(000)	436
Absorption correction	numerical Bruker SADABS
Absorption coefficient /mm <sup>-1</sup>	5.210
Structure solution /refinement	Direct methods, SHELXS/XL-97
Data/restraints/parameters	661 / 0 / 35
N( <i>hkl</i> )	3478
N'( <i>hkl</i> ) unique with <i>I</i> > 2σ( <i>I</i> )	661
R <sub>int</sub>	0.0730
R <sub>1</sub> ( <i>I</i> > 2σ); wR <sub>2</sub> ( <i>I</i> > 2σ)	0.0791; 0.1781
R <sub>1</sub> (all); wR <sub>2</sub> (all)	0.1227; 0.2231
Goof	1.175
Extinction coefficient	0.015(5)
$\Delta F_{max}$ ; $\Delta F_{min}$ /e · Å <sup>-3</sup>	1.061; -1.517
XRD measuring unit	Bruker AXS Smart CCD 1000

The interatomic distances compare well with the ones found for RbGaCl<sub>4</sub> [11], CsGaCl<sub>4</sub> [11] and TlGaCl<sub>4</sub> [12], which also crystallize in the “baryte” crystallographic type of

structure. The Ga-Cl distances in  $[\text{NH}_4]\text{GaCl}_4$  are slightly shorter than the ones observed by  $\text{LiGaCl}_4$  [13] and  $\text{KGaCl}_4$  [14], which crystallize in different structural types. The coordination of chlorine atoms around the ammonium cation have the same geometry, namely the fourfold capped distorted octahedron (C.N. = 6+4), already described for  $\text{TlAlCl}_4$ .

**Tab.14** Selected distances and angles for  $[\text{GaCl}_4]^-$  tetrahedral unit of  $[\text{NH}_4]\text{GaCl}_4$

Distance	d/pm		Angle	$^\circ$	
Ga(1)-Cl(4)	214.5(10)	1x	Cl(4)-Ga(1)-Cl(1)	113.4(3)	1x
Ga(1)-Cl(1)	215.4(9)	1x	Cl(4)-Ga(1)-Cl(2)	109.89(1)	2x
Ga(1)-Cl(2)	215.7(6)	2x	Cl(1)-Ga(1)-Cl(2)	108.4(1)	2x
			Cl(2)-Ga(1)-Cl(2)	106.6(2)	1x

**Tab.15** Selected N-Cl distances

N-Cl	d/pm	Equivalent distances
N(1)-Cl(4)	330.0(20)	1x
N(1)-Cl(2)	337.0(2)	2x
N(1)-Cl(2)'	347.0(2)	2x
N(1)-Cl(1)	350.0(2)	1x
N(1)-Cl(1)'	384.0(1)	2x
N(1)-Cl(4)'	387.0(2)	2x

**Tab.16** Atomic coordinates and equivalent isotropic displacement parameters ( $\text{\AA}^2$ ) for  $[\text{NH}_4]\text{GaCl}_4$

Atom	x/a	y/b	z/c	S.O.F.	$U_{eq}$
Ga(1)	0.06625	$1/4$	0.31180	0.50000	0.03548
Cl(2)	0.07659	0.00338	0.17379	1.00000	0.06666
Cl(1)	0.22304	$1/4$	0.45086	0.50000	0.08450
Cl(4)	-0.10363	$1/4$	0.42565	0.50000	0.11444
N(1)	-0.31595	$1/4$	0.67606	0.50000	0.06727

### 2.1.2.2 XRD-powder diffraction

In all analyzed samples a strong diffused scattering was observed (the background of the presented spectra was smoothed via software processing), which can be attributed to a glass phase, which accompanies the crystalline phase, in a relatively high quantity, or to absorption processes. All the products were confirmed by powder patterns, sign of a nearly complete conversion of the reaction. By  $TiAlCl_4$  and  $TiGaCl_4$  systems, no educt peaks were found; for  $[NH_4]GaCl_4$  were observed a few peaks, which do not match the simulated powder pattern. A part of these peaks could be attributed to boron oxide and silicon oxide (from the glass ampoule), however not all the other “foreign” peaks could be assigned. The foreign peaks belong either to a different modification of the main compound, to an unknown structural modification of the reagents, or to an unknown compound.

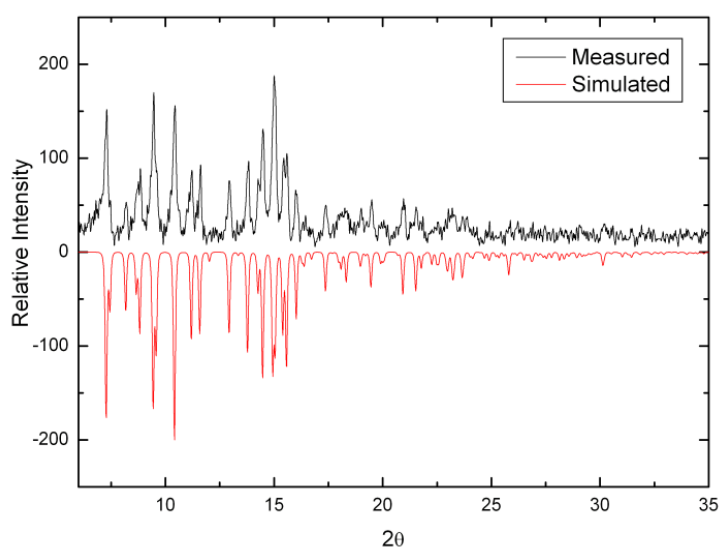


**Fig.20** XRD-Powder pattern of  $TiAlCl_4$   
(measured on a Huber G670 diffractometer/ $MoK\alpha$  radiation)

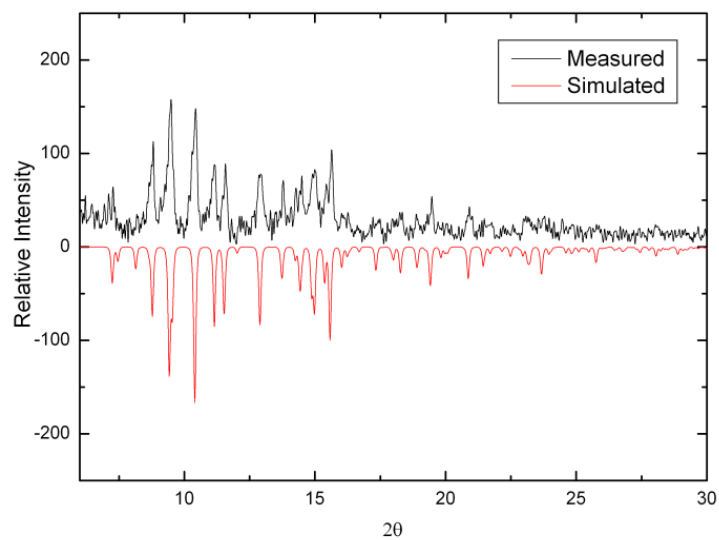


**Fig.21** XRD-Powder pattern of TiGaCl<sub>4</sub>  
(measured on a Huber G670 diffractometer/MoK $\alpha$  radiation)

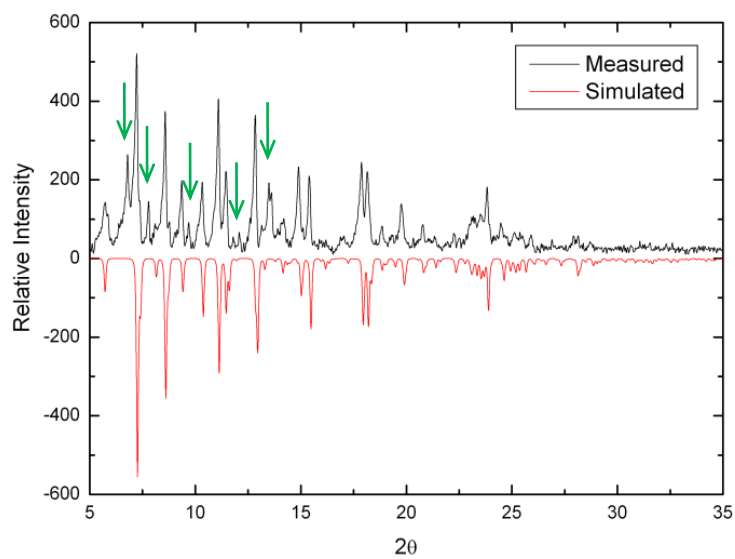


**Fig.22** XRD-Powder pattern of [NH<sub>4</sub>]<sup>+</sup>GaCl<sub>4</sub><sup>-</sup>  
(green arrows show the byproduct/s peaks)  
(measured on a Huber G670 diffractometer/MoK $\alpha$  radiation)

## 2.2 $M^I M^{III} X_4$ salts crystallizing in the $P 2_1 / c$ space group

Thallium(I) tetraiodidoaluminate, thallium(I) tetrabromidogallate, thallium(I) tetraiodidogallate, caesium tetraiodidoaluminate and caesium tetraiodidogallate crystallize in the space group  $P 2_1 / c$ . This space group is less common for the tetrahalogenidoaluminates as for tetrahalogenidogallates (table 1, table 2). For the tetraiodidoaluminates two exceptions are known to date [15][16], which do not crystallize in this structural type.

### 2.2.1 Preparation

The reactions were carried out in sealed and evacuated borosilicate glass ampoules.

$TlAlI_4$  was prepared by mixing  $TlI$  and  $AlI_3$  in a 1:1 molar ratio (0.733 mmol); the mixture was sealed in a glass ampoule and heated with  $30^\circ\text{C}/\text{h}$  to  $200^\circ\text{C}$  (annealed at this temperature for 24 h); the probe was cooled to  $25^\circ\text{C}$  with a rate of  $10^\circ\text{C}/\text{h}$ .

$TlGaBr_4$  was prepared in a glass ampoule from the mixture of  $TlBr$  and  $GaBr_3$  in a 1:1 molar ratio (0.527 mmol). The ampoule was heated with  $10^\circ\text{C}/\text{h}$  to  $200^\circ\text{C}$ , annealed at this temperature for 96 h, and then cooled to room temperature with  $2^\circ\text{C}/\text{h}$ .

$TlGaI_4$  was obtained from  $TlI$  and  $GaI_3$  in a 1:1 molar ratio (0.453 mmol), in a sealed glass ampoule. The probe was heated with  $10^\circ\text{C}/\text{h}$  to  $250^\circ\text{C}$ , annealed for 96 h at this temperature, and cooled with  $2^\circ\text{C}/\text{h}$  to room temperature.

$CsAlI_4$  and  $CsGaI_4$  were obtained as follows:  $CsI$  and  $AlI_3$  in a 1:1 molar ratio (0.368 mmol), respectively  $CsI$  and  $GaI_3$  in a 1:1 molar ratio (0.368 mmol) were mixed, sealed in glass ampoules, and heated with  $10^\circ\text{C}/\text{h}$  to  $250^\circ\text{C}$ . After annealing at this temperature for 120 h, the probes were cooled to room temperature with a rate of  $2^\circ\text{C}/\text{h}$ .

All products are colourless, and irregularly shaped crystals were observed under the microscope. A second phase with glass-like appearance was observed in all these reactions. The crystals were isolated under inert atmosphere, mounted in glass capillaries, and measured at room temperature.

## 2.2.2 Structural aspects

### 2.2.2.1 Crystal structure of TlAlI<sub>4</sub>, TlGaI<sub>4</sub>, CsAlI<sub>4</sub>, CsGaI<sub>4</sub> and TlGaBr<sub>4</sub>

TlAlI<sub>4</sub> and TlGaI<sub>4</sub> crystallize isotypic in a distorted LiAlCl<sub>4</sub> type of structure: monoclinic space group  $P 2_1 / c$  (no.14), with four formula units in the unit cell ( $a = 822.5(9)$  pm,  $b = 784.4(7)$  pm,  $c = 1597.3(16)$  pm,  $\beta = 96.02(2)^\circ$ ;  $V = 1024.8(18) \cdot 10^6$  pm<sup>3</sup> for TlAlI<sub>4</sub>, and  $a = 813.52(6)$  pm,  $b = 777.29(5)$  pm,  $c = 1592.04(9)$  pm,  $\beta = 96.06^\circ$ ;  $V = 713.9(6) \cdot 10^6$  pm<sup>3</sup> for TlGaI<sub>4</sub>). The asymmetric unit of TlAlI<sub>4</sub> and TlGaI<sub>4</sub> contains one crystallographically independent Tl(I) cation, one M(III) cation (M = Al, Ga) and four I<sup>-</sup> anions.

CsAlI<sub>4</sub> and CsGaI<sub>4</sub> crystallize in the  $P 2_1 / c$  (no.14) space group, with four formula units in the unit cell ( $a = 729.61(5)$  pm,  $b = 1854.32(9)$  pm,  $c = 836.77(5)$  pm,  $\beta = 107.076(7)^\circ$ ,  $V = 1082.18(11) \cdot 10^6$  pm<sup>3</sup> for CsAlI<sub>4</sub>, and  $a = 724.13(6)$  pm,  $b = 1842.25(10)$  pm,  $c = 833.07(6)$  pm,  $\beta = 107.011(9)^\circ$ ,  $V = 1062.72(13) \cdot 10^6$  pm<sup>3</sup> for CsGaI<sub>4</sub>). The asymmetric units of both CsAlI<sub>4</sub> and CsGaI<sub>4</sub> contain one crystallographically independent Cs<sup>+</sup> cation, one M(III) cation and four I<sup>-</sup> anions.

TlGaBr<sub>4</sub> adopts an own structural type. It crystallizes in the space group  $P 2_1 / c$  (no.14), with **eight** formula units in the unit cell ( $a = 1229.49(10)$  pm,  $b = 1105.66(10)$  pm,  $c = 12.6512(11)$ ,  $\beta = 107.943(10)^\circ$ ;  $V = 1636.2(2) \cdot 10^6$  pm<sup>3</sup>), while its asymmetric unit contains two symmetrically independent Tl(I) cations, two independent Ga(III) cations and eight Br<sup>-</sup> anions.

2.2.2.1.1 TlAlI<sub>4</sub> and TlGaI<sub>4</sub>**Tab.17** Crystallographic and refinement data for TlAlI<sub>4</sub> and TlGaI<sub>4</sub>

Empirical formula	TlAlI <sub>4</sub>	TlGaI <sub>4</sub>
Formula weight /amu	738.95	781.69
Crystal system	monoclinic	monoclinic
Space group (no.)	<i>P</i> 2 <sub>1</sub> / <i>c</i> (no. 14)	<i>P</i> 2 <sub>1</sub> / <i>c</i> (no. 14)
Unit cell dimensions /pm	<i>a</i> = 822.5(9) <i>b</i> = 784.4(7) <i>c</i> = 1597.3(16) ; β = 96.02(2)°	<i>a</i> = 813.52(6) <i>b</i> = 777.29(5) <i>c</i> = 1592.04(9) ; β = 96.06°
<i>V</i> /Å <sup>3</sup>	1024.8(18)	1001.10(11)
ρ <sub>xray</sub> /g · cm <sup>-3</sup>	4.789	5.186
<i>Z</i>	4	4
Theta range	2.49° ≤ θ ≤ 25°	2.57° ≤ θ ≤ 25.10°
Temperature	T = 298.(2) K	T = 298.(2) K
F(000)	1224	1296
Absorption correction	numerical Bruker SADABS	semiempirical Oxford CRYSLIS RED
Absorption coefficient /mm <sup>-1</sup>	27.809	31.014
Structure solution /refinement	Direct methods, SIR-92/ SHELXL-97	Direct methods, SIR-92/ SHELXL-97
Data/restraints/parameters	1736 / 0 / 56	7924 / 0/1778
N( <i>hkl</i> )	2606	7924
N'( <i>hkl</i> ) unique with I > 2σ(I)	1736	1778
R <sub>int</sub>	0.1445	0.1000
R <sub>1</sub> (I>2σ); wR <sub>2</sub> (I>2σ)	0.1080; 0.2640	0.0500; 0.1118
R <sub>1</sub> (all); wR <sub>2</sub> (all)	0.2293; 0.3357	0.1008; 0.1781
GooF	0.891	0.855
Extinction coefficient	0.0118(16)	0.0118(16)
ΔF <sub>max</sub> ; ΔF <sub>min</sub> /e · Å <sup>-3</sup>	2.880; -1.972	2.369; -2.272
XRD measuring unit	Bruker AXS Smart CCD 1000	Oxford Excalibur II CCD Sapphire

The [AlI<sub>4</sub>]<sup>-</sup> and [GaI<sub>4</sub>]<sup>-</sup> tetrahedra come close to the ideal T<sub>d</sub> symmetry (fig.23 and fig.24). The Al-I, respectively Ga-I lengths vary in the range of 0.48-1.03 pm (for Ga-I), and 1.65-5.97 pm (for Al-I) range. Both compounds crystallize in the LiAlCl<sub>4</sub> type of structure. The coordination polyhedron around Tl(I) is strongly distorted.

There are no known to date crystal structures of analogous alkali metallates RbAlI<sub>4</sub> and RbGaI<sub>4</sub>, and thus no structural comparison can be made.

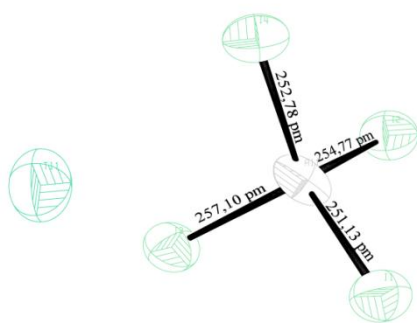


**Fig.23** Structural unit of  $TlAlI_4$

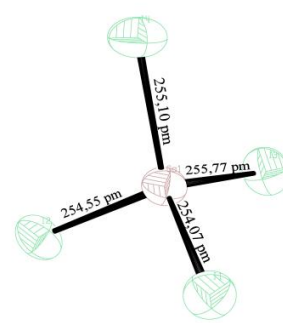


**Fig.24** Structural unit of  $TlGaI_4$

**Tab.18** Distances and angles for  $[AlI_4]^-$  unit

Al-I	d/ pm	I-Al-I	$^\circ$
Al-I(1)	251.0(16)	I(1)-Al(1)-I(4)	110.02
Al-I(2)	254.5(17)	I(1)-Al(1)-I(2)	113.80
Al-I(3)	257.3(18)	I(4)-Al(1)-I(2)	108.15
Al-I(4)	252.9(17)	I(1)-Al(1)-I(3)	108.73
		I(4)-Al(1)-I(3)	108.82
		I(2)-Al(1)-I(3)	107.20

**Tab.19** Distances and angles for  $[GaI_4]^-$  unit

Ga-I	d/ pm	I-Ga-I	$^\circ$
Ga-I(1)	254.0(3)	I(1)-Ga(1)-I(4)	108.66(12)
Ga-I(2)	254.5(3)	I(1)-Ga(1)-I(2)	108.44(12)
Ga-I(3)	255.7(4)	I(4)-Ga(1)-I(2)	109.80(13)
Ga-I(4)	255.1(3)	I(1)-Ga(1)-I(3)	113.46(13)
		I(4)-Ga(1)-I(3)	108.50(12)
		I(2)-Ga(1)-I(3)	107.96(13)

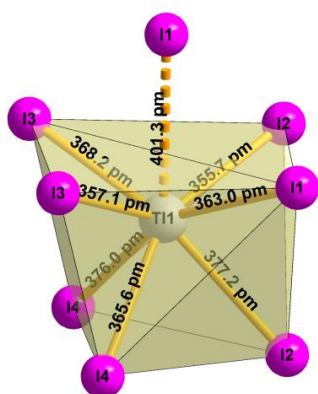


**Fig.25** Coordination surrounding for Tl(I) in  $TlAlI_4$

The coordination polyhedron of  $Li^+$  in the  $LiAlCl_4$  crystallographic type of structure [17] has been described as a distorted octahedron; two of these octahedra are edge-linked, and alternate in the crystal lattice, connecting further through vertices with other four identical entities. Returning to  $TlAlI_4$ , no recognizable regular polyhedron (fig.25) could be observed for the coordination environment (C.N. = 8); nevertheless the edge-linked two-polyhedral assembly is similar to the case of  $LiAlCl_4$ . The following figures present the translation of the coordination polyhedron items and anionic tetrahedra, first through the unit cell (fig. 26), and then a projection through crystallographic axis b (fig.27).

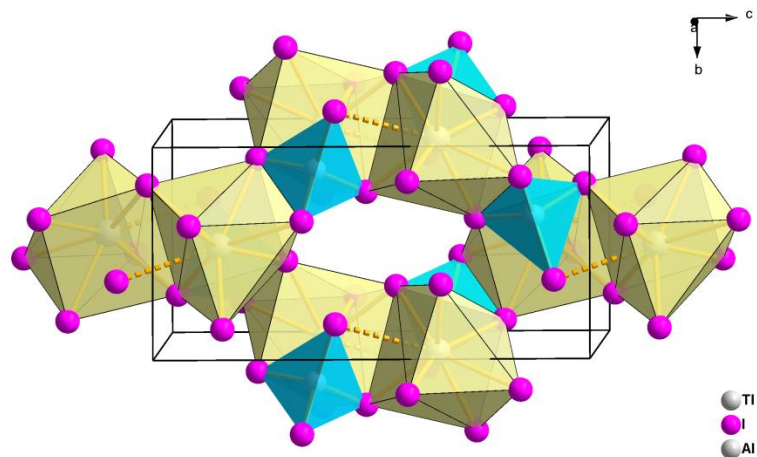


**Fig.26** Unit cell of TlAlI<sub>4</sub>- view along axis a

**Tab.20** Atomic coordinates and equivalent isotropic displacement parameters ( $\text{\AA}^2$ ) for TlAlI<sub>4</sub>

Atom	x/a	y/b	z/c	S.O.F.	$U_{eq}$
Tl(1)	1.7445(4)	-1.0006(5)	0.6382(2)	1.0000	0.098(1)
Al(1)	1.2440(20)	-1.1400(20)	0.6401(11)	1.0000	0.063(5)
I(1)	1.1419(6)	-0.8527(6)	0.5892(3)	1.0000	0.074(2)
I(2)	1.0178(6)	-1.3530(6)	0.6600(3)	1.0000	0.081(2)
I(3)	1.4183(6)	-1.2675(7)	0.5309(3)	1.0000	0.082(2)
I(4)	1.4205(6)	-1.1099(6)	0.7788(2)	1.0000	0.076(2)

**Tab.21** Atomic coordinates and equivalent isotropic displacement parameters ( $\text{\AA}^2$ ) for TlGaI<sub>4</sub>

Atom	x/a	y/b	z/c	S.O.F.	$U_{eq}$
Tl(1)	0.25705	-0.00117	0.86139	1.0000	0.08164
Ga(1)	0.75595	0.14211	0.86073	1.0000	0.04685
I(1)	0.85899	-0.15230	0.91174	1.0000	0.05804
I(2)	0.57977	0.10532	0.71998	1.0000	0.05951
I(3)	0.98864	0.35454	0.84051	1.0000	0.06602
I(4)	0.58133	0.26901	0.96948	1.0000	0.06680

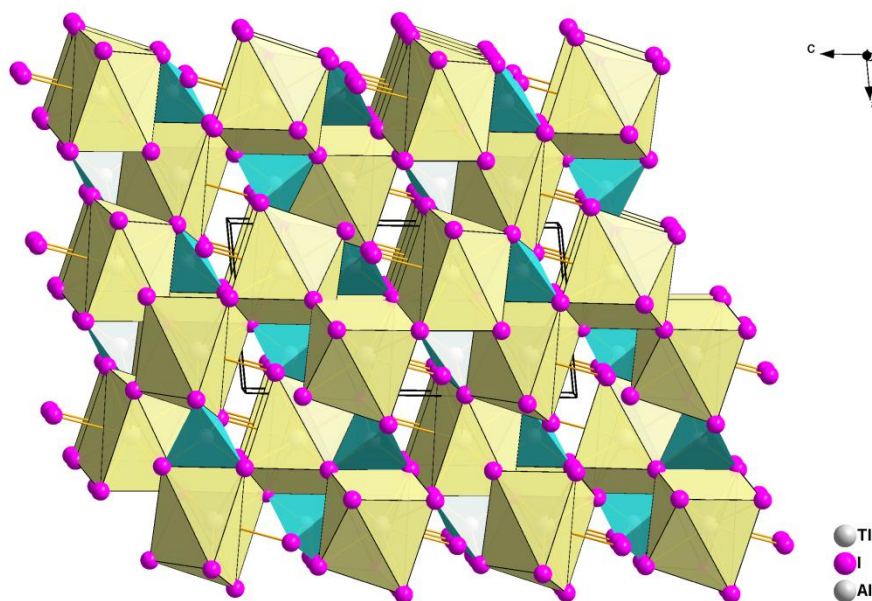


**Fig.27** Crystal structure of  $\text{TlAlI}_4$  - projection along the b axis

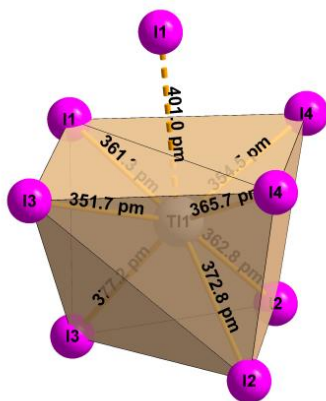
**Tab.22** Selected Tl-I distances for  $\text{TlAlI}_4$

Tl-I	d/pm	Equivalent distances
Tl(1)-I(1)	401.3(7)	1x
Tl(1)-I(2)	377.2(6)	1x
Tl(1)-I(3)	357.1(6)	1x
Tl(1)-I(1)'	363.0(7)	1x
Tl(1)-I(4)	365.6(6)	1x
Tl(1)-I(3)'	368.2(6)	1x
Tl(1)-I(4)'	376.0(6)	1x
Tl(1)-I(2)'	355.7(7)	1x

**Tab.23** Selected Tl-I distances for  $\text{TlGaI}_4$

Tl-I	d/pm	Equivalent distances
Tl(1)-I(1)	401.0(2)	1x
Tl(1)-I(1)'	361.3(2)	1x
Tl(1)-I(3)	351.7(3)	1x
Tl(1)-I(3)'	377.2(2)	1x
Tl(1)-I(4)	354.5(2)	1x
Tl(1)-I(4)'	365.6(2)	1x
Tl(1)-I(2)	372.7(2)	1x
Tl(1)-I(2)'	362.7(2)	1x

The coordination environment around the thallium ion in the case of  $\text{TlGaI}_4$  (fig.28) is identical to  $\text{TlAlI}_4$ , a monocapped irregular polyhedron (C.N.=8). As it can be seen in table 22, respectively 23, the Tl-I distances vary, for the case of both compounds, almost in the same length range.

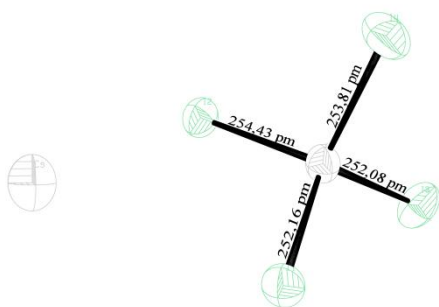
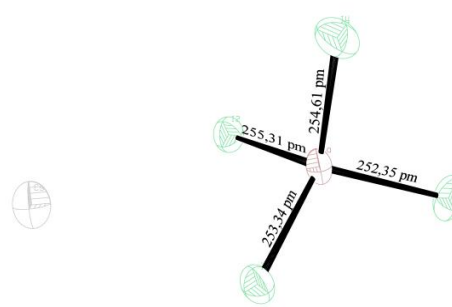


**Fig.28** Coordination of iodine around thallium in  $\text{TlGaI}_4$

2.2.2.1.2 CsAlI<sub>4</sub> and CsGaI<sub>4</sub>**Tab.24** Crystallographic and refinement data for CsAlI<sub>4</sub> and CsGaI<sub>4</sub>

Empirical formula	CsAlI <sub>4</sub>	CsGaI <sub>4</sub>
Formula weight /amu	667.49	710.23
Crystal system	monoclinic	monoclinic
Space group (no.)	<i>P2<sub>1</sub>/c</i> (no.14)	<i>P2<sub>1</sub>/c</i> (no.14)
Unit cell dimensions /pm	<i>a</i> = 729.61(5) <i>b</i> = 1854.32(9) <i>c</i> = 836.77(5); $\beta$ = 107.076(7)°	<i>a</i> = 724.13 <i>b</i> = 1842.25(10) <i>c</i> = 833.07(6); $\beta$ = 107.011(9)°
<i>V</i> /Å <sup>3</sup>	1082.18(11)	1062.72(13)
$\rho_{xray}$ /g · cm <sup>-3</sup>	4.097	4.439
<i>Z</i>	4	4
Theta range	2.77° ≤ $\theta$ ≤ 27.59°	3.14° ≤ $\theta$ ≤ 27.71°
Temperature	293(2) K	293(2)K
F(000)	1120	1192
Absorption correction	semiempirical Oxford CRYCALIS RED	semiempirical Oxford CRYCALIS RED
Absorption coefficient /mm <sup>-1</sup>	14.833	17.502
Structure solution /refinement	Direct methods, SIR-92/ SHELXL-97	Direct methods, SIR-92/ SHELXL-97
Data/restraints/parameters	2514 / 0 / 55	2470 / 0 / 55
<i>N</i> ( <i>hkl</i> )	7822	7039
<i>N'</i> ( <i>hkl</i> ) unique with <i>I</i> > 2σ( <i>I</i> )	2514	2470
<i>R</i> <sub>int</sub>	0.0312	0.0329
<i>R</i> <sub>1</sub> ( <i>I</i> > 2σ); <i>wR</i> <sub>2</sub> ( <i>I</i> > 2σ)	0.0268; 0.0508	0.0475, 0.1281
<i>R</i> <sub>1</sub> (all); <i>wR</i> <sub>2</sub> (all)	0.0650; 0.0679	0.0775, 0.1348
GooF	0.899	0.951
Extinction coefficient	-	-
$\Delta F_{max}$ ; $\Delta F_{min}$ /e · Å <sup>-3</sup>	1.245; -0.807	2.403; -2.096
XRD measuring unit	Oxford Excalibur II CCD Sapphire	Oxford Excalibur II CCD Sapphire

Like for all the previously mentioned compounds, the tetraiodidoaluminate (fig.29) and tetraiodidogallate (fig.30) tetrahedra show high, almost undistorted, tetrahedral symmetry; the bond lengths differences are in the 0.99-2.96 pm range for [AlI<sub>4</sub>]<sup>-</sup> unit (tab.25), and in the 0.08-2.35 pm range for [GaI<sub>4</sub>]<sup>-</sup> unit (tab.26).

**Fig.29** Structural unit of CsAlI<sub>4</sub>**Fig.30** Structural unit of CsGaI<sub>4</sub>

**Tab.25** Distances and angles for  $[\text{AlI}_4]^-$  unit

Al-I	d/ pm	I-Al-I	$^\circ$
Al-I(1)	252.1(3)	I(1)-Al(1)-I(4)	109.01
Al-I(2)	254.4(2)	I(1)-Al(1)-I(2)	109.21
Al-I(3)	252.1(2)	I(4)-Al(1)-I(2)	108.22
Al-I(4)	253.8(3)	I(1)-Al(1)-I(3)	113.11
		I(4)-Al(1)-I(3)	108.51
		I(2)-Al(1)-I(3)	108.67

**Tab.26** Distances and angles for  $[\text{GaI}_4]^-$  unit

Ga-I	d/ pm	I-Ga-I	$^\circ$
Ga-I(1)	253.3(1)	I(1)-Ga(1)-I(4)	109.32
Ga-I(2)	255.3(1)	I(1)-Ga(1)-I(2)	109.19
Ga-I(3)	252.3(1)	I(4)-Ga(1)-I(2)	108.20
Ga-I(4)	254.6(2)	I(1)-Ga(1)-I(3)	112.78
		I(4)-Ga(1)-I(3)	108.62
		I(2)-Ga(1)-I(3)	108.63

**Tab.27** Atomic coordinates and equivalent isotropic displacement parameters ( $\text{\AA}^2$ ) for  $\text{CsAlI}_4$ 

Atom	x/a	y/b	z/c	S.O.F.	$U_{eq}$
Cs(1)	0.18216	0.63161	0.29413	1.0000	0.06343
Al(1)	0.19351	0.37230	0.29604	1.0000	0.03838
I(1)	0.27851	0.44543	0.07383	1.0000	0.04532
I(2)	0.27214	0.44497	0.56561	1.0000	0.04647
I(3)	0.37114	0.25405	0.35451	1.0000	0.05760
I(4)	-0.16392	0.34657	0.20411	1.0000	0.06076

**Tab.28** Atomic coordinates and equivalent isotropic displacement parameters ( $\text{\AA}^2$ ) for  $\text{CsGaI}_4$ 

Atom	x/a	y/b	z/c	S.O.F.	$U_{eq}$
Cs(1)	0.18130	0.63216	0.29544	1.0000	0.05597
Ga(1)	0.19315	0.37252	0.29622	1.0000	0.03289
I(1)	0.27993	0.44627	0.07196	1.0000	0.03839
I(2)	0.27361	0.44580	0.56806	1.0000	0.03975
I(3)	0.36855	0.25262	0.35477	1.0000	0.05190
I(4)	-0.16863	0.34784	0.20293	1.0000	0.05270

The structural difference between  $\text{TlAlI}_4/\text{TlGaI}_4$  and  $\text{CsAlI}_4/\text{CsGaI}_4$  is that the coordination polyhedron around  $\text{Cs}^+$  is double capped (fig.31 and fig.32), whereas the coordination polyhedron for  $\text{Tl}^{+1}$  is monocapped (in the case of  $\text{TlAlI}_4$  and  $\text{TlGaI}_4$ ). For  $\text{LiAlCl}_4$ , the crystal structure shows two edge-linked octahedra, which repeat in three dimensions, connected through common vertices with other identical units. In the case of caesium tetraiodidoaluminate and caesium tetraiodidogallate each coordination polyhedron connects with the other three neighboring polyhedra through three edges. The structural differences between the above named compounds can be attributed to the larger volume of caesium, compared to thallium ( $R_{\text{vdW}}^{\text{Cs}} = 2.9 \text{ \AA} > R_{\text{vdW}}^{\text{Tl}} = 2.0 \text{ \AA}$ , whereby  $R_{\text{vdW}} = \text{van der Waals radius}$ ) [7], from which the increased coordination number for caesium compared to the coordination number for thallium ( $\text{C.N.}_{\text{Cs}} = 9 > \text{C.N.}_{\text{Tl}} = 8$ ).

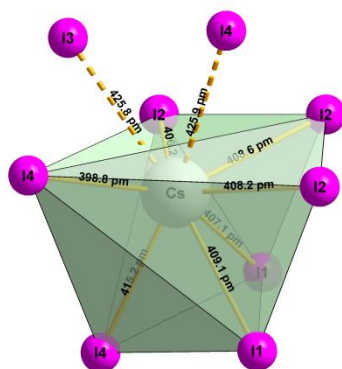


**Fig.31** Coordination around Cs in  $\text{CsAlI}_4$

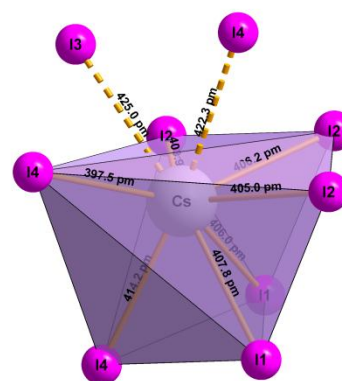


**Fig.32** Coordination around Cs in  $\text{CsGaI}_4$

**Tab.29** Selected Cs-I distances for  $\text{CsAlI}_4$

Cs-I	d/pm	Equivalent distances
Cs(1)-I(1)	407.09(7)	1x
Cs(1)-I(2)	406.23(10)	1x
Cs(1)-I(3)	425.84(10)	1x
Cs(1)-I(1')	409.15(9)	1x
Cs(1)-I(4)	415.2(1)	1x
Cs(1)-I(2')	408.24(9)	1x
Cs(1)-I(4')	398.84(7)	1x
Cs(1)-I(2'')	408.6(1)	1x
Cs(1)-I(4'')	425.9(1)	1x

**Tab.30** Selected Cs-I distances for  $\text{CsGaI}_4$

Cs-I	d/pm	Equivalent distances
Cs(1)-I(1)	407.8(1)	1x
Cs(1)-I(1')	406.0(1)	1x
Cs(1)-I(3)	425.03(15)	1x
Cs(1)-I(2)	405.0(1)	1x
Cs(1)-I(4)	397.46(14)	1x
Cs(1)-I(4')	414.23(12)	1x
Cs(1)-I(2')	406.24(12)	1x
Cs(1)-I(2'')	403.85(14)	1x
Cs(1)-I(4'')	422.3(1)	1x

Since the structures of  $\text{CsAlI}_4$  and  $\text{CsGaI}_4$  are isotypic, only representations for  $\text{CsAlI}_4$  are presented. Figure 33 shows the arrangement of coordination polyhedra in the unit cell, while the fig. 34 presents a projection of the structural units along the crystallographic axis  $a$ .

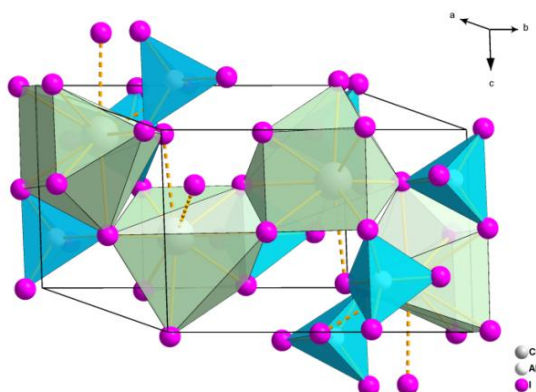


**Fig.33** Unit cell of  $\text{CsAlI}_4$

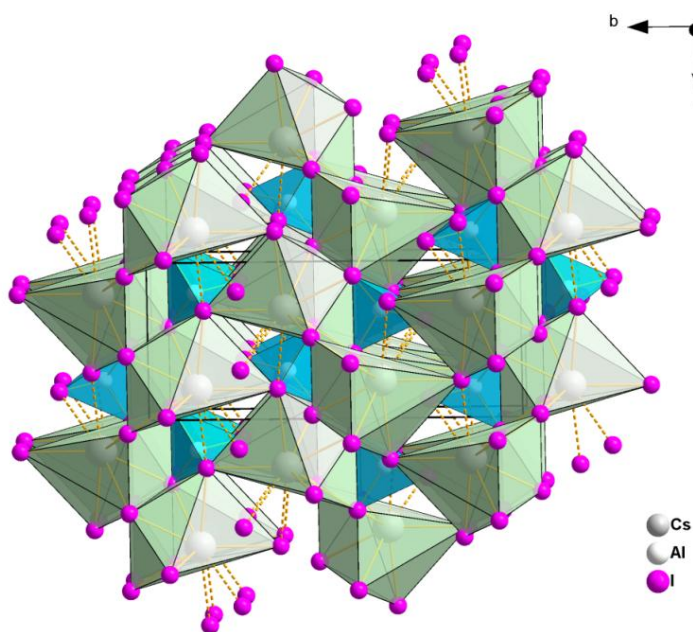


**Fig.34** Crystal structure of  $\text{CsAlI}_4$ -projection along the  $a$  axis

### 2.2.2.1.3 $\text{TlGaBr}_4$

$\text{TlGaBr}_4$  is different from all other discussed compounds. It crystallizes also in the  $P 2_1/c$  space group, but it has a larger unit cell, with eight formula units inside, compared to four formula units per unit cell for the other compounds from this subchapter. In  $\text{TlGaBr}_4$

thallium has two different coordination surroundings.

**Tab.32** Crystallographic and refinement data for TlGaBr<sub>4</sub>

Empirical formula	TlGaBr <sub>4</sub>
Formula weight /amu	593.73
Crystal system	monoclinic
Space group (no.)	<i>P2<sub>1</sub>/c</i> (no. 14)
Unit cell dimensions /pm	<i>a</i> = 1229.49(10) <i>b</i> = 1105.66(10) <i>c</i> = 1265.12(11) ; $\beta$ = 107.943(10)°
<i>V</i> /Å <sup>3</sup>	1636.2(2)
$\rho_{xray}$ /g · cm <sup>-3</sup>	4.821
<i>Z</i>	8
Theta range	3.30° ≤ $\theta$ ≤ 25°
Temperature	T = 298(2)K
F(000)	2016
Absorption correction	semiempirical Oxford CRYSTALIS RED
Absorption coefficient /mm <sup>-1</sup>	42.392
Structure solution /refinement	Direct methods, SHELXS/XL-97
Data/restraints/parameters	2851 / 0 / 110
N( <i>hkl</i> )	7128
N'( <i>hkl</i> ) unique with I > 2σ(I)	2851
R <sub>int</sub>	0.1080
R <sub>1</sub> (I > 2σ); wR <sub>2</sub> (I > 2σ)	0.0391; 0.0656
R <sub>1</sub> (all); wR <sub>2</sub> (all)	0.1648; 0.1158
Goof	0.721
Extinction coefficient	-
$\Delta F_{max}$ ; $\Delta F_{min}$ /e · Å <sup>-3</sup>	1.170; -1.029
XRD measuring unit	Oxford Excalibur II CCD Sapphire

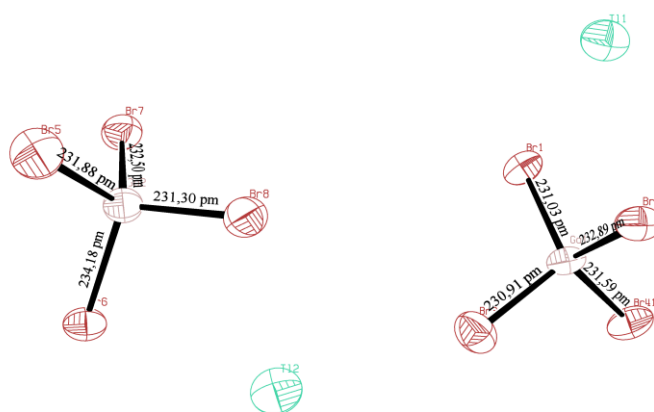


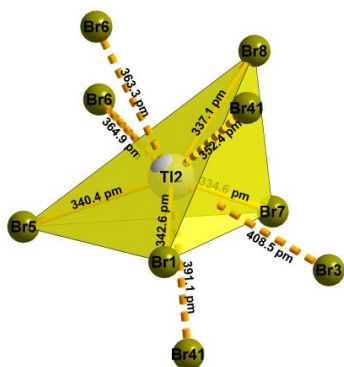
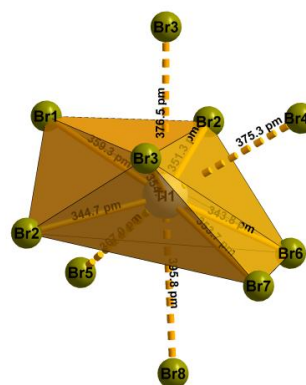
**Fig.35** Formula units of TlGaBr<sub>4</sub>

The tetrabromidogallate tetrahedra are nearly undistorted; the bond length variation lies in the range of 0.09-2.9 pm (tab.33). The average Ga-Br bond length is in accordance with similar compounds, like LiGaBr<sub>4</sub> [18].

**Tab.33** Distances and angles for the  $[\text{GaBr}_4]^-$  units

Ga-Br	d/ pm	Br-Ga-Br	$^\circ$	Ga-Br	d/ pm	Br-Ga-Br	$^\circ$
Ga <sub>(1)</sub> -Br(1)	231.0(4)	Br(3)-Ga <sub>(1)</sub> -Br(1)	111.91(19)	Ga <sub>(2)</sub> -Br(5)	231.9(5)	Br(8)-Ga <sub>(2)</sub> -Br(5)	107.70(19)
Ga <sub>(1)</sub> -Br(2)	232.9(4)	Br(3)-Ga <sub>(1)</sub> -Br(4)	108.26(18)	Ga <sub>(2)</sub> -Br(6)	234.2(5)	Br(8)-Ga <sub>(2)</sub> -Br(7)	113.16(19)
Ga <sub>(1)</sub> -Br(3)	230.9(5)	Br(1)-Ga <sub>(1)</sub> -Br(4)	107.86(16)	Ga <sub>(2)</sub> -Br(7)	232.5(4)	Br(5)-Ga <sub>(2)</sub> -Br(7)	109.72(18)
Ga <sub>(1)</sub> -Br(4)	231.6(4)	Br(3)-Ga <sub>(1)</sub> -Br(2)	107.31(16)	Ga <sub>(2)</sub> -Br(8)	231.3(5)	Br(8)-Ga <sub>(2)</sub> -Br(6)	106.97(18)
		Br(1)-Ga <sub>(1)</sub> -Br(2)	110.35(18)			Br(5)-Ga <sub>(2)</sub> -Br(6)	110.63(18)
		Br(4)-Ga <sub>(1)</sub> -Br(2)	111.16(19)			Br(7)-Ga <sub>(2)</sub> -Br(6)	108.64(17)

The two crystallographically independent Tl(I) cations which are found in the structure of  $\text{TlGaBr}_4$ , have both distorted coordination polyhedra. One polyhedron can be characterized as a distorted triangular anti-prism (fig.37), capped by four additional bromide anions (C.N. = 6+4). The second coordination polyhedron resembles a flattened tetrahedron (fig.36), capped by five extra bromide ions (C.N. = 4+5).

**Fig.36** Coordination around Tl(2) in  $\text{TlGaBr}_4$ **Fig.37** Coordination around Tl(1) in  $\text{TlGaBr}_4$ 

The distorted tetrahedra (fig. 36) are isolated from each other in the lattice, sharing with the other (same polyhedral type) two capping bromines. The distorted triangular anti-prism polyhedra (fig.37) are connected in rows through one bromine ion with other similar anti-prism coordination polyhedral. Along the crystallographic axis  $c$ , these triangular anti-prism coordinating polyhedra are linked in rows under an angle of  $74.3^\circ$  (fig.41). The previously mentioned rows are connected to each other by capping bromines (the connecting capping bromine from one polyhedron is a vertex of the other one). Figure 40 presents the

distorted triangular anti-prism coordination polyhedra, as they reveal a chain-like connection along the crystallographic axis  $c$ .

The two different polyhedral species are connected in the crystal lattice by two vertices and one capping bromine ion.

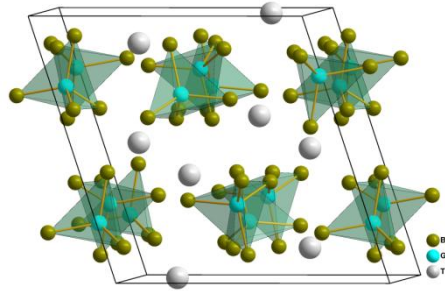


**Fig.38** Unit cell of  $\text{TlGaBr}_4$

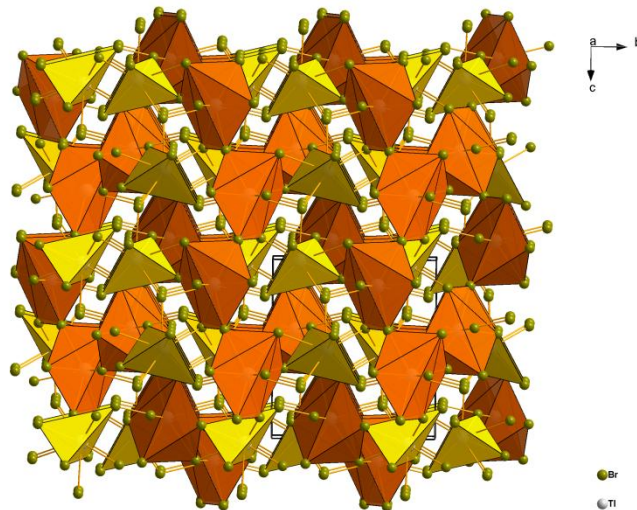


**Fig.39** Coordination polyhedral around thallium in  $\text{TlGaBr}_4$

The view along crystallographic axis  $c$  shows the angle in the anti-prismatic coordination polyhedron rows (fig.41).

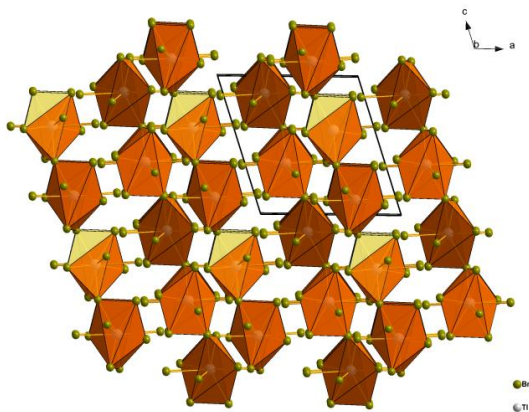


**Fig.40** View along the  $b$  axis for  $\text{TlGaBr}_4$

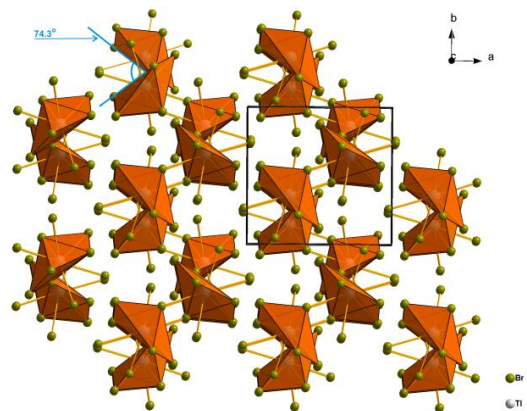


**Fig.41** View along the  $c$  axis for  $\text{TlGaBr}_4$

**Tab.34** Selected Tl-Br distances

<b>Tl(1)-Br</b>	<b>d/pm</b>		<b>Tl(2)-Br</b>	<b>d/pm</b>	
Tl(1)-Br(6)	343.8(22)	1x	Tl(2)-Br(7)	334.6(6)	1x
Tl(1)-Br(2)	344.7(7)	1x	Tl(2)-Br(8)	337.1(11)	1x
Tl(1)-Br(2)′	351.3(7)	1x	Tl(2)-Br(5)	340.4(5)	1x
Tl(1)-Br(7)	353.7(5)	1x	Tl(2)-Br(1)	342.6(12)	1x
Tl(1)-Br(3)	354.1(13)	1x	Tl(2)-Br(4)	352.4(16)	1x
Tl(1)-Br(1)	359.3(4)	1x	Tl(2)-Br(6)	363.3(8)	1x
Tl(1)-Br(5)	367.0(5)	1x	Tl(2)-Br(6)′	364.9(18)	1x
Tl(1)-Br(4)	375.3(5)	1x			
Tl(1)-Br(3)′	376.5(4)	1x			
Tl(1)-Br(8)	395.8(5)	1x			

**Tab.35** Atomic coordinates and equivalent isotropic displacement parameters ( $\text{\AA}^2$ ) for TlGaBr<sub>4</sub>

<b>Atom</b>	<b>x/a</b>	<b>y/b</b>	<b>z/c</b>	<b>S.O.F.</b>	<b>U<sub>eq</sub></b>
Tl(1)	0.2926(1)	0.1424(2)	0.3778(1)	1.0000	0.068(1)
Tl(2)	0.2111(1)	0.8369(2)	0.0154(1)	1.0000	0.074(1)
Ga(1)	0.4802(3)	0.3623(3)	0.2105(2)	1.0000	0.042(1)
Ga(2)	0.0010(3)	0.9221(3)	0.2223(3)	1.0000	0.046(1)
Br(1)	0.4987(3)	0.3786(3)	0.3974(2)	1.0000	0.051(1)
Br(2)	0.3506(3)	0.2100(3)	0.1291(2)	1.0000	0.057(1)
Br(3)	0.4135(3)	0.5392(3)	0.1156(3)	1.0000	0.066(1)
Br(4)	0.6593(3)	0.3219(4)	0.1947(3)	1.0000	0.063(1)
Br(5)	-0.1932(3)	0.9547(4)	0.1873(3)	1.0000	0.077(1)
Br(6)	0.0802(3)	1.0713(3)	0.1369(2)	1.0000	0.048(1)
Br(7)	0.0931(3)	0.9278(3)	0.4126(3)	1.0000	0.058(1)
Br(8)	0.0229(3)	0.7394(3)	0.1420(3)	1.0000	0.072(1)

### 2.2.2.2 XRD-powder diffraction

From the above presented compounds XRD-powder diffractograms were measured for  $\text{TlAlI}_4$ ,  $\text{TlGaBr}_4$  and  $\text{TlGaI}_4$ . Even though in all the cases the diffuse scattering (in the presented XRD powder diffractograms the background was smoothed via software) is observed (caused by the glass phase fraction or absorption phenomena), the low quality of the  $\text{TlGaBr}_4$  XRD-powder diffractogram made the analysis impossible. For  $\text{TlAlI}_4$  and  $\text{TlGaI}_4$  the measured powder patterns match the simulated ones (fig.42 and fig.43). For both compounds there is one relatively intense peak to observe which do not find an analogue one in the simulated diffractogram; however this “foreign” peak probably belongs to a silicon dioxide XRD-powder pattern or to an unknown byproduct XRD pattern.

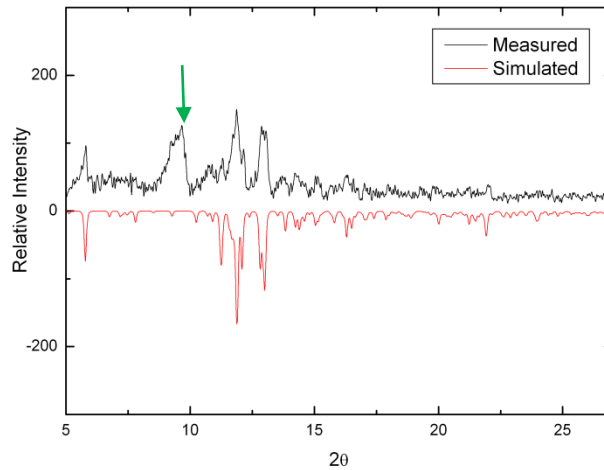


**Fig.42** XRD-Powder pattern of  $\text{TlAlI}_4$

(measured on a Huber G670 diffractometer/ $\text{MoK}\alpha$  radiation)

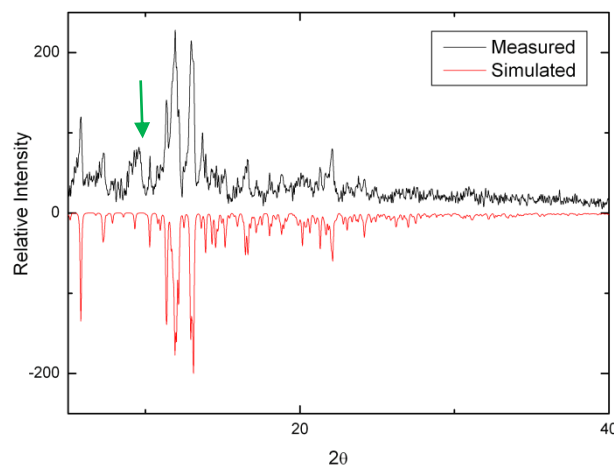


**Fig.43** XRD-Powder pattern of  $\text{TlGaI}_4$

(measured on a Huber G670 diffractometer/ $\text{MoK}\alpha$  radiation)

\*In the **fig.42** and **fig.43** the green arrows represent the byproduct peak

## 2.3 InAlI<sub>4</sub>

Indium tetraiodidoaluminate [16], does not belong to one of the two large classes of crystallization presented above. It crystallizes in the space group  $P 2_1/m$  (no. 11), which is of higher symmetry than  $P 2_1/c$  (no. 14) space group ( $P 2_1/c$  is a crystallographic  $k$  I1b type subgroup of the  $P 2_1/m$  space group) [19]. No other known salt from the analysed ones crystallizes in this space group, therefore indium tetraiodidoaluminate represents an exception.

### 2.3.1 Preparation

InAlI<sub>4</sub> was obtained as follows: 0.150 g (1.306 mmol) In powder, 0.322 g (0.649 mmol) InI<sub>3</sub> and 0.795 g (1.950 mmol) AlI<sub>3</sub> (In:InI<sub>3</sub>:AlI<sub>3</sub> = 2:1:3 molar ratio) were introduced in a borosilicate glass ampoule. The sealed ampoule was placed in a programmable oven and heated with 10°C/h to 250°C, and was held at this temperature for 144 hours. The probe was cooled to room temperature with 5°C/h. Under the microscope transparent, pale yellow, irregularly shaped crystals were observed. Suitable crystals were selected and placed in glass capillaries for XRD single crystal analysis.

### 2.3.2 Structural aspects

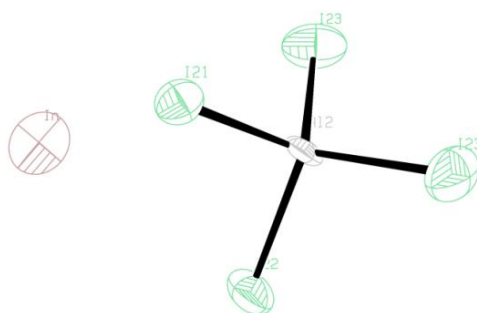
#### 2.3.2.1 Crystal structure of InAlI<sub>4</sub>

InAlI<sub>4</sub> crystallizes in the space group  $P 2_1/m$  (no.11), with four formula units in the unit cell ( $a = 713.5(4)$  pm,  $b = 1182.2(3)$  pm,  $c = 1208.3(6)$  pm,  $\beta = 96.23(6)^\circ$ ;  $V=1013.2(8)\cdot 10^6$  pm<sup>3</sup>). The asymmetric unit of InAlI<sub>4</sub> contains one crystallographically independent In(I) cation, two Al(III) cations and six I<sup>-</sup> anions.

The InAlI<sub>4</sub> structure is dominated by the tetraiodidoaluminate motif. The [AlI<sub>4</sub>]<sup>-</sup> tetrahedra are just slightly distorted from the ideal T<sub>d</sub> symmetry, with deformations in the same range as by the other reported compounds (TlAlI<sub>4</sub>, CsAlI<sub>4</sub>); the bond lengths (tab.37) are comparable with the ones observed by similar salts, such as NaAlI<sub>4</sub> [15].

**Tab.36** Crystallographic and refinement data for InAlI<sub>4</sub>

Empirical formula	InAlI <sub>4</sub>
Formula weight /amu	649,4
Crystal system	monoclinic
Space group (no.)	<i>P</i> 2 <sub>1</sub> / <i>m</i> (no. 11)
Unit cell dimensions /pm	<i>a</i> = 713.5(4) <i>b</i> = 1182.2(3) <i>c</i> = 1208.3(6); $\beta$ = 96.23(6)°
<i>V</i> /Å <sup>3</sup>	1013.2(8)
$\rho_{xray}$ /g · cm <sup>-3</sup>	4.257
<i>Z</i>	4
Theta range	2.42° ≤ $\theta$ ≤ 20.00°
Temperature	293(2)K
F(000)	1096
Absorption correction	numerical Stoe X-SHAPE/ X-RED
Absorption coefficient /mm <sup>-1</sup>	14.520
Structure solution /refinement	Direct methods, SHELXS/XL-97
Data/restraints/parameters	981 / 0 / 60
N( <i>hkl</i> )	3904
N'( <i>hkl</i> ) unique with <i>I</i> > 2σ( <i>I</i> )	981
R <sub>int</sub>	0.3082
R <sub>1</sub> ( <i>I</i> > 2σ); wR <sub>2</sub> ( <i>I</i> > 2σ)	0.0401, 0.0733
R <sub>1</sub> (all); wR <sub>2</sub> (all)	0.2208, 0.1508
Goof	0.457
Extinction coefficient	-
$\Delta F_{max}$ ; $\Delta F_{min}$ /e · Å <sup>-3</sup>	0.838; -1.113
XRD measuring unit	Stoe IPDS

**Fig.44** Formula unit of InAlI<sub>4</sub>

The coordination around indium(I) by iodine atoms can be characterized as a distorted square pyramid (fig.45), which is capped by three additional iodine ions (C.N. = 5+3). Two coordination polyhedra are connected by a common edge; these units connect further through vertices, creating undulated chains along the *b* axis (fig.46).

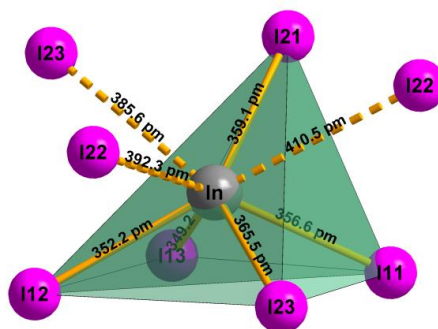


**Fig.45** Coordination environment of In (I) in InAlI<sub>4</sub>

**Tab.37** Distances and angles for the [AlI<sub>4</sub>]<sup>-</sup> units

Al <sub>(1)</sub> -I	d/ pm	I-Al <sub>(1)</sub> -I	/°	Al <sub>(2)</sub> -I	d/ pm	I-Al <sub>(2)</sub> -I	/°
Al <sub>(1)</sub> -I <sub>(11)</sub>	255(3)	I <sub>(11)</sub> -Al <sub>(1)</sub> -I <sub>(12)</sub>	104.9(8)	Al <sub>(2)</sub> -I <sub>(21)</sub>	259(3)	I <sub>(21)</sub> -Al <sub>(2)</sub> -I <sub>(22)</sub>	103.7(8)
Al <sub>(1)</sub> -I <sub>(12)</sub>	258(2)	I <sub>(12)</sub> -Al <sub>(1)</sub> -I <sub>(13)</sub>	109.9(1)	Al <sub>(2)</sub> -I <sub>(22)</sub>	255(2)	I <sub>(21)</sub> -Al <sub>(2)</sub> -I <sub>(13)</sub>	110.1(1)
Al <sub>(1)</sub> -I <sub>(13)</sub>	251(13)	I <sub>(13)</sub> -Al <sub>(1)</sub> -I <sub>(13)</sub>	110.4(2)	Al <sub>(2)</sub> -I <sub>(23)</sub>	252.2(14)	I <sub>(23)</sub> -Al <sub>(2)</sub> -I <sub>(23)</sub>	113.4(2)
		I <sub>(13)</sub> -Al <sub>(1)</sub> -I <sub>(11)</sub>	110.8(1)			I <sub>(23)</sub> -Al <sub>(2)</sub> -I <sub>(21)</sub>	109.5(1)

**Tab.38** Atomic coordinates and equivalent isotropic displacement parameters (Å<sup>2</sup>) for InAlI<sub>4</sub>

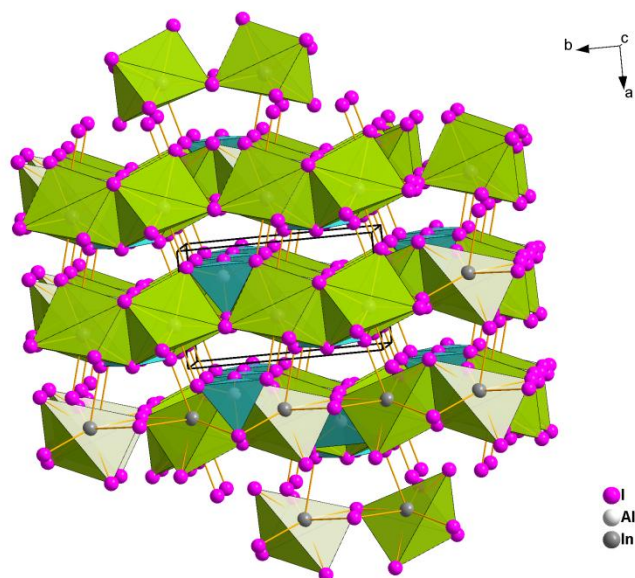
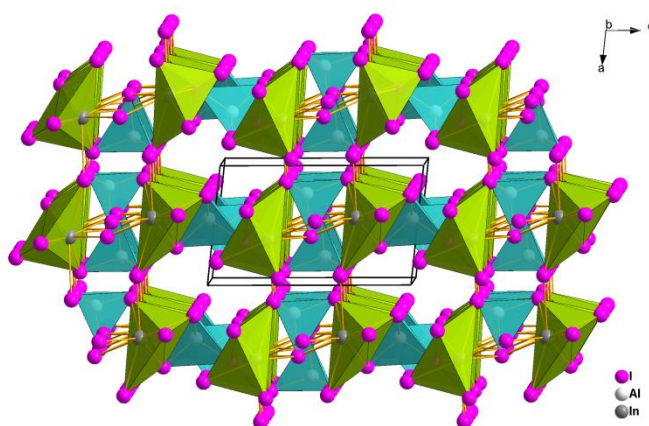
Atom	x/a	y/b	z/c	S.O.F.	U <sub>eq</sub>
In(1)	0.5910(9)	0.0149(6)	0.2934(5)	1.0000	0.085(2)
Al(1)	0.5710(30)	1/4	0.0250(20)	0.5000	0.031(5)
I(11)	0.3356(8)	1/4	0.1689(6)	0.5000	0.056(2)
I(12)	0.3672(14)	1/4	-0.1650(6)	0.5000	0.079(3)
I(13)	0.7728(7)	0.0755(6)	0.431(5)	1.0000	0.069(2)
Al(2)	0.7790(30)	1/4	0.5560(2)	0.5000	0.031(5)
I(21)	0.9007(8)	1/4	0.3617(5)	0.5000	0.049(2)
I(22)	0.4218(8)	1/4	0.5120(6)	0.5000	0.061(2)
I(23)	0.8854(7)	0.0717(5)	0.6589(5)	1.0000	0.073(2)

**Tab.39** In-I distances in  $\text{InAlI}_4$ 

In-I	d/pm	
In-I(13)	349.2(9)	1x
In-I(12)	352.2(8)	1x
In-I(11)	356.5(8)	1x
In-I(21)	359.1(8)	1x
In-I(23)	365.5(8)	1x
In-I(23)′	385.6(8)	1x
In-I(22)	392.3(8)	1x
In-I(22)′	410.5(9)	1x

The chains formed by the connection of the coordination polyhedra (fig.45) are linked to the parallel chains from the vicinity through tetraiodidoaluminate tetrahedra and by sharing capping iodide ions along the crystallographic axis a (the capping iodides of one chain are vertices for the chain situated above (fig.46); along crystallographic axis c each coordinating polyhedra of indium shares

the remaining two capping iodides with other six coordinating polyhedra (fig.47).

**Fig.46** Crystal structure of  $\text{InAlI}_4$ -projection along the c axis**Fig.47** Crystal structure of  $\text{InAlI}_4$ -projection along the b axis

## 2.4 TlAlBr<sub>4</sub>

The second compound which makes an exception by the classification presented in this thesis is thallos tetrabromidoaluminate. TlAlBr<sub>4</sub> crystallizes in a space group not commonly adopted by this class of compounds, namely  $P 2 / c$  (no.13). From all known to date tetrahalogenidoaluminates and tetrahalogenidogallates, only four of these salts crystallize in this space group, and these are: KAlBr<sub>4</sub>, InAlBr<sub>4</sub> and InGaBr<sub>4</sub> [20]. There can be made no comparison to RbAlBr<sub>4</sub>, since the structure of this one is to date unknown.

### 2.4.1 Preparation

TlAlBr<sub>4</sub> is synthesized by mixing TlBr and AlBr<sub>3</sub> in equimolar ratio (0,735 mmol); the reaction mixture was sealed in a glass ampoule and heated with 10°C/h to 150°C. At this temperature the probe was annealed for 48 h, and then cooled to room temperature with a rate of 2°C/h. After completion of the reaction, colourless, transparent and prismatic shaped crystals were observed under the microscope.

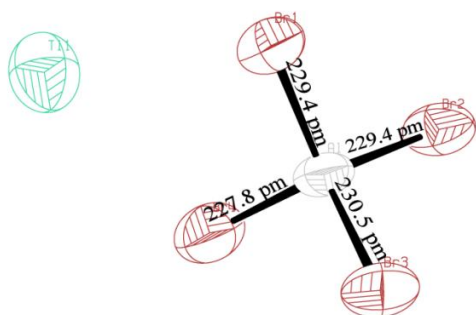
### 2.4.2 Structural aspects

#### 2.4.2.1 Crystal structure of TlAlBr<sub>4</sub>

TlAlBr<sub>4</sub> crystallize isotypic with KAlBr<sub>4</sub> in the monoclinic space group  $P 2 / c$  (no.13), with four formula units per unit cell ( $a = 899.8(9)$  pm,  $b = 739.9(7)$  pm,  $c = 1303.8(13)$ ,  $\beta = 106.51(2)^\circ$ ,  $V = 1001.10(11) \cdot 10^6$  pm<sup>3</sup>). Its asymmetric unit contains two crystallographically independent Tl(I) ions, one independent Al(III) cation and four Br<sup>-</sup> anions. The tetrabromidoaluminate tetrahedron (fig.48) shows a slightly distortion. Thallium shows two coordination environments.

**Tab.40** Crystallographic and refinement data for TlAlBr<sub>4</sub>

Empirical formula	<b>TlAlBr<sub>4</sub></b>
Formula weight /amu	550.99
Crystal system	monoclinic
Space group (no.)	<i>P2/c</i> (no. 13)
Unit cell dimensions /pm	<i>a</i> = 8.998(9) <i>b</i> = 7.399(7) <i>c</i> = 13.038(13); $\beta$ = 106.51(2)°
<i>V</i> /Å <sup>3</sup>	832.2(14)
$\rho_{\text{Xray}}$ /g · cm <sup>-3</sup>	4.398
<i>Z</i>	4
Theta range	2.36° ≤ $\theta$ ≤ 50°
Temperature	T = 298(2)K
F(000)	936
Absorption correction	numerical Bruker SADABS
Absorption coefficient /mm <sup>-1</sup>	38.609
Structure solution /refinement	Direct methods, SIR 92/ SHELXL-97
Data/restraints/parameters	1465 / 0 / 57
N( <i>hkl</i> )	4536
N'( <i>hkl</i> ) unique with I > 2σ(I)	1465
R <sub>int</sub>	0.2760
R <sub>1</sub> (I > 2σ); wR <sub>2</sub> (I > 2σ)	0.1353; 0.3455
R <sub>1</sub> (all); wR <sub>2</sub> (all)	0.1998; 0.3866
GooF	1.001
Extinction coefficient	0.017(4)
$\Delta F_{\text{max}}$ ; $\Delta F_{\text{min}}$ /e · Å <sup>-3</sup>	2.541; -1.923
XRD measuring unit	Bruker AXS Smart CCD 1000

**Fig.48** Structural unit of TlAlBr<sub>4</sub>

The tetrabromidoaluminate tetrahedron is only distorted to a small extent from the ideal T<sub>d</sub> symmetry (fig.48). The Al-Br bond lengths are in the expected range, if compared to similar compounds, like CsAlBr<sub>4</sub> [21].

**Tab.41** Distances and angles for the [AlBr<sub>4</sub>]<sup>-</sup> units

Al-Br	d/pm		Br-Al-Br	/°	
Al(1)-Br(4)	227.8(15)	1x	Br(4)-Al(1)-Br(1)	109.9(5)	1x
Al(1)-Br(2)	229.4(13)	2x	Br(4)-Al(1)-Br(2)	112.4(6)	1x
Al(1)-Br(3)	230.5(12)	1x	Br(1)-Al(1)-Br(2)	108.3(5)	1x
			Br(4)-Al(1)-Br(3)	109.1(5)	1x
			Br(1)-Al(1)-Br(3)	108.3(6)	1x
			Br(2)-Al(1)-Br(3)	108.7(5)	1x

The coordination polyhedron of Tl(1) ion (fig.50) is a slightly distorted square anti-prism (C.N.=8); the environment formed by the coordination of Tl(2) ion (fig.49) is a flattened polyhedron containing six bromine ions, capped by four additional bromines (C.N.=6+4). This coordinating type is similar to the one in TlGaBr<sub>4</sub>. The two different coordination polyhedra alternate along crystallographic axis a, connecting by edges. The formed polyhedral chains are linked along crystallographic axis b by vertices (shared by the two different polyhedra), and along crystallographic axis c through the capping bromine ions from the coordination environment of Tl(2). Furthermore, the four capping bromine ions from the coordination environment of Tl(2) are vertices for four other Tl(1) coordination polyhedra, and vertices for other two Tl(2) coordination polyhedra. In the *ab* plane the two crystallographic independent thallium ions are positioned in layers (fig.52).

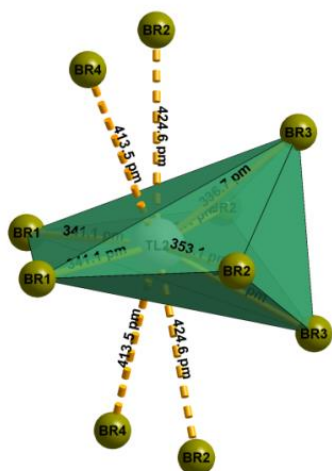


**Fig.49** Coordination environment for Tl(2)

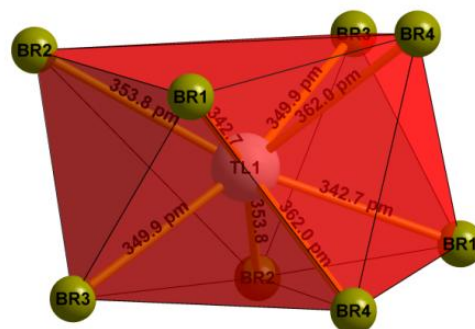


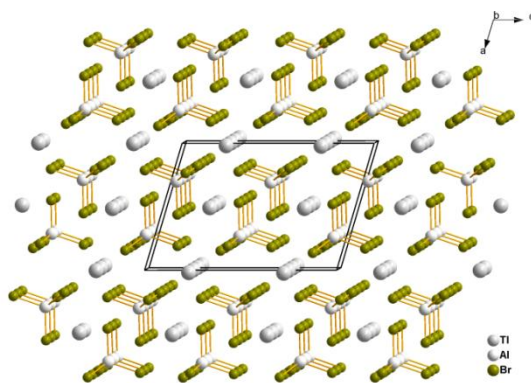
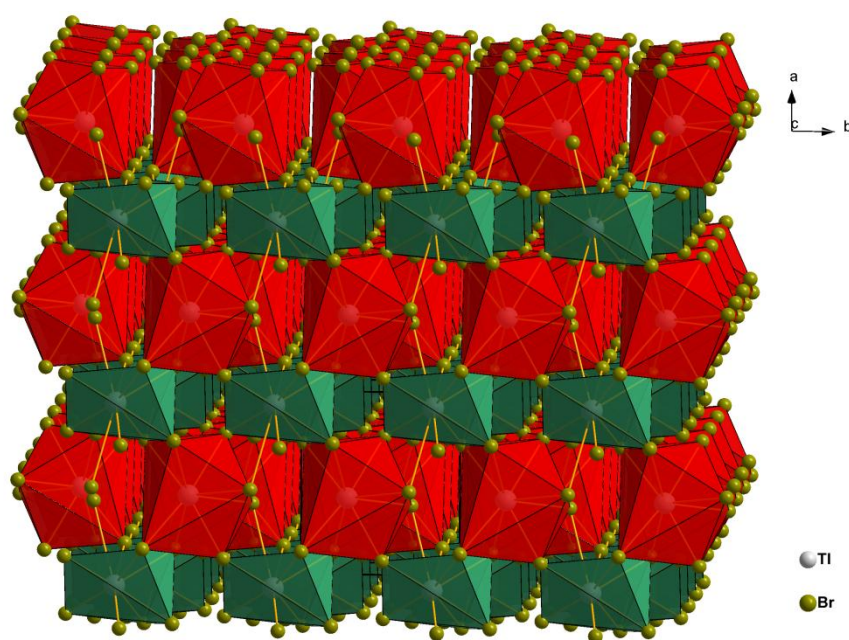
**Fig.50** Coordination environment for Tl(1)

**Tab.42** Selected Tl-Br distances

Tl-Br	d/pm		Tl-Br	d/pm	
Tl(1)-Br(1)	342.7(28)	2x	Tl(2)-Br(3)	336.8(16)	2x
Tl(1)-Br(3)	349.8(23)	2x	Tl(2)-Br(1)	341.2(15)	2x
Tl(1)-Br(2)	353.8(31)	2x	Tl(2)-Br(2)	353.0(23)	2x
Tl(1)-Br(4)	362.0(9)	2x			

**Tab.43** Atomic coordinates and equivalent isotropic displacement parameters ( $\text{\AA}^2$ ) for  $\text{TlAlBr}_4$ 

$\text{TlAlBr}_4$	$x/a$	$y/b$	$z/c$	$U_{eq}$
Tl(1)	1/2	0.6525(5)	1/4	0.121(2)
Tl(2)	0	0.1147(5)	1/4	0.189(3)
Al(1)	0.2843(15)	0.2160(17)	0.0438(9)	0.069(3)
Br(1)	0.1659(6)	0.4259(6)	0.1237(3)	0.082(2)
Br(2)	0.2122(7)	-0.0666(6)	0.0842(4)	0.093(2)
Br(3)	0.1969(7)	0.2569(8)	-0.1388(3)	0.101(2)
Br(4)	0.5459(7)	0.2563(10)	0.0990(5)	0.115(2)

**Fig.51** Crystal structure of  $\text{TlAlBr}_4$ -projection along the  $b$  axis**Fig.52** Coordination polyhedra of Tl(1)(red) and Tl(2)(green) along axis  $c$  in  $\text{TlAlBr}_4$

## 2.5 Summary

The symmetry of the tetrahedral  $[\text{MX}_4]^-$  unit, is in all cases close to the ideal  $T_d$  symmetry. The angles between the central atom and the halide ions in tetrahedron deviate within a range of  $10^\circ$ . It seems that the strong Lewis character of aluminium and gallium is reflected through this high symmetry, low influences being observed by changing the counter ion. These tetrahedra items act as an almost non deformable building unit.

The coordination around the heavy metal was taken into focus to analyse if a perceivable effect of the lone-pair of electrons plays a role in the deformation from the ideal symmetry. It was shown that the inert-pair effect becomes visible if interactions of covalent nature are involved [22]. Since the  $[\text{MX}_4]^-$  units can be considered as relatively weakly coordinating anions, they should not play a strong polarisable role, and thus give heavy metals the “freedom” to reveal an inert-pair effect. By comparing the structures of the  $\text{InAlCl}_4$ ,  $\text{InAlI}_4$ ,  $\text{TlAlCl}_4$ ,  $\text{TlAlBr}_4$ ,  $\text{TlAlI}_4$ ,  $\text{TlGaCl}_4$ ,  $\text{TlGaBr}_4$  and  $\text{TlGaI}_4$  to analogous alkali metal compounds, it should be possible to reveal eventual symmetry perturbations. However through this study there was no reduction in symmetry (which could be assumed to the “lone pair” effect) observed, since also the analogous alkali metal cations show similar coordination environments. The symmetry distortions can be attributed to the volume demand (depending on the surroundings) of different atoms, with other words, the packing effects.

$\text{TlAlCl}_4$ ,  $\text{TlGaCl}_4$ , and  $\text{RbAlCl}_4$ , respectively  $\text{RbGaCl}_4$  crystallize isotypic, all showing a similar distortion from the “barium sulphate” type of structure.  $\text{KAlCl}_4$  shows also the distorted “baryte” type of structure, but at higher temperatures (above  $114^\circ\text{C}$ );  $\text{InAlCl}_4$  shows also a structural distorted “baryte” type. Having these new compounds analysed, and considering also the known to date structures of analogous compounds, it can be affirmed that an astonishing amount of the analysed systems crystallize in a deformed “baryte” type. More precisely,  $P n m a$  is the preferred space group candidate for the tetrachloridoaluminates and tetrachloridogallates.

Tetrabromidogallate and tetrabromidoaluminate compounds seem to be a transit group, since in this segment occur the most structural exceptions. For example, TlGaBr<sub>4</sub> crystallizes in  $P 2_1 / c$ , while RbGaBr<sub>4</sub> crystallize in the  $P n m a$  space group. InGaBr<sub>4</sub> crystallizes also differently comparing to its analogue, the KGaBr<sub>4</sub>. InAlBr<sub>4</sub> crystallizes in the same space group with its analogue, KAlBr<sub>4</sub>. RbAlBr<sub>4</sub> have no known to date structure, and therefore no statement can be make on the structural compatibility with the “pseudo-alkali” thallium compound.

Unidentified to date are the crystal structures of RbAlI<sub>4</sub> and RbGaI<sub>4</sub>, therefore it makes impossible a comparison with the crystal structures of TlAlI<sub>4</sub> and TlGaI<sub>4</sub>. However the tetraiodidoaluminate and tetraiodidogallate compounds crystallize almost exclusively in the  $P 2_1 / c$  space group. There are only two exceptions known to date in the considered systems (these are NaAlI<sub>4</sub>-crystallizes in the  $P n m a$  space group and InAlI<sub>4</sub>-crystallizes in the  $P 2_1 / m$  space group). Throughout this study the new reported crystal structures of TlAlI<sub>4</sub>, TlGaI<sub>4</sub>, CsAlI<sub>4</sub> and CsGaI<sub>4</sub> confirm the above specified statement. InAlI<sub>4</sub> seems to present a light structural deviation from the trend, namely the  $P 2_1 / m$  space group.

## 2.6 Literature

- [1] J. Kendall, E. D. Crittenden, H. K. Miller, *J. Am. Chem. Soc.* **1923**, *45*, 963-996.
- [2] G. Mairesse, P. Barbier, J. P. Wignacourt, A. Rubbens, F. Wallart, *Can. J. Chem.* **1978**, *56*, 764-771.
- [3] T. Staffel, G. Meyer, *Z. Anorg. Allg. Chem.* **1987**, *552*, 108-112.
- [4] A. P. Wilkinson, A. K. Cheetham, D. E. Cox, *Acta Crystallogr., Sect. B: Struct. Sci.* **1991**, *47*, 155-161.
- [5] J. M. van den Berg, *Acta Crystallogr.* **1966**, *20*, 905-910.
- [6] T. Timofte, A.-V. Mudring, *Acta Crystallogr., Sect. E: Struct. Rep. Online* **2005**, *61*, i199-i200.
- [7] S. S. Batsanov, *J. Mol. Struct. (Theochem)* **1999**, *468*, 151-159.
- [8] C. E. Housecroft, A. G. Sharpe, *Anorganische Chemie*, Pearson Studium, München, **2006**.
- [9] N. N. Greenwood, A. Earnshaw, *Chemie der Elemente*, VCH, Weinheim, **1988**.
- [10] J.-X. Mi, H. Zhang, J.-F. Deng, S.-Y. Mao, J.-T. Zhao, *Z. Kristallogr. - New Cryst. Struct.* **2002**, *217*, 479-480.
- [11] G. Meyer, E. Schwan, *Z. Naturforsch., B: Chem. Sci.* **1980**, *35b*, 117-118.
- [12] M. Gorlov, A. Fischer, L. Kloo, *Acta Crystallogr., Sect. E: Struct. Rep. Online* **2003**, *59*, i70-i71.
- [13] G. Meyer, T. Staffel, M. Irmler, *Thermochim. Acta* **1990**, *160*, 63-70.
- [14] G. Meyer, E. Schwan, *Z. Anorg. Allg. Chem.* **1980**, *468*, 82-90.
- [15] R. Burnus, D. J. Hinz, G. Meyer, *Z. Kristallogr.* **1994**, *209(6)*, 544.
- [16] T. Timofte, A.-V. Mudring, *Z. Anorg. Allg. Chem.* **2008**, *634(4)*, 622-623.
- [17] E. Perenthaler, H. Schulz, A. Rabenau, *Z. Anorg. Allg. Chem.* **1982**, *491*, 259-265.
- [18] W. Höhle, A. Simon, *Z. Naturforsch., B: Chem. Sci.* **1986**, *41B(11)*, 1391-1398.
- [19] T. Hahn, *International Tables for Crystallography-Vol.A (5<sup>th</sup> Edition)*, Kluwer Academic Publishers, **2002**.

- [20] T. Staffel, G. Meyer, *Z. Anorg. Allg. Chem.* **1990**, 585, 38-48.
- [21] R. W. Berg, *Acta Chemica Scandinavica* **1997**, 51, 455-461.
- [22] A.-V. Mudring, *Eur. J. Inorg. Chem.* **2007**, 6, 882-890.

### 3. Indium heptachloridogallate - $\text{InGa}_2\text{Cl}_7$

Phase diagrams show the existence of the  $\text{M}^{\text{I}}\text{M}^{\text{III}}_2\text{X}_7$  form for the cases presented in the previous chapters, in the thermal behavior of the  $\text{M}^{\text{I}}\text{X}\cdot\text{M}^{\text{III}}\text{X}_3$  systems [1]. The synthesis route applied is the same as in the case of  $\text{M}^{\text{I}}\text{M}^{\text{III}}\text{X}_4$  compounds, only the stoichiometry and reaction temperature differ. Little is known about the structure of the alkali metal and pseudo-alkali metal heptahalogenidodigallates and heptahalogenidodialuminates. Furthermore no systematic structural study, like in the case of  $\text{M}^{\text{I}}\text{M}^{\text{III}}\text{X}_4$ , is known. From the whole class of alkali metal and pseudo-alkali metal heptahalogenidodigallates and heptahalogenidodialuminates, only the crystal structures of  $\text{KGa}_2\text{Cl}_7$  [2],  $\text{KAl}_2\text{Br}_7$  [3],  $\text{CsGa}_2\text{I}_7$  [4] and  $\text{Ga}_3\text{Cl}_7$  [5] are reported. As an analogous compound, the structure of  $\text{NH}_4\text{Al}_2\text{Br}_7$  is also known [6]. In this section is presented the structure of  $\text{InGa}_2\text{Cl}_7$  [7]. The conformation of  $[\text{Al}_2\text{Cl}_7]^-$  is reported in a cluster compound [8], also vibrational spectroscopic studies on  $[\text{Al}_2\text{Cl}_7]^-$  and  $[\text{Al}_2\text{Br}_7]^-$  [9] are available.

#### 3.1 Preparation

$\text{InGa}_2\text{Cl}_7$  was obtained by reacting (sealed glass ampoule, under argon gas) Bi pieces (8.709 mmol), In powder (0.870 mmol) and  $\text{GaCl}_3$  (8.709 mmol) - molar ratio  $\text{Bi}:\text{In}:\text{GaCl}_3=10:1:10$  - together with 0.4 g of 1-butyl-3-methyl-imidazolium tetrakis(nonafluoro-tert-butoxy)aluminate (used as reaction medium), at  $100^\circ\text{C}$  (heating with a rate of  $30^\circ\text{C}/\text{h}$ ), and annealing at this temperature for 24 h; then cooling to room temperature with  $10^\circ\text{C}/\text{h}$ . After the reaction took place, the mixture in the ampoule had a brick-like red color. Under the microscope irregularly shaped, transparent and deep red crystals, surrounded by a black byproduct mass could be observed. Suitable crystals for X-ray diffraction analysis could be isolated under inert atmosphere in glass capillaries. Because of the reaction mixture consistence, no XRD-powder diffraction data of sufficient quality could be provided.

## 3.2 Structural aspects

### 3.2.1 Crystal structure of $\text{InGa}_2\text{Cl}_7$

$\text{InGa}_2\text{Cl}_7$  crystallizes isotypic with  $\text{KGa}_2\text{Cl}_7$  and  $\text{Ga}_3\text{Cl}_7$  ( $\text{Ga}[\text{GaCl}_4]$ ) in the acentric orthorhombic space group  $Pna2_1$  (no. 33), containing four formula units in the unit cell ( $a = 1185.7(2)$ ,  $b = 891.4(4)$ ,  $c = 1071.6(2)$  pm,  $V = 1132.6(3) \cdot 10^6$  pm<sup>3</sup>). The asymmetric unit of  $\text{InGa}_2\text{Cl}_7$  contains one crystallographic independent  $\text{In}^{+1}$  ion, two  $\text{Ga}^{+3}$  cations, and seven chlorine anions.

**Tab.44** Crystallographic and refinement data for  $\text{InGa}_2\text{Cl}_7$

Empirical formula	$\text{InGa}_2\text{Cl}_7$
Formula weight /amu	502.41
Crystal system	orthorhombic
Space group (no.)	$Pna2_1$ (no.33)
Unit cell dimensions /pm	$a = 1185.73(18)$ $b = 891.37(15)$ $c = 1071.63(15)$
$V/\text{\AA}^3$	1132.6(3)
$\rho_{\text{XRAY}}/\text{g}\cdot\text{cm}^{-3}$	2.946
Z	4
Theta range	$2.86^\circ \leq \theta \leq 24.98^\circ$
Temperature	293(2) K
F(000)	920
Absorption correction	numerical Stoe X-SHAPE/X-RED
Absorption coefficient / $\text{mm}^{-1}$	8.326
Structure solution /refinement	Direct methods, SIR-92/ SHELXL-97
Data/restraints/parameters	1994 / 1 / 93
N(hkl)	8449
N'(hkl) unique with $I > 2\sigma(I)$	1994
$R_{\text{int}}$	0.1554
$R_1 (I > 2\sigma)$ ; $wR_2 (I > 2\sigma)$	0.0692; 0.1842
$R_1$ (all); $wR_2$ (all)	0.0780; 0.1964
GooF	1.040
Extinction coefficient	0.021(2)
$\Delta F_{\text{max}}$ ; $\Delta F_{\text{min}} / e \cdot \text{\AA}^{-3}$	1.501; -1.232
Flack-Parameter	0.00(5)
XRD measuring unit	Stoe IPDS

In this case the structural motif is created by connecting two  $[\text{GaCl}_4]^-$  tetrahedral through a chlorine vertice. In each of both, the tetrahedron is slightly elongated at the bridging chlorine atom. As it was previously determined [5], the chlorine connecting the two gallium

atoms shows no linear bridging, but a given angle of  $109.012^\circ$ , which is slightly larger than in the case of  $\text{KGa}_2\text{Cl}_7$  ( $108.624^\circ$ ) [2].

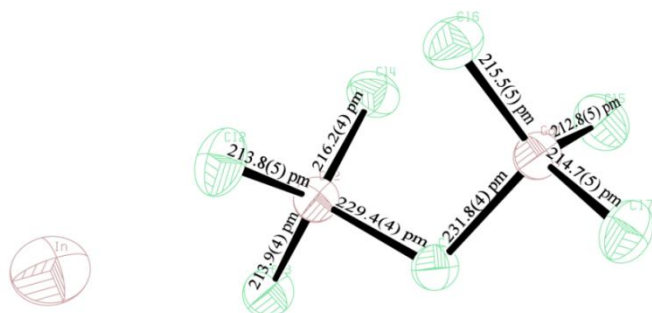


**Fig.53** Structural unit of  $\text{InGa}_2\text{Cl}_7$

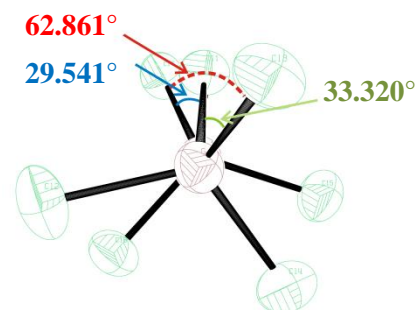


**Fig.54** Torsion angles of  $[\text{Ga}_2\text{Cl}_7]^-$

The  $[\text{Ga}_2\text{Cl}_7]^-$  anion adopts a gauche-like conformation, the torsion angle being  $62.861^\circ$ . The difference between angles and the fact that bridging bonds are longer than the other bonds in the tetrahedron are explained by making an analogy to the  $\text{Cl}_2\text{O}_7$  structure and by using VSEPR theory principles [2].

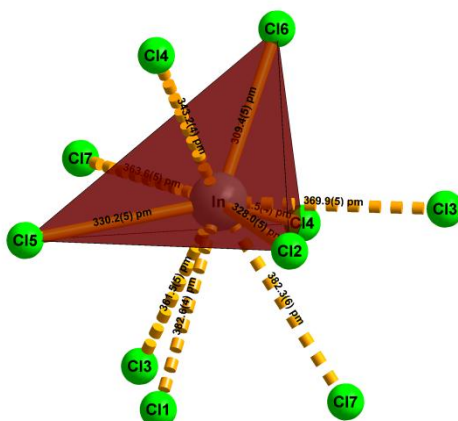
**Tab.45** Distances and angles for the  $[\text{Ga}_2\text{Cl}_7]^-$  units

Ga-Cl	d/pm		Cl-Ga-Cl	$l^\circ$	
Ga(1)-Cl(5)	212.8(5)	1x	Cl(5)-Ga(1)-Cl(1)	104.8(2)	1x
Ga(1)-Cl(7)	214.7(5)	1x	Cl(6)-Ga(1)-Cl(1)	105.6(2)	1x
Ga(1)-Cl(6)	215.5(5)	1x	Cl(7)-Ga(1)-Cl(1)	101.2(2)	1x
Ga(1)-Cl(1)	231.8(4)	1x	Cl(5)-Ga(1)-Cl(6)	114.6(2)	1x
			Cl(6)-Ga(1)-Cl(7)	113.4(2)	1x
			Cl(7)-Ga(1)-Cl(5)	115.3(2)	1x
Ga(2)-Cl(3)	213.9(4)	1x	Cl(2)-Ga(2)-Cl(1)	106.1(2)	1x
Ga(2)-Cl(2)	213.8(5)	1x	Cl(3)-Ga(2)-Cl(1)	105.2(2)	1x
Ga(2)-Cl(4)	216.2(4)	1x	Cl(4)-Ga(2)-Cl(1)	103.7(1)	1x
Ga(2)-Cl(1)	229.4(4)	1x	Cl(2)-Ga(2)-Cl(3)	113.0(2)	1x
			Cl(3)-Ga(2)-Cl(4)	113.1(2)	1x
			Cl(4)-Ga(2)-Cl(1)	114.5(2)	1x

**Tab.46** Atomic coordinates and equivalent isotropic displacement parameters ( $\text{\AA}^2$ )

Atom	x/a	y/b	z/c	$U_{eq}$
In	0.1144(2)	0.3657(3)	0.8790(3)	0.121(1)
Ga1	0.3875(1)	0.3809(2)	0.2427(2)	0.049(1)
Ga2	0.1755(1)	0.4304(2)	0.4997(2)	0.049(1)
Cl1	0.2569(3)	0.2591(4)	0.3677(3)	0.051(1)
Cl2	0.2890(4)	0.4546(6)	0.6534(4)	0.074(1)
Cl3	0.0174(3)	0.3335(5)	0.5520(4)	0.067(1)
Cl4	0.1575(3)	0.6289(4)	0.3856(4)	0.064(1)
Cl5	0.904(4)	0.4807(6)	0.0978(4)	0.072(1)
Cl6	0.4718(3)	0.5386(5)	0.3633(5)	0.067(1)
Cl7	0.4928(3)	0.1971(6)	0.1861(4)	0.063(1)

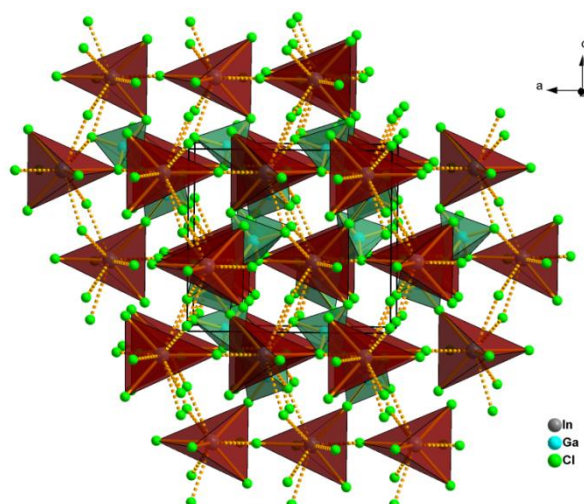
The coordination around indium is accomplished by ten chlorine atoms (C.N. = 8+2). Considering that these ten atoms find themselves at different distances from the central atom, a characterization dependent on lengths order is reported for similar compounds [2][5]. The In-Cl distances could be divided in two categories: four In-Cl distances are the shortest from the whole ten chlorine ions coordinating around indium, and which build a distorted tetrahedron (fig.55); the remaining six chlorines cap this tetrahedron at different distances, one relatively close, at 343.2 pm, three chlorines at longer distances (361.5-369.9 pm), and another two situated outside the sum of the van der Waals radii of both elements, at 382.3-382.6 pm.

**Fig.55** Coordination environment of In in  $\text{InGa}_2\text{Cl}_7$

**Tab.47** Selected In-Cl distances for  $\text{InGa}_2\text{Cl}_7$ 

In-Cl	d/ pm	In-Cl	d/ pm
In(1)-Cl(6)	309.4(5)	In(1)-Cl(3)	361.5(5)
In(1)-Cl(4)	322.5(5)	In(1)-Cl(7)	363.6(5)
In(1)-Cl(2)	328.0(5)	In(1)-Cl(3)′	369.92(53)
In(1)-Cl(5)	330.2(5)	In(1)-Cl(7)′	382.3(6)
In(1)-Cl(4)′	343.2(4)	In(1)-Cl(1)	382.6(4)

While in the case of  $\text{KGa}_2\text{Cl}_7$  [2] the capping chlorines can be divided into two groups (three chlorines with intermediate distances - an 350 pm average range, and three with long, 380 pm average distances), in the case of  $\text{Ga}_3\text{Cl}_7$  the classification divides the capping chlorines in three groups (two with short, 350 pm average distances, two with intermediate, 360 pm average distances, and two with long, 380 pm average distances); with this last example resembles most the presented  $\text{InGa}_2\text{Cl}_7$ . In table 47, the first four shortest distances belong to the coordination tetrahedron, and the remaining six distances belong to the capping chlorine ions: one short, three intermediate, and two long distances.

**Fig.56** Crystal structure of  $\text{InGa}_2\text{Cl}_7$ - projection along crystallographic axis b

One type of coordination is observed by this compound around indium. Each coordinating tetrahedron connects with other four tetrahedra in its surroundings, through the capping chlorines: two of these tetrahedra share each two capping chlorines with the central

tetrahedron (the red dotted bonds in fig.57), while the other two remaining tetrahedra connect each through one capping chlorine, as follows: one capping chlorine atom of the central tetrahedron is vertex for the next tetrahedron, and a vertex of the central tetrahedron is capping chlorine for the remaining tetrahedron (the yellow dotted bonds in fig.57). The blue dotted bond represents in fig.57 the only capping chlorine which do not link to another coordinating tetrahedron.

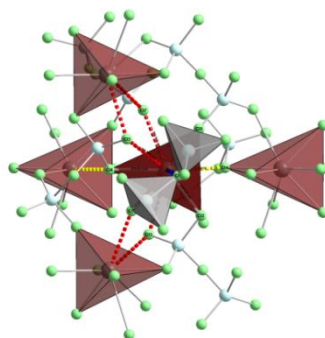


**Fig.57** The coordinating tetrahedra connectivity in the structure of  $\text{InGa}_2\text{Cl}_7$   
red: 2-fold connectivity between coordinating tetrahedra  
yellow: 1-fold connectivity between coordinating tetrahedra  
blue: distance to capping chlorine which do not link to further coordinating tetrahedra

Fig.58 reveals the layer-wise orientation of the heptachloridodigallate anions. The violet-coloured tetrahedra represent the heptachloridodigallate anions which belong to the further parallel (to the presented one) layer. While the  $[\text{Ga}_2\text{Cl}_7]^-$  layers are parallel along crystallographic axis b, along the crystallographic axis a the orientation of the anions from one layer make with the orientation of the anions from the next layer a  $95.97^\circ$  angle.

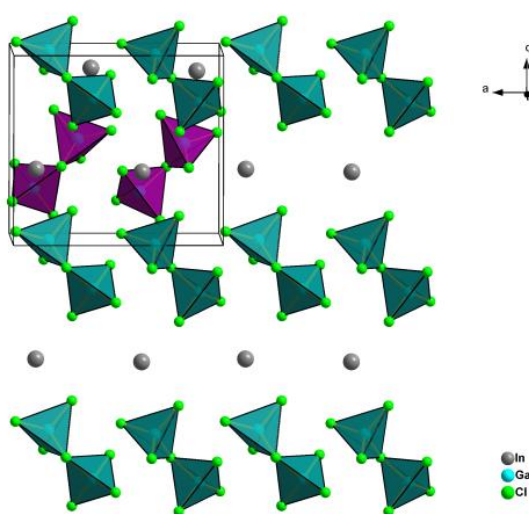


**Fig.58** Layer-wise representation of the  $[\text{Ga}_2\text{Cl}_7]^-$  anions along the crystallographic plane ac  
 \*in violet are presented the  $[\text{Ga}_2\text{Cl}_7]^-$  anions from the layer behind the presented layer

### 3.3 Summary

A first conclusion is that no observable inert pair effect is manifested for this case, since the potassium analogue crystallizes isotypic and show the same coordination environment around potassium. Indeed bond length in  $[\text{Ga}_2\text{Cl}_7]^-$  vary between both analogous compounds with an average value of 1 pm, and by the torsion angles the medium difference is about  $1^\circ$ . Also In-Cl distances in the coordinating environment are similar to those found by  $\text{KGa}_2\text{Cl}_7$  and  $\text{Ga}_3\text{Cl}_7$ , in this case the variations are within a 10 pm range.

With respect to the previous classifications, an analogy could be observed between  $\text{KGa}_2\text{Cl}_7$  and  $\text{InGa}_2\text{Cl}_7$ ; these two above named and  $\text{Ga}_3\text{Cl}_7$  are the structurally known heptachloridodialuminates, respectively heptachloridodigallates, and crystallize without exception in the acentric  $Pna2_1$  (no. 33) space group.

The only two known structures of heptabromidodialuminates crystallize in different space groups:  $\text{KAl}_2\text{Br}_7$  in  $P2_1/c$  (no. 14), while  $[\text{NH}_4]\text{Al}_2\text{Br}_7$  crystallizes in  $Pna2_1$  (no. 33).

The only crystallographically characterized heptaiodidodigallate is  $\text{CsGa}_2\text{I}_7$ , and it crystallizes in a different space group, namely  $Pbcm$  (no. 57).

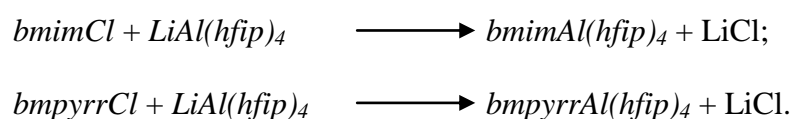
### 3.4 Literature

- [1] J. Kendall, E. D. Crittenden, H. K. Miller, *J. Am. Chem. Soc.* **1923**, *45*, 963-966.
- [2] D. Mascherpa-Corral, P. Vitse, A. Potier, J. Darriet, *Acta Crystallogr., Sect. B: Struct. Sci.* **1976**, *32*, 247-250.
- [3] E. Rytter, B. E. D. Rytter, H. A. Oye, J. Krogh-Moe, *Acta Crystallogr., Sect. B: Struct. Sci.* **1973**, *29(7)*, 1541-1543.
- [4] D. Mascherpa-Corral, A. Potier, *J. Inorg. Nucl. Chem.* **1976**, *38*, 211-213.
- [5] W. Frank, W. Hönle, A. Simon, *Z. Naturforsch., B: Chem. Sci.* **1990**, *45b*, 1-7.
- [6] E. Rytter, B. E. D. Rytter, H. A. Oye, *Acta Crystallogr., Sect. B: Struct. Sci.* **1975**, *31*, 2177-2181.
- [7] T. Timofte, A.-V. Mudring, *Z. Anorg. Allg. Chem.* **2008**, *634(4)*, 624-625.
- [8] T. W. Couch, D. A. Lokken, J. D. Corbett, *Inorg. Chem. (Washington, DC, U. S.)* **1972**, *11(2)*, 357-362.
- [9] A. Grodzicki, A. Potier, *J. Inorg. Nucl. Chem.* **1973**, *35*, 61-66.

## 4. Ionic liquids with weakly coordinating anions

### 4.1 General preparation

The ionic liquids presented in this work were obtained by metathesis reaction (often used for ionic liquid synthesis [1]), as presented in the following schemes:



**Tab.48** Educt/Product abbreviation

Abbreviation	Full name
<i>bmimCl</i>	1-butyl-3-methylimidazolium chloride
<i>bmpyrrCl</i>	1-butyl-1-methylpyrrolidinium chloride
<i>LiAl(hfip)<sub>4</sub></i>	lithium tetrakis(hexafluoroisopropyl)aluminate
<i>bmimAl(hfip)<sub>4</sub></i>	1-butyl-3-methylimidazolium tetrakis(hexafluoroisopropyl)aluminate [2]
<i>bmpyrrAl(hfip)<sub>4</sub></i>	1-butyl-1-methylpyrrolidinium tetrakis(hexafluoroisopropyl)aluminate [2]

Dichloromethane proved to be a convenient reaction medium (solvent) for these reactions, in such a way that the product (ionic liquid) is soluble in it, but the byproduct, which is lithium chloride, not.

Due to the hygroscopicity and moisture sensitivity of the educts and products, all the manipulations were carried out under inert atmosphere using glove box (MBraun, Germany) and Schlenk techniques.

The dichloromethane used for the reactions was distilled, moisture level repeatedly checked by Karl-Fischer titration (moisture level under 10 ppm), and then stored under argon atmosphere.

The educts used for the metathesis reactions were synthesized as follows:

1-butyl-3-methylimidazolium chloride (*bmimCl*) was synthesized according to the literature [3] by refluxing for 24 h 1-methylimidazole with an excess of 1-chlorobutane. The volatile fraction was removed under vacuum and the crude *bmimCl* recrystallized from a acetonitrile/ethyl acetate mixture. The product quality was checked through  $^1\text{H-NMR}$  - the obtained spectra match the theoretical chemical shifts and previous reports [4]; a few additional “foreign” peaks were identified as belonging to silicone grease and acetonitrile fraction (which was removed by applying high vacuum, and light heating).  $^1\text{H-NMR}$  (200 MHz;  $\text{CDCl}_3$ ):  $\delta(\text{ppm}) = 0.995(\text{t}), 1.368(\text{sext}), 1.899(\text{p}), 4.122(\text{s}), 4.322(\text{t}), 7.24(\text{m}), 7.31(\text{m}), 11.00(\text{s})$ . The white crystalline powder of *bmimCl* was stored under argon.

1-butyl-1-methylpyrrolidinium chloride (*bmpyrrCl*) was obtained following a literature procedure [5]: a slight excess of 1-chlorobutane was added while cooling to a solution of 1-methylpyrrolidine in propan-2-ol; the mixture was refluxed for 24 h; recrystallization was carried out from a 2-propanol/ethyl acetate mixture. The white powder of *bmpyrrCl* was dried under high vacuum. NMR was used to verify the quality of this intermediate compound, which confirms the theoretical and literature values [5];  $^1\text{H-NMR}$  (300 MHz,  $\text{CDCl}_3$ ):  $\delta(\text{ppm}) = 0.960(\text{t}), 1.415(\text{sextet}), 1.734(\text{p}), 2.267(\text{m}), 3.303(\text{s}), 3.644(\text{t}), 3.85(\text{m})$ . *BmpyrrCl* was stored under argon.

Lithium tetrakis(hexafluoroisopropyl)aluminate  $\{\text{LiAl}(\text{hfip})_4\}$  was synthesized [6] by adding 1,1,1,3,3,3-hexafluoroisopropanol at  $0^\circ\text{C}$  to a suspension of  $\text{LiAlH}_4$  (prior purified [7]) in toluene, in a 4:1 molar ratio (gas evolution). By refluxing this mixture for 12 h, a clear homogenous solution was obtained. Cooling this solution to approximately  $-20^\circ\text{C}$  leads to the precipitation of  $\text{LiAl}(\text{hfip})_4$ . This product was filtered out under argon stream, dried under vacuum, and then sublimated under vacuum, at approximately  $120^\circ\text{C}$ .  $^{27}\text{Al}$ -,  $^{19}\text{F}$ -, and  $^1\text{H}$ -NMR prove the purity of the product, and the obtained spectra correspond well to the reported data [6]:  $^1\text{H-NMR}$  (300 MHz;  $\text{CDCl}_3+5\% \text{ THF}$ ):  $\delta(\text{ppm}) = 4.436(\text{septet})$ ;  $^{27}\text{Al-NMR}$  (78 MHz,  $\text{CDCl}_3 + 5\% \text{ THF}$ )  $\delta(\text{ppm}) = 59.97(\text{s})$ ;  $^{19}\text{F-NMR}$  (282 MHz,  $\text{CDCl}_3 + 5\% \text{ THF}$ )

$\delta(\text{ppm}) = -77.23(\text{d})$ , and a small impurity peak at  $-76.97(\text{d})$ , which can be diminished through multiple sublimations of the reaction product.

## 4.2 1-butyl-3-methylimidazolium tetrakis(hexafluoroisopropyl)aluminate

### 4.2.1 Preparation

*BmimCl* and *LiAl(hfip)<sub>4</sub>* were mixed in a 1:1 molar ratio (5,698 mmol) and introduced in a Schlenk flask – additionally 20 ml dry dichloromethane were added; all work was carried under argon atmosphere. The suspension was rapidly stirred for 48 h at 30°C. The solution was decanted and filtered. The white residual powder was dried under high vacuum. From the filtrate, the solvent was removed under vacuum, when a white, light sticky solid, *bmimAl(hfip)<sub>4</sub>*, was obtained in high yield (approximately 80%).

Combustion analysis (CHNS analyzer) measured for the obtained product gives the results: calculated C(28.79%); H(2.30%); N(3.36%); found C(28.51%); H(2.275%); N(3.165%).

XRD-powder analysis confirmed that the residual solid which separate after the reaction took place, is lithium chloride, resulted as a byproduct of the metathesis reaction.

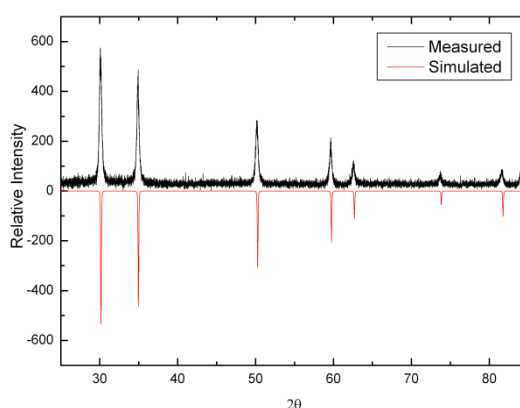


**Fig.59** XRD-Powder pattern of residual substance compared with simulated LiCl XRD-pattern (measured on Stoe Stadi P diffractometer/CuK $\alpha$  radiation)

## 4.2.2 Structural aspects

### 4.2.2.1 $^{27}\text{Al}$ -, $^{19}\text{F}$ -, $^1\text{H}$ -NMR

$^{27}\text{Al}$ -,  $^{19}\text{F}$ -,  $^1\text{H}$ -NMR were measured. For all three measurements deuterated chloroform was used.

$^{27}\text{Al}$ -NMR shows only one peak, a singlet at 59.879 ppm. A similar shift is observed for  $^{27}\text{Al}$  in the NMR spectra of the educt  $\text{LiAl}(\text{hfip})_4$ .

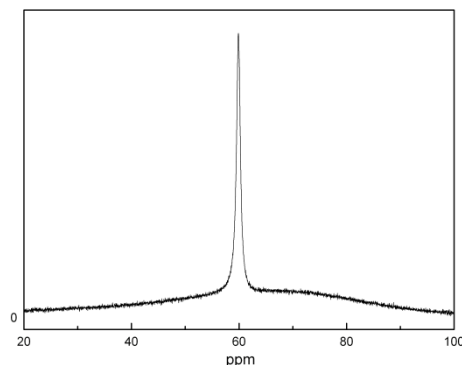


**Fig.60**  $^{27}\text{Al}$ -NMR spectra of  $\text{bmimAl}(\text{hfip})_4$

The  $^{19}\text{F}$ -NMR spectra is also almost identical with the one of the educt  $\text{LiAl}(\text{hfip})_4$ . The peak of the product is a doublet, because of the J-coupling between the fluorine atoms and the only proton of the complex anion. The coupling constant  $^3J$  is in this case 6.131 Hz and vary slightly from the educt. The small impurity peak exhibits the same coupling constant as the product peak. The ratio between product and impurity peak is 26:1. Observing same multiplicity and same coupling constant, means that in the impurity the hexfluoro-isopropyl segment remains intact.

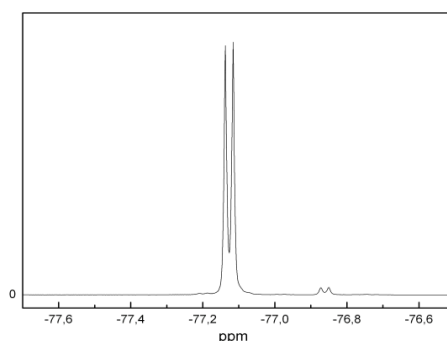


**Fig.61**  $^{19}\text{F}$ -NMR spectra of  $\text{bmimAl}(\text{hfip})_4$

The  $^1\text{H-NMR}$  spectrum of  $\text{bmimAl}(\text{hfip})_4$  matches the  $\text{bmimCl}$  one, with the exception that a new peak appears at 4.511 ppm, which belongs to the proton from the anion. By integrating the peak intensities, is observed that the ratio between the protons in spectrum matches the ratio from the chemical formula of this ionic liquid.

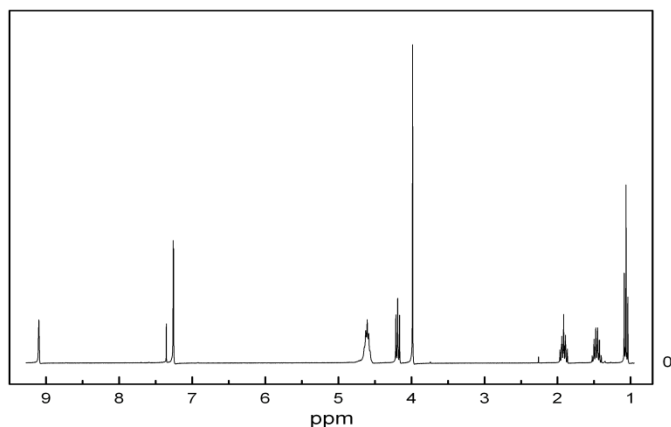


**Fig.62**  $^1\text{H-NMR}$  spectra of  $\text{bmimAl}(\text{hfip})_4$

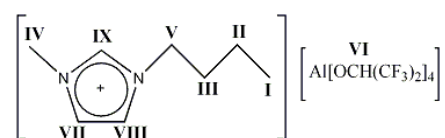


**Fig.63** Notation for identifying protons in the  $^1\text{H-NMR}$  spectra

**Tab.49** Chemical shift, integrals, multiplicity and coupling constants for  $^1\text{H-NMR}$

Chemical shift (ppm)	Integral	Multiplicity	$^2\text{J}/^3\text{J}(\text{Hz})$	Atom group
0.970	3	t	7.245	$\text{CH}_3$ (I)
1.360	2.07	sextet	7.477	$\text{CH}_2$ (II)
1.820	2.04	p	7.645	$\text{CH}_2$ (III)
3.890	3.01	s	-	$\text{CH}_3$ (IV)
4.090	2.09	t	7.645	$\text{CH}_2$ (V)
4.511	3.82	septet	5.791	CH (VI)
7.161	0.76	s	-	CH (VII)
7.166	0.83	s	-	CH (VIII)
7.260	0.31	s	-	$\text{CDCl}_3$
9.004	0.94	s	-	CH (IX)

#### 4.2.2.2 Crystal structure

*BmimAl(hfip)<sub>4</sub>* forms irregularly shaped, pale yellow, transparent crystals. A few suitable crystals were isolated and sealed in glass capillaries, checked for quality with Laue photographs, and then subjected to XRD single crystal analysis.

**Tab.50** Crystallographic and refinement data for *bmimAl(hfip)<sub>4</sub>*

Empirical formula	$C_{20}H_{19}AlF_{24}N_2O_4$
Formula weight /amu	834.35
Crystal system	monoclinic
Space group (no.)	$P 2_1/c$ (no.14)
Unit cell dimensions /pm	$a = 1620.4(2)$ $b = 1108.70(13)$ $c = 1797.7(3); \beta = 90.868(12)^\circ$
$V / \text{\AA}^3$	3229.3(8)
$\rho_{xray} / \text{g} \cdot \text{cm}^{-3}$	1.716
Z	4
Theta range	$2.16^\circ \leq \theta \leq 20.00^\circ$
Temperature	173(2) K
F(000)	1656
Absorption correction	numerical Stoe X-SHAPE/X-RED
Absorption coefficient / $\text{mm}^{-1}$	0.232
Structure solution /refinement	Direct Methods; SHELXS/XL-97
Data/restraints/parameters	3020 / 0 / 478
N( <i>hkl</i> )	21653
N'( <i>hkl</i> ) unique with $I > 2\sigma(I)$	3020
$R_{int}$	0.0764
$R_1 (I > 2\sigma); wR_2 (I > 2\sigma)$	0.0451; 0.0957
$R_1$ (all); $wR_2$ (all)	0.0901; 0.1073
GooF	0.887
Extinction coefficient	-
$\Delta F_{max}; \Delta F_{min} / e \cdot \text{\AA}^{-3}$	0.320; -0.219
XRD measuring unit	Stoe IPDS

*BmimAl(hfip)<sub>4</sub>* crystallizes in the monoclinic  $P 2_1 / c$  (no.14) space group (unit cell  $a=1620.4(2)$  pm;  $b=1108.70(13)$  pm;  $c=1797.7(3)$  pm;  $\beta=90.868^\circ$ ;  $V = 3229.3(8) \text{\AA}^3$ ) with four formula units per unit cell. There is one crystallographically independent aluminium atom, four oxygen, two nitrogen, twenty carbon, and twenty-four fluorine atoms.

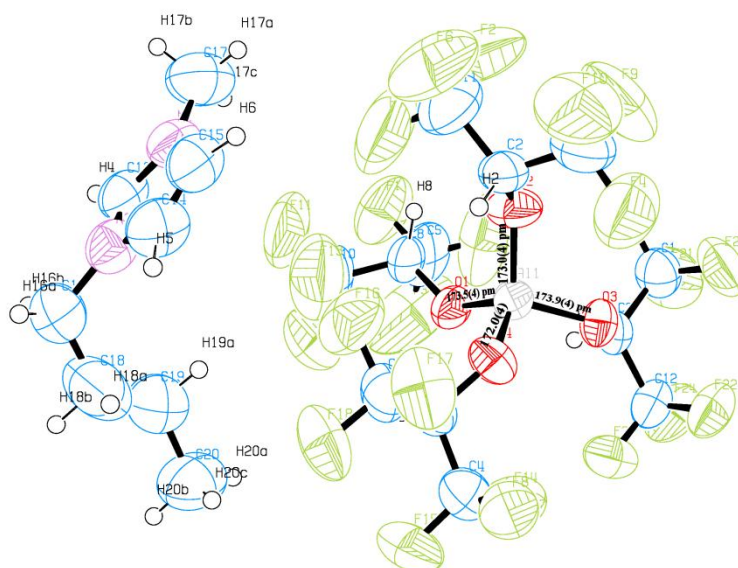


**Fig.64** Structural unit of *bmimAl(hfip)<sub>4</sub>*

The symmetry of the complex aluminate tetrahedron is fairly high. The bond lengths and O-Al-O angles of this tetrahedron confirm this statement (tab.51/tab.52). The high symmetry, the screening of basic centers by -CF<sub>3</sub> groups, large ionic volume and the charge distribution make this fluorinated aluminate a very weakly coordinating anion. Indeed theoretical studies [8] showed for LiAl[C(CF<sub>3</sub>)<sub>3</sub>]<sub>4</sub>, that the largest surface charge ( $q_{surf}$ ) found on the fluorine atom is -0.20 ( fluorine atom).

**Tab.51** Selected bond lengths (pm) for *bmimAl(hfip)<sub>4</sub>*

Bond	d/pm	Bond	d/pm	Bond	d/pm	Bond	d/pm
Al(1)-O(4)	172.0(4)	F(10)-C(9)	133.8(8)	F(23)-C(12)	130.6(7)	C(8)-C(10)	149.9(11)
Al(1)-O(2)	173.0(4)	F(11)-C(10)	131.8(9)	F(24)-C(12)	133.1(6)	C(13)-N(2)	129.6(8)
Al(1)-O(1)	173.5(4)	F(12)-C(10)	121.8(12)	O(1)-C(8)	137.1(6)	C(13)-N(1)	132.6(8)
Al(1)-O(3)	173.9(4)	F(13)-C(10)	136.7(10)	O(2)-C(2)	135.4(7)	C(14)-C(15)	129.7(10)
F(1)-C(5)	134.9(8)	F(14)-C(4)	132.9(7)	O(3)-C(3)	137.6(6)	C(14)-N(2)	137.7(8)
F(2)-C(11)	129.3(10)	F(15)-C(4)	131.9(7)	O(4)-C(6)	137.1(6)	C(15)-N(1)	135.2(8)
F(3)-C(5)	133.8(11)	F(16)-C(7)	133.8(7)	C(1)-C(3)	150.2(8)	C(16)-C(18)	145.9(11)
F(4)-C(9)	132.1(8)	F(17)-C(7)	130.0(7)	C(2)-C(11)	150.4(10)	C(16)-N(2)	148.2(8)
F(5)-C(5)	123.3(10)	F(18)-C(7)	131.8(7)	C(2)-C(9)	151.7(10)	C(17)-N(1)	146.1(8)
F(6)-C(11)	133.5(9)	F(19)-C(1)	131.5(7)	C(3)-C(12)	152.1(8)	C(18)-C(19)	130.0(10)
F(7)-C(11)	129.5(10)	F(20)-C(1)	132.6(7)	C(4)-C(6)	151.0(9)	C(19)-C(20)	151.6(10)
F(8)-C(4)	131.4(7)	F(21)-C(1)	132.0(7)	C(5)-C(8)	150.8(10)		
F(9)-C(9)	126.4(8)	F(22)-C(12)	132.5(6)	C(6)-C(7)	151.0(8)		

**Tab.52** Selected angles for *bmimAl(hfip)<sub>4</sub>*

Angle	d/°	Angle	d/°
O(4)-Al(1)-O(2)	109.33(19)	F(3)-C(5)-C(8)	107.8(8)
O(4)-Al(1)-O(1)	112.04(19)	F(1)-C(5)-C(8)	110.3(9)
O(2)-Al(1)-O(1)	109.13(19)	O(4)-C(6)-C(7)	109.3(5)
O(4)-Al(1)-O(3)	108.28(19)	O(4)-C(6)-C(4)	110.4(5)
O(2)-Al(1)-O(3)	110.00(19)	C(7)-C(6)-C(4)	111.3(6)
O(1)-Al(1)-O(3)	108.04(17)	F(17)-C(7)-F(16)	105.9(6)
C(8)-O(1)-Al(1)	131.5(3)	F(18)-C(7)-F(16)	105.7(6)
C(2)-O(2)-Al(1)	133.5(4)	F(17)-C(7)-C(6)	115.2(6)
C(3)-O(3)-Al(1)	127.7(3)	F(18)-C(7)-C(6)	112.9(6)
C(6)-O(4)-Al(1)	131.7(3)	F(16)-C(7)-C(6)	109.2(6)
F(19)-C(1)-F(21)	106.4(6)	O(1)-C(8)-C(10)	111.5(6)
F(19)-C(1)-F(20)	105.8(6)	O(1)-C(8)-C(5)	108.6(5)
F(21)-C(1)-F(20)	106.8(6)	C(10)-C(8)-C(5)	111.9(7)
F(19)-C(1)-C(3)	110.8(6)	F(9)-C(9)-F(4)	110.0(9)
F(21)-C(1)-C(3)	113.4(6)	F(9)-C(9)-F(10)	107.2(7)
F(20)-C(1)-C(3)	113.1(6)	F(4)-C(9)-F(10)	105.0(8)
O(2)-C(2)-C(11)	109.1(6)	F(9)-C(9)-C(2)	113.4(8)
O(2)-C(2)-C(9)	109.0(6)	F(4)-C(9)-C(2)	109.3(6)
O(3)-C(3)-C(1)	109.7(5)	F(10)-C(9)-C(2)	111.6(7)
O(3)-C(3)-C(12)	108.6(5)	F(12)-C(10)-F(11)	113.0(9)
C(1)-C(3)-C(12)	112.5(5)	F(12)-C(10)-F(13)	105.4(10)
F(8)-C(4)-F(15)	106.9(6)	F(11)-C(10)-F(13)	101.2(9)
F(8)-C(4)-F(14)	105.4(6)	F(12)-C(10)-C(8)	117.4(9)
F(15)-C(4)-F(14)	107.7(6)	F(13)-C(10)-C(8)	105.2(8)
F(8)-C(4)-C(6)	113.6(6)	F(2)-C(11)-F(7)	107.7(10)
F(15)-C(4)-C(6)	112.7(6)	F(2)-C(11)-F(6)	108.8(9)
F(14)-C(4)-C(6)	110.2(6)	F(7)-C(11)-F(6)	106.3(9)
F(5)-C(5)-F(3)	109.8(11)	F(2)-C(11)-C(2)	113.4(8)
F(5)-C(5)-F(1)	109.7(9)	F(7)-C(11)-C(2)	109.5(8)
F(3)-C(5)-F(1)	105.5(8)	F(6)-C(11)-C(2)	110.8(8)
F(5)-C(5)-C(8)	113.5(8)	F(23)-C(12)-F(22)	106.5(6)
F(23)-C(12)-F(24)	108.3(6)	C(19)-C(18)-C(16)	127.4(9)
F(22)-C(12)-F(24)	105.6(5)	C(18)-C(19)-C(20)	124.5(10)
F(23)-C(12)-C(3)	111.3(5)	C(13)-N(1)-C(15)	107.0(7)
F(22)-C(12)-C(3)	112.3(5)	C(13)-N(1)-C(17)	126.3(8)
F(24)-C(12)-C(3)	112.6(5)	C(15)-N(1)-C(17)	126.7(8)
N(2)-C(13)-N(1)	109.1(7)	C(13)-N(2)-C(14)	108.1(7)
C(15)-C(14)-N(2)	106.8(7)	C(13)-N(2)-C(16)	125.8(7)
C(14)-C(15)-N(1)	109.1(7)	C(14)-N(2)-C(16)	126.1(9)
C(18)-C(16)-N(2)	114.5(7)		

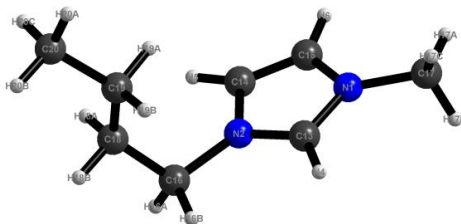


**Fig.65** Conformation of the butyl chain in *bmimAl(hfip)<sub>4</sub>*

In figure 65 is shown the adopted orientation of the butyl chain. The angle between imidazolium ring plane and C<sub>(18)</sub>,C<sub>(16)</sub> atoms from the alkyl chain is 114.55°, and the two remained C-C-C angles in the butyl chain are 124.48° (<C<sub>(18)</sub>C<sub>(19)</sub>C<sub>(20)</sub>) and 127.29° (<C<sub>(16)</sub>C<sub>(18)</sub>C<sub>(19)</sub>). The catenary torsion angle is 45.027° in the C<sub>4</sub> alkyl chains (gauche-like conformation).

**Tab.53** Atomic coordinates and equivalent isotropic displacement parameters (Å<sup>2</sup>)

Atom	x/a	y/b	z/c	U <sub>eq</sub>
Al(1)	0.2595(1)	0.2312(1)	0.0390(1)	0.058(1)
F(1)	0.3300(3)	0.5098(4)	-0.1679(2)	0.158(2)
F(2)	0.5111(4)	0.3650(7)	0.0907(4)	0.209(3)
F(3)	0.2118(6)	0.4238(7)	-0.1707(3)	0.245(4)
F(4)	0.3773(4)	0.0800(4)	0.1761(3)	0.163(2)
F(5)	0.3200(5)	0.3207(5)	-0.1566(3)	0.212(3)
F(6)	0.4819(3)	0.4106(5)	0.2027(3)	0.197(3)
F(7)	0.4117(5)	0.4789(5)	0.1127(4)	0.230(3)
F(8)	0.0482(2)	0.1591(4)	0.1870(2)	0.112(1)
F(9)	0.4905(4)	0.1288(6)	0.1269(4)	0.215(3)
F(10)	0.4661(3)	0.1808(5)	0.2364(3)	0.181(2)
F(11)	0.2818(4)	0.6441(4)	-0.0550(3)	0.191(2)
F(12)	0.1643(4)	0.5611(5)	-0.0561(5)	0.241(4)
F(13)	0.2380(4)	0.5553(5)	0.0380(5)	0.199(3)
F(14)	0.0402(2)	0.1637(4)	0.0702(2)	0.131(2)
F(15)	-0.0195(2)	0.2993(4)	0.1346(2)	0.135(2)
F(16)	0.2047(3)	0.4536(4)	0.1865(2)	0.137(2)
F(17)	0.1578(3)	0.3157(4)	0.2544(2)	0.124(2)
F(18)	0.0778(3)	0.4504(4)	0.2128(2)	0.127(1)
F(19)	0.3852(2)	0.0832(4)	-0.0915(2)	0.133(2)
F(20)	0.3453(2)	-0.0940(4)	-0.0696(3)	0.130(2)
F(21)	0.3216(3)	-0.0144(4)	-0.1752(2)	0.144(2)
F(22)	0.1818(2)	-0.1254(3)	-0.0419(2)	0.100(1)
F(23)	0.1032(2)	0.0225(4)	-0.0632(2)	0.121(1)
F(24)	0.1628(2)	-0.0672(3)	-0.1528(2)	0.115(1)

(continuation)

O(1)	0.2348(2)	0.3360(3)	-0.0294(2)	0.069(1)
O(2)	0.3588(2)	0.2582(4)	0.0716(2)	0.083(1)
O(3)	0.2535(2)	0.0883(3)	-0.0006(2)	0.062(1)
O(4)	0.1924(2)	0.2369(3)	0.1121(2)	0.072(1)
C(1)	0.3236(4)	0.0079(7)	-0.1031(4)	0.087(2)
C(2)	0.3917(4)	0.2795(6)	0.1400(4)	0.078(2)
C(3)	0.2443(3)	0.0595(5)	-0.0746(3)	0.059(2)
C(4)	0.0480(4)	0.2334(7)	0.1300(4)	0.090(2)
C(5)	0.2871(7)	0.4168(9)	-0.1393(6)	0.131(3)
C(6)	0.1253(4)	0.3089(5)	0.1252(3)	0.067(2)
C(7)	0.1403(5)	0.3799(7)	0.1958(4)	0.090(2)
C(8)	0.2777(4)	0.4326(5)	-0.0566(4)	0.076(2)
C(9)	0.4333(5)	0.1655(9)	0.1683(5)	0.112(2)
C(10)	0.2365(8)	0.5496(8)	-0.0379(7)	0.138(3)
C(11)	0.4508(7)	0.3837(10)	0.1356(6)	0.132(3)
C(12)	0.1723(4)	-0.0275(6)	-0.0834(4)	0.076(2)
C(13)	0.2839(6)	0.8669(6)	0.1198(4)	0.081(2)
C(14)	0.2586(7)	0.7653(8)	0.2197(4)	0.102(2)
C(15)	0.3323(6)	0.7374(7)	0.1983(5)	0.099(2)
C(16)	0.1465(5)	0.9084(7)	0.1723(5)	0.123(3)
C(17)	0.4255(5)	0.7938(7)	0.0934(4)	0.131(3)
C(18)	0.0761(6)	0.8287(11)	0.1590(6)	0.164(4)
C(19)	0.0681(5)	0.7473(9)	0.1072(7)	0.168(4)
C(20)	-0.0079(5)	0.6696(7)	0.0954(5)	0.142(3)
N(1)	0.3492(4)	0.7988(6)	0.1354(4)	0.085(2)
N(2)	0.2280(4)	0.8481(5)	0.1693(4)	0.086(2)

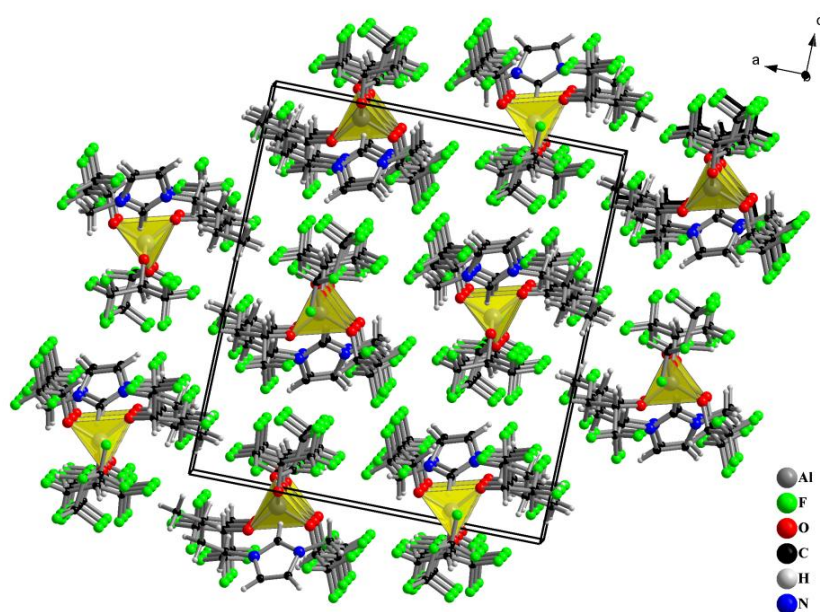


**Fig.66** Crystal structure of *bmimAl(hfip)<sub>4</sub>* -view along crystallographic axis *b*

No  $\pi$ - $\pi$  interactions occur in  $bmimAl(hfip)_4$ , since the imidazolium rings are at a distance of 1108.7 pm from each other, practically isolated in solid state, as it is possible to see in fig.67.

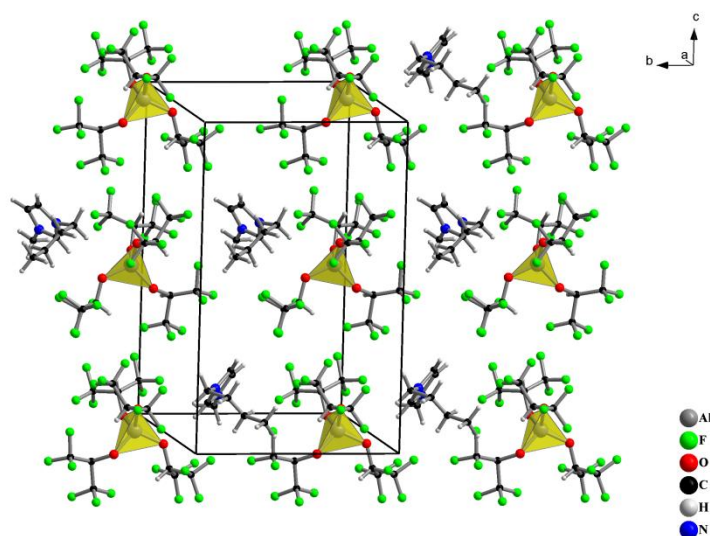


**Fig.67** Crystal structure of  $bmimAl(hfip)_4$  -view along crystallographic axis a

The shortest H $\cdots$ F distances are 241.34 pm and 245.39 pm in the hexafluoroisopropoxy unit. Between the fluorine atoms of the anion and the protons of the cation, the H $\cdots$ F distances are in the 266.17 pm – 284.43 pm range.

#### 4.2.2.3 IR/Raman spectroscopy

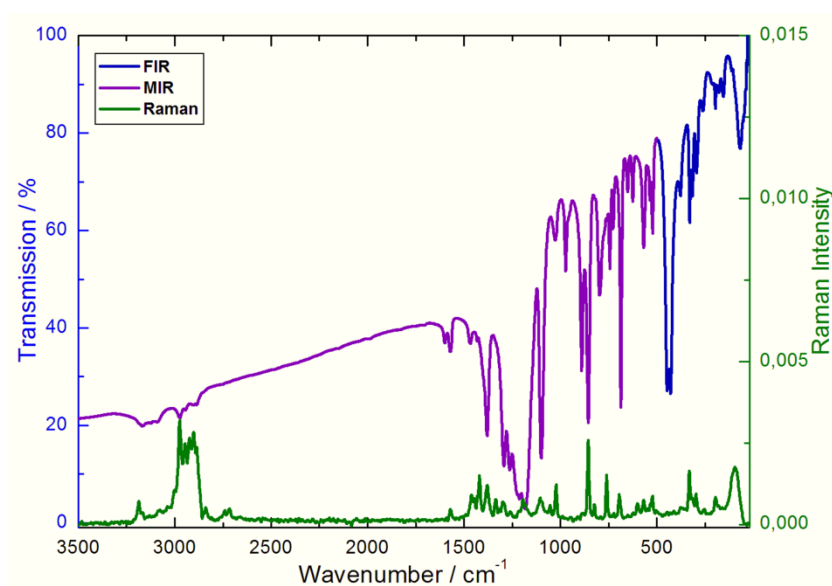


**Fig.68** FIR/MIR and Raman spectra of  $bmimAl(hfip)_4$

**Tab.54** Assignment of vibrational frequencies in the IR/Raman spectra of *bmimAl(hfip)<sub>4</sub>*

IR			Raman	
Wavenumber /cm <sup>-1</sup>	Intensity	Assignment	Wavenumber /cm <sup>-1</sup>	Intensity
68	m		-	
-			95	s
155	w		-	
197	w		197	m
294	m	ν Al-O	294	m
331	m		331	s
429	s		429	w
447	s		447	w
523	m		522	m
569	m	ν Al-O	569	m
-			600	m
625	w	C-N-C(ring)	625	w
652	w	N-C-C(chain)	652	w
686	s	ν Al-O	686	m
727	w		727	w
744	m	=C-H(ring)	-	
760	m		760	s
796	m		796	w
-			824	m
856	s	-CH <sub>2</sub> -	856	s
891	s	ν C-C(hfip)	891	w
974	m	ν Al-O; ν C-O	-	
1030	w	ν C-O	1030	s
-		C-C(chain)	1053	m
1101	s		1101	m
1184	s	ν C-O	1184	m
1263	s	-CF <sub>3</sub>	1263	w
1294	s		1294	m
1381	s		1381	s
-			1419	s
1469	w	C-N-C(ring)	1469	m
1572	w	C-C(ring)	1572	w
1599	w		-	
-			2715	w
2897	w	ν -CH <sub>2</sub> - ν -CH <sub>3</sub> ν CH	2897	s
2903	s		2903	s
2972	w		2972	s
3093	w		3093	w
3167	w		3167	w
3186	m		3186	m

\*w/m/s refer to the intensity of the peaks and are the abbreviations from w=weak; m=medium; s=strong

The assignment of the peaks was made using IR/Raman tables [9], and literature values for similar compounds (which contain either the cation, or the anion of the discussed ionic liquids) [10][11]. Poor transmission in IR spectra does not permit to achieve a proper interpretation in the C-H stretching region (peaks above 2500 cm<sup>-1</sup>), which would have been useful in evaluating the extent of hydrogen bonding in this ionic liquid. On the other side, the Raman spectra possesses a sufficient quality to allow an interpretation in the above specified

region. As theory shows, a hydrogen bond of the C-H...X type would weaken the C-H bond, and therefore shift the stretching peak of this bond to lower wavenumbers [12]. In contrast, weakly coordinating anions are poor hydrogen bond acceptors, and should lead to a “stabilization” of the C-H bond, therefore a shifting of the C-H stretching peak to higher wavenumbers should occur. Indeed, by comparing the last peak of the Raman spectra ( $3186\text{ cm}^{-1}$ , attributed to C-H stretching vibrations) with the analogue peak from the spectra of *bmimCl* ( $3153\text{ cm}^{-1}$ ) [13], it is evident the shifting to higher wavenumbers, hence weaker hydrogen bonds.

### 4.2.3 Physico-chemical properties

#### 4.2.3.1 Differential scanning calorimetry

The thermal behavior of *bmimAl(hfip)<sub>4</sub>* was investigated from  $-60^{\circ}\text{C}$  to  $140^{\circ}\text{C}$ . This ionic compound melts endothermic at  $34.15^{\circ}\text{C}$ , and because it has a melting point below  $100^{\circ}\text{C}$ , formally belongs to the class of ionic liquids. Supercooling occurs with a difference between melting point and crystallization point of  $53.37^{\circ}\text{C}$  (the crystallization takes place at  $-19.22^{\circ}\text{C}$ ). No glass phase transition could be observed in this thermal segment, with the applied heating/cooling rate of  $5^{\circ}\text{C}/\text{min}$ . Moreover, no decomposition in the above given domain was detected, and the measurement runs are fully reversible.

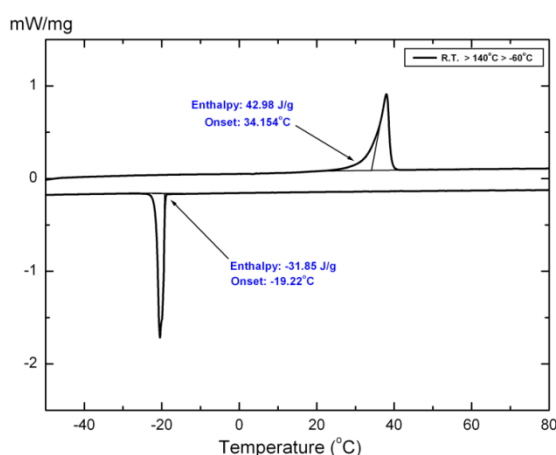


**Fig.69** DSC-Thermogram of *bmimAl(hfip)<sub>4</sub>*

The compound is at room temperature liquid, but with a very high viscosity.

In this metastable liquid state, the compound has an opaque white-pale gray color.

#### 4.2.3.2 Cyclic voltammetry

The electro-chemical stability of the alkyl-imidazolium based ionic liquids, toward reduction, is known in many cases, and it is expected to be in the region -3.5V to -4V [1]. Nevertheless, theoretical studies on the stability of the fluorinated alkoxyaluminates, predict that the low energy of HOMO level makes the compound resistant toward oxydation [8].

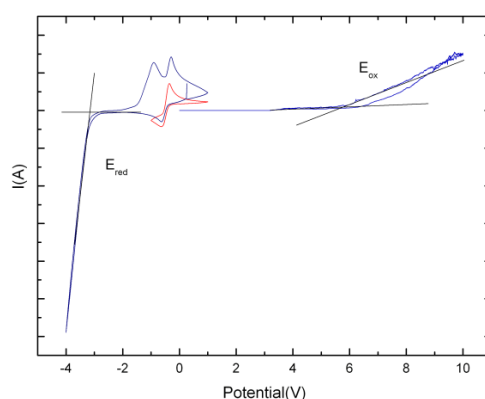


**Fig.70** Cyclic voltammogram of *bmimAl(hfip)<sub>4</sub>*

As it can be seen in figure 70, the reduction of the substituted imidazolium cation starts at approximately -2.26 V, while the oxidation of the anion starts with a slow ascending curve at approximately +6.64 V (vs. Fc/Fc<sup>+</sup>, used as internal standard). This is in accordance with computational study, for the case of the fluorinated anion, since oxidation occurs late, at high potentials. Therefore the ionic liquid shows an incredibly wide potential window (almost 9 V), which would make it suitable for electrochemical applications. It is one of the widest known to date ionic liquid potential window [1]. A small amount of Cl<sup>-</sup> (in form of LiCl impurity) was removed electrochemically, however an oxidative peak can be observed in the 0 V to -1 V range. This impurity should be removable through additional purification steps.

#### 4.2.3.3 Viscosity

For potential applications as reaction medium, the viscosity of the molten *bmimAl(hfip)<sub>4</sub>* was analyzed. The kinematic viscosity was measured in the glove box, by using a self-designed silicone oil thermostat-bath system, coupled with an Ubbelohde

viscosimeter (Schott AG, Germany) which was immersed (measuring region and reservoir section) and stabilized in the oil bath. The temperature was set to 60°C, and three measurements were run. The arithmetic mean value for the kinematic viscosity is 7.85 mm<sup>2</sup>/s (cSt), surprisingly when compared to other ionic liquids with fluorinated anions (e.g. *bmimBF<sub>4</sub>* at 60°C have a kinematic viscosity of 20 mm<sup>2</sup>/s) [14].

### 4.3 1-butyl-1-methylpyrrolidinium tetrakis(hexafluoroisopropyl)aluminate

#### 4.3.1 Preparation

*BmpyrrCl* and *LiAl(hfip)<sub>4</sub>* were mixed under inert atmosphere in a 1.021:1 molar ration (14.244 mmol of *LiAl(hfip)<sub>4</sub>*, and 13.949 mmol *bmpyrrCl*), and introduced into a Schlenk flask; 45 ml dry CH<sub>2</sub>Cl<sub>2</sub> were added. The suspension was stirred for 24 h at approximately 30°C. The obtained solution was decanted and filtrated, whereas the residual white solid powder dried under vacuum. From the filtrate the solvent (CH<sub>2</sub>Cl<sub>2</sub>) was removed under high vacuum. The estimated yield of the reaction is 91%.

Combustion analysis (CHNS) reveal the following results: calculated 30.12% C, 2.89% H, 1.67% N; measured 29.91% C, 3.86% H, 1.58% N.

The XRD-powder pattern confirms that the precipitate is lithium chloride.

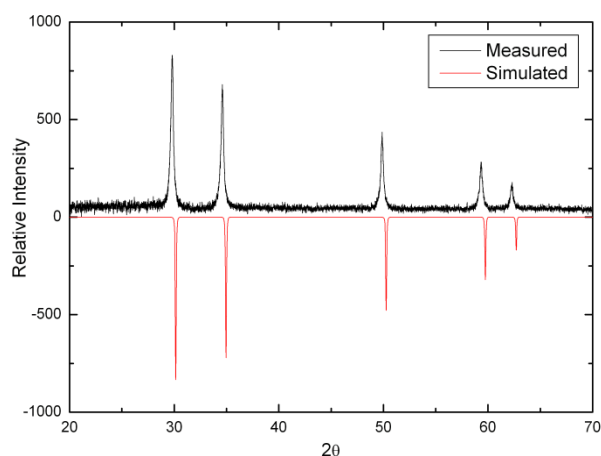


**Fig.71** XRD-powder pattern of rest, compared with the simulated XRD-powder pattern of LiCl (measured on Stoe Stadi P diffractometer/ CuK $\alpha$  radiation)

### 4.3.2 Structural aspects

#### 4.3.2.1 $^{27}\text{Al}$ -, $^{19}\text{F}$ - and $^1\text{H}$ - NMR

In order to get structural information about the product, and also to check the purity of this one,  $^{27}\text{Al}$ -,  $^{19}\text{F}$ - and  $^1\text{H}$ -NMR were measured. Deuterated chloroform was used as a solvent for the NMR measurements.

$^{27}\text{Al}$ -NMR spectrum consists of one peak, as expected, and confirms that in solution exists only one type of chemical environment for aluminium. By  $\text{LiAl}(\text{hfiip})_4$ , this peak shows at 59.9 ppm; in the case of  $\text{bmpyrrAl}(\text{hfiip})_4$  the peak appears at 59.726 ppm. The broad “hill” which appears in spectrum is associated to aluminium oxide found in glass (NMR tube).

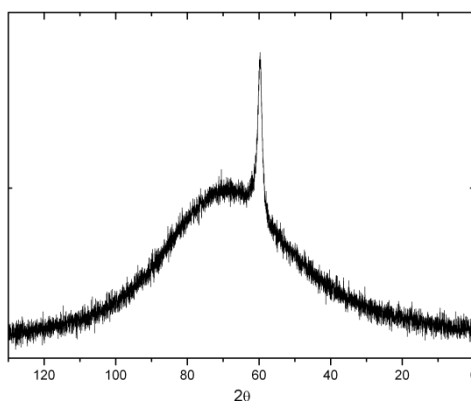


**Fig.72**  $^{27}\text{Al}$ -NMR of  $\text{bmpyrrAl}(\text{hfiip})_4$

The  $^{19}\text{F}$ -NMR spectrum contains a doublet at -76.955 ppm, and an impurity (doublet) at -75.707 ppm. The ratio between product peak and the impurity is approximately 59:1. Coupling constants are the same for product and impurity, namely 6.131 Hz. One conclusion might be, that this impurity contains the hexafluoroisopropyl fragment.

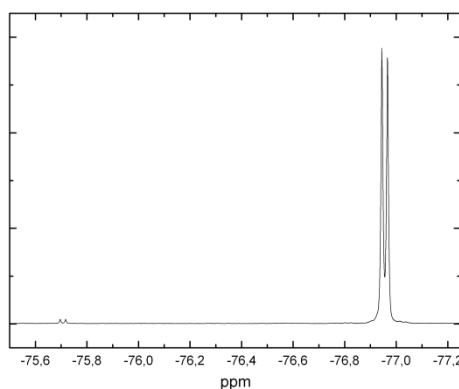


**Fig.73**  $^{19}\text{F}$ -NMR of  $\text{bmpyrrAl}(\text{hfiip})_4$

The  $^1\text{H-NMR}$  spectrum of  $\text{bmpyrrAl}(\text{hfip})_4$  reflects the peak positions found in the NMR spectra of the educts ( $\text{bmpyrrCl}$  and  $\text{LiAl}(\text{hfip})_4$ ). Also the coupling constants were compared and the resemblance confirm, together with the chemical shift, integrals and multiplicity, the same chemical environments. A peak which could not be attributed to the product was observed at 2.1 ppm; this singlet peak could be assigned to acetonitrile, which remained in the sample after the synthesis (this can be removed under high vacuum and light heating). The peak integration was correlated to the  $\text{CH}_3$  group of butyl chain.

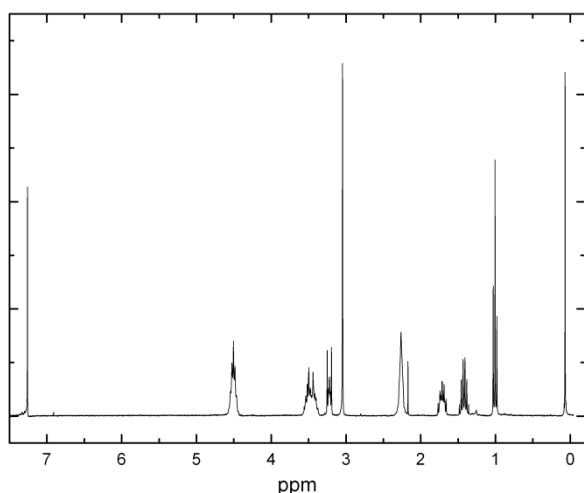


**Fig.74**  $^1\text{H-NMR}$  spectra of  $\text{bmpyrrAl}(\text{hfip})_4$

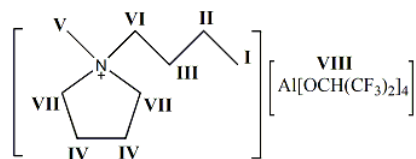


**Fig.75** Notation for identifying the protons in the  $^1\text{H-NMR}$  spectra

**Tab.55**  $^1\text{H-NMR}$  spectral data for  $\text{bmpyrrAl}(\text{hfip})_4$

Chemical shift (ppm)	Integral	Multiplicity	$^2\text{J}/^3\text{J}$ (Hz)	Atom group
1.006	3.00	t	7.176	$\text{CH}_3$ (I)
1.421	2.12	sextet	7.250	$\text{CH}_2$ (II)
1.713	2.05	p	7.648	$\text{CH}_2$ (III)
2.264	3.91	(s-broad)/m	-	$\text{CH}_2$ (IV)
3.046	2.92	s	-	$\text{CH}_3$ (V)
3.221	1.98	m	-	$\text{CH}_2$ (VI)
3.468	4.00	m	-	$\text{CH}_2$ (VII)
4.504	3.91	septet	5.665	CH (VIII)
7.26	-	s	-	$\text{CDCl}_3$

## 4.3.2.2 IR/Raman spectroscopy

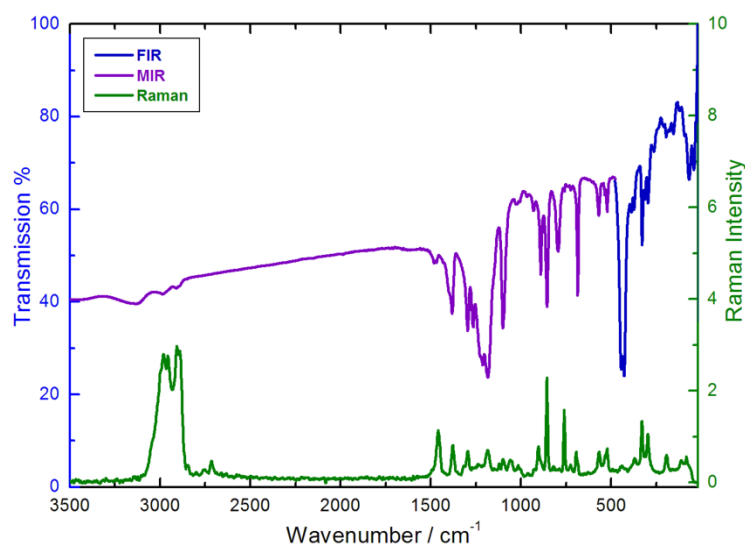


**Fig.76** FIR/MIR and Raman spectra of *bmpyrrAl(hfip)<sub>4</sub>*

For the infrared spectrum, the comparison with *bmpyrrPF<sub>6</sub>* [15] matched almost all the peaks, the few unmatched ones being probably “masked” due to poor transmission. The same is to report for the anionic part [10]. Also the Raman spectrum was compared with literature reports [16].

**Tab.56** Assignment of vibrational frequencies in the IR/Raman spectra of *bmpyrrAl(hfip)<sub>4</sub>*

IR			Raman	
Wavenumber /cm <sup>-1</sup>	Intensity	Assignment	Wavenumber /cm <sup>-1</sup>	Intensity
42	s		-	
68	s		-	
-			83	m
-			112	m
119	w		-	
155	w		-	
-			162	w
196	w		195	m
206	w		-	
263	w		-	
296	m	ν Al-O	297	s
314	m		-	
330	s		330	s
374	m		370	m
387	m		-	
428	s		424	w
445	s		440	w
522	m		523	m
536	w		534	m
569	m		567	m
686	s	ν Al-O N-C-C(chain)	694	m

(continuation)

725	w		725	w
760	w	C-C(hfip)	760	s
794	s	=CH <sub>2</sub> (ring)	-	
-			822	w
856	s	C-C(ring)	856	s
891	s		905	m
929	w		-	
968	w	ν C-O	960	w
1020	w		1016	w
1030	w		-	
-			1061	m
1101	s	C-C(chain)	1099	m
1184	s	ν C-O	1184	m
1213	s		1238	w
1265	s	-CF <sub>3</sub> C-N-C(ring) C-C(ring)	-	
1296	s		1294	m
1383	s		1379	m
1483	w		1460	s
-			2715	m
-			2754	w
-			2798	w
-			2847	w
-		ν -CH <sub>2</sub> - ν -CH <sub>3</sub>	2891	s
2910	w		2906	s
-			2957	s
2987	w		2982	s
3136	w		-	

\*w/m/s refer to the intensity of the peaks and are the abbreviations from w=weak; m=medium; s=strong

### 4.3.3 Physico-chemical properties

#### 4.3.3.1 Differential scanning calorimetry

In this case the calorimetric measurements reveal an endothermic solid-solid transition, what is not quite a surprise, since there are reports showing that ionic liquids/molten salts containing N-alkyl-N-methylpyrrolidinium cation show often glass phase transitions, or plastic crystallinity [17][18]. The thermogram was measured in the range  $-70^{\circ}\text{C}$  to  $130^{\circ}\text{C}$ , with a cooling/heating rate of  $5^{\circ}\text{C}/\text{min}$ . No glass phase transition or decomposition was observed. The solid-solid transition occurs at  $20.6^{\circ}\text{C}$ , and the endothermic melting at  $46.8^{\circ}\text{C}$ . Supercooling can be observed also for this ionic liquid: solidification occurs at  $25.0^{\circ}\text{C}$  (the difference between peaks is  $21.8^{\circ}\text{C}$ ). *Timmermans* presented that typically plastic crystal phases have fusion entropies lower than  $20\text{ J/mol}\cdot\text{K}$  [19]. On the other side, considering more rotational degrees of freedom, it was proposed that the fusion entropy for plastic crystals could be in some cases even higher than  $20\text{ J/mol}\cdot\text{K}$ . For *bmpyrrTf<sub>2</sub>N*, (1-butyl-1-methylpyrrolidinium bis(trifluoromethanesulphonyl)imide) was found an entropy of fusion of approximately  $41\text{ J/mol}\cdot\text{K}$  [17]. For in this work reported compound, the entropy of fusion has the value of  $42.92\text{ J/mol}\cdot\text{K}$  ( $\Delta S_{\text{fusion}} = \Delta H_{\text{fusion}}/T_{\text{m}}$ ).

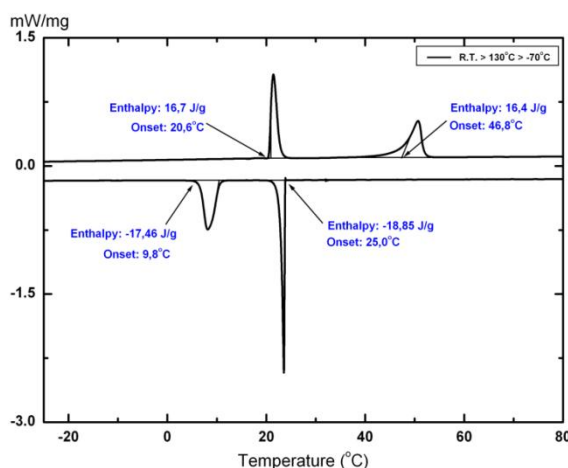


**Fig.77** DSC-Thermogram of *bmpyrrAl(hfip)<sub>4</sub>*

This is in agreement with the observation that no crystals of sufficient quality for XRD single crystal analysis could be obtained at room temperature, although the material showed

reflections on the diffractometer. To obtain measurable crystals, these should be picked at low temperatures (below 10°C). If indeed a plastic crystalline phase occurs for this ionic liquid, this should be reflected in even better ionic conductivity properties [20].

#### 4.3.3.2 Cyclic voltammetry

Similar compounds with weakly coordinating anions (first generation of WCAs), show relatively large potential windows. For example, *1-methyl-1-propylpyrrolidinium tetrafluoroborate* has a potential window of approximately 4V (-2.25V to +2.5V, vs. Ag/Ag<sup>+</sup>) [20], *1-butyl-1-methylpyrrolidinium bis(trifluoromethanesulphonyl)imide* has an even broader potential window of approximately 5V (from -3V to +2.5V, vs. Ag/Ag<sup>+</sup>) [17]. From figure 78 it can be seen that the reduction process starts for the cationic unit at approximately -3V, while the oxidation of the anion starts at +6.451V (vs. Fc/Fc<sup>+</sup>). This data reveals a potential window of approximately 9.5V, even wider than in the case of the formerly mentioned ionic liquid.

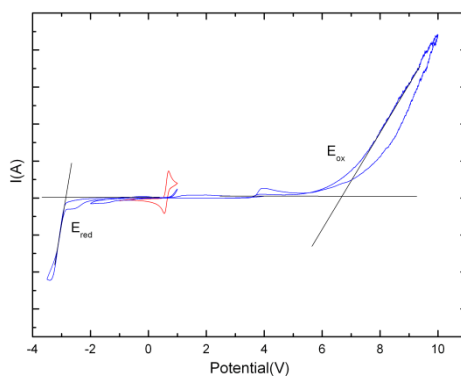


**Fig.78** Cyclic voltammogram of *bmpyrrAl(hfip)*<sub>4</sub>

#### 4.3.3.3 Viscosity

The kinematic viscosity of *bmpyrrAl(hfip)*<sub>4</sub> was measured with the same experimental setup used to measure the viscosity for the previous compound. The measurements were run in a glove box, at a temperature of 60°C. Also three measurements were undertaken, and the arithmetic mean value is 12.92 mm<sup>2</sup>/s (cSt). Like for *bmimAl(hfip)*<sub>4</sub>, the viscosity of *bmpyrrAl(hfip)*<sub>4</sub> is far smaller than for analogous compounds. For example, the dynamic

viscosity of *bmpyrrTf<sub>2</sub>N* at 60°C is approximately 70 mPa·s [21], and the density of *bmpyrrTf<sub>2</sub>N* at 25°C is 1.41 g/cm<sup>3</sup> [1] (no density of this ionic liquid was reported for the temperature of 60°C). However, it is known that the density of ionic liquids is the physical parameter which varies the least with temperature [1]. Therefore for the calculation of the kinematic viscosity this density (at 25°C) was considered. In consequence the approximative density at 60°C would be around 49.64 mm<sup>2</sup>/s. Even if the density of *bmpyrrTf<sub>2</sub>N* will drop at 60°C to half of the above given value, the viscosity of *bmpyrrAl(hfip)<sub>4</sub>* is still much lower than that of *bmpyrrTf<sub>2</sub>N* (the formula to calculate the kinematic viscosity,  $\nu$ , from the dynamic viscosity,  $\eta$ , is  $\nu = \eta/\rho$ , where  $\rho$  is the density of the respective substance).

#### 4.4 Summary

The two above presented ionic liquids have application potential as versatile electrolytes, in different electrochemical applications (batteries, solar cells, electrochemical processes, etc.). The melting points are low (almost room-temperature ionic liquids), due to weak interactions between cationic and anionic parts: first of all the hydrogen bonds are proved to be very weak in these two ILs (comparing to, for example, *bmimCl* or *bmpyrrCl*), the alkyl chains from the cations are not long enough to produce a raise in the melting point (van der Waals interactions), but enough long to produce a given disorder, which sinks the melting point, the volumes of the both cationic and anionic entities are quite big, influencing the coulombic forces between charges; finally, the symmetry of the anion could be approximated as spherical, whereby the cation does not present such a symmetry. No  $\pi$ - $\pi$  interactions were observed, and as a proof (since anions are the same, and for *bmpyrrAl(hfip)<sub>4</sub>* no crystallographic structural data are available), both ILs melt at comparatively similar temperatures compared to each other (34.15°C for *bmimAl(hfip)<sub>4</sub>*, and 46.8°C for *bmpyrrAl(hfip)<sub>4</sub>*). But the greatest advantages of these two compounds are the broad potential windows (approximately 9 V in both cases), and also very low viscosities in the liquid phase

(hence good transport properties). It must be said that the viscosity is very low as soon as the compounds melt. Another advantage is the facile preparation and separation from the by-product. Although LiCl was discovered in the product fraction, its small amounts can be removed by a few several purifying steps. A disadvantage of these two ILs is that the anionic unit is unstable toward hydrolysis [6]. Therefore these ionic liquids are moisture sensitive. Thermally, the stability was checked until 130-140°C, without observing any decomposition peaks in the DSC analysis. General studies [1] suggest that weakly coordinating anions should bring the thermal stability of the ionic liquids to the edge (in this case probably 300-400°C, supported by the heterocyclic segment). This conclusion should be verified however by further measurements (thermogravimetric analysis).

#### 4.5 Literature

- [1] P. Wasserscheid, T. Welton, *Ionic Liquids in Synthesis, 2nd Edition*, VCH, Weinheim, **2008**.
- [2] T. Timofte, S. Pitula, A.-V. Mudring, *Inorg. Chem. (Washington, DC, U.S.)* **2007**, *46*, 10938-10940.
- [3] J. S. Wilkes, J. A. Levisky, R. A. Wilson, C. L. Hussey, *Inorg. Chem. (Washington, DC, U.S.)* **1982**, *21*, 1263-1264.
- [4] P. A. Z. Suarez, S. Einloft, J. E. L. Dullius, R. F. de Souza, J. Dupont, *Journal de Chimie Physique et de Physico-Chimie Biologique* **1998**, *95*, 1626-1639.
- [5] L. Crowhurst, N. L. Lancaster, J. M. Perez-Arlandis, T. Welton, *J. Am. Chem. Soc.* **2004**, *126(37)*, 11549-11555.
- [6] I. Krossing, *Chem.--Eur. J.* **2001**, *7(2)*, 490-502.
- [7] D. D. Perrin, W. L. F. Armarego, *Purification of Laboratory Chemicals (3<sup>rd</sup> Edition)*, Pergamon Press, **1988**.
- [8] I. Krossing, I. Raabe, *Chem.--Eur. J.* **2004**, *10*, 5017-5030.
- [9] J. Weidlein, U. Müller, K. Dehnicke, *Schwingungsfrequenzen I-Hauptgruppenelemente*, Georg Thieme, Stuttgart, **1981**.
- [10] A. Bihlmeier, M. Gonsior, I. Raabe, N. Trapp, I. Krossing, *Chem.--Eur. J.* **2004**, *10*, 5041-5051.
- [11] R. W. Berg, M. Deetlefs, K. R. Seddon, I. Shim, J. M. Thompson, *J. Phys. Chem. B*, **2005**, *109*, 19018-19025.
- [12] A. Elaiwi, P. B. Hitchcock, K. R. Seddon, N. Srinivasan, Y. M. Tan, T. Welton, J. A. Zora, *J. Chem. Soc., Dalton Trans.*, **1995**, *21(1)*, 3467-3472.
- [13] M. B. Alves, V. O. Santos Jr., V. C. D. Soares, P. A. Z. Suarez, J. C. Rubim, *J. Raman Spectrosc.* **2008**, *39(10)*, 1388-1395.
- [14] K. R. Harris, M. Kanakubo, L. A. Woolf, *J. Chem. Eng. Data* **2007**, *52*, 2425-2430.

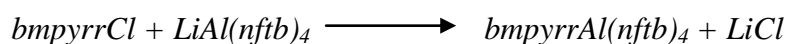
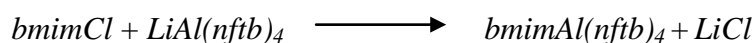
- [15] J. Golding, N. Hamid, D. R. MacFarlane, M. Forsyth *et al.*, *Chem. Mater.* **2001**, *13*, 558-564.
- [16] O. B. Babushkina, S. Ekres, G. E. Nauer, *J. Phys. Chem. A* **2008**, *112*, 8288-8294.
- [17] D. R. MacFarlane, P. Meakin, J. Sun, N. Amini, M. Forsyth, *J. Phys. Chem. B* **1999**, *103*, 4164-4170.
- [18] W. A. Henderson, V. G. Young Jr., W. Pearson, S. Passerini, H. C. De Long, P. C. Trulove, *J. Phys.: Condens. Matter* **2006**, *18*, 10377-10390.
- [19] J. Timmermans, *J. Phys. Chem. Solids* **1961**, *18*, 1-8.
- [20] S. Forsyth, J. Golding, D. R. MacFarlane, M. Forsyth, *Electrochim. Acta* **2001**, *46*, 1753-1757.
- [21] J. Salminen, N. Papaiconomou, R. A. Kumara, J.-M. Lee *et al.*, *Fluid Phase Equilib.* **2007**, *261*, 421-426.

## 5. Molten salts with weakly coordinating anions

### 5.1 General preparation

The preparation methods are identical with those presented in the same section of the previous chapter. All the work was carried under inert conditions, using dry chemicals. As solvent was used dry dichloromethane. The synthesis of *1-butyl-3-methylimidazolium chloride* (*bmimCl*) and *1-butyl-1-methylpyrrolidinium chloride* (*bmpyrrCl*) was presented in the section 4.1.

The reaction schemes are:



Lithium tetrakis(nonafluoro-tert-butyl)aluminate was prepared according to literature [1]: to a suspension of LiAlH<sub>4</sub> (purified) in toluene, nonafluoro-tert-butanol was added under argon stream at 0°C, stepwise, in a molar ratio LiAlH<sub>4</sub>:(CF<sub>3</sub>)<sub>3</sub>COH = 1:4 (gas evolution). After adding the complete amount of alcohol, the solution was refluxed for approximately 12 hours. Then the solution was set aside to cool; the clear transparent solution at room temperature was cooled further to -20°C and stirred, until the product crystallizes. The product was decanted at -20°C, and the remaining solvent removed by applying high vacuum for several hours. After this step, the product was sublimed twice under low pressure at 150°C. <sup>27</sup>Al- and <sup>19</sup>F-NMR: <sup>27</sup>Al-NMR (78 MHz, CDCl<sub>3</sub>) δ(ppm) = 34.485(s); <sup>19</sup>F-NMR (282 MHz, CDCl<sub>3</sub>) δ(ppm) = -75.63(s), and two small impurity peaks at -75.534(s), respectively at -76.739(s, broad) ppm. The ratio between product and impurity can be increased through multiple sublimations.

## 5.2 1-butyl-3-methylimidazolium tetrakis(nonafluoro-tert-butyl)aluminate

### 5.2.1 Preparation

*BmimCl* and *LiAl(nftb)<sub>4</sub>* were mixed in a 1:1 molar ratio (1.026 mmol), introduced in a Schlenk flask with 50 ml dry  $\text{CH}_2\text{Cl}_2$ , and stirred at 30°C for 24 h under an inert atmosphere. After this step, the clear solution was filtrated and moved to another flask. The remaining white powder was dried under vacuum and the presence of LiCl was confirmed by XRD-powder analysis (fig.79).

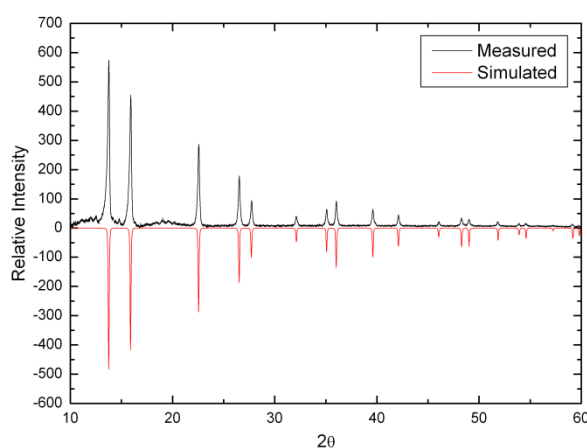


**Fig.79** XRD-Powder pattern of rest, compared with simulated powder pattern of LiCl (measured on Stoe Stadi P diffractometer/  $\text{CuK}\alpha$  radiation)

From the clear filtrate, the solvent was removed by applying vacuum and light heating; finally a white solid remained. The yield is approximately 75.24% and the amount of the residual powder was larger than calculated, suggesting that a part of the product (or educt) remained in the byproduct fraction.

Combustion analysis (CHNS analysis) also confirms the identity of the expected product: calculated 26.039% C, 2.531% N and 1.356% H; found 25.925% C, 2.455% N and 1.13% H.

## 5.2.2 Structural aspects

### 5.2.2.1 $^{27}\text{Al}$ - and $^{19}\text{F}$ - NMR

$^{27}\text{Al}$ - and  $^{19}\text{F}$ -NMR were measured. As solvent for the NMR measurements a mixture of deuterated chloroform and tetrahydrofuran in the volumic ratio of 95:5 was used.

$^{27}\text{Al}$ -NMR shows only one singlet, as in the spectrum of the educt ( $\text{LiAl}(\text{nftb})_4$ ). The chemical shift moves only 0.1 ppm upfield ( $\delta=34.353$  ppm), with respect to the educt peak.

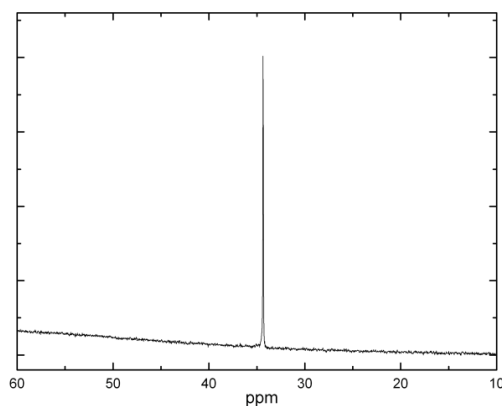


**Fig.80**  $^{27}\text{Al}$ -NMR spectrum of  $\text{bmimAl}(\text{nftb})_4$

In the  $^{19}\text{F}$ -NMR spectrum a broad singlet impurity peak ( $\delta=-76.800$  ppm) is observed, next to the product peak at  $-75.749$  ppm(s). The product and impurity peaks are shifted lightly upfield (with approximately 0.1 ppm) with respect to the educt spectrum. The ratio between product and impurity is quite low (2:1); one way to diminish the impurity amount would be to apply extra sublimation steps to  $\text{LiAl}(\text{nftb})_4$  educt. The other impurity peak observed in the  $^{19}\text{F}$ -NMR spectrum of  $\text{LiAl}(\text{nftb})_4$  was not found in this spectrum; it was obviously removed during the synthesis stages.

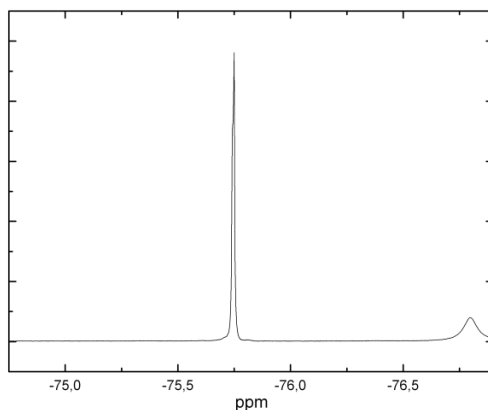


**Fig.81**  $^{19}\text{F}$ -NMR spectrum of  $\text{bmimAl}(\text{nftb})_4$

Moreover, since in literature [1] is specified that the anionic unit is stable toward hydrolysis, the product should be also hydrolysis stable (as the cationic part is hydrolysis stable). This fact was checked by measuring  $^{27}\text{Al}$ - and  $^{19}\text{F}$ -NMR spectra of a probe containing  $\text{bmimAl}(\text{nftb})_4$  mixed with distilled water, tetrahydrofuran and chloroform. The spectra show practically no change at product peaks, but there is interesting to observe that the impurity reacts with water, since the impurity peak moves downfield (less screening around fluorine atoms comparing to the precedent spectrum).

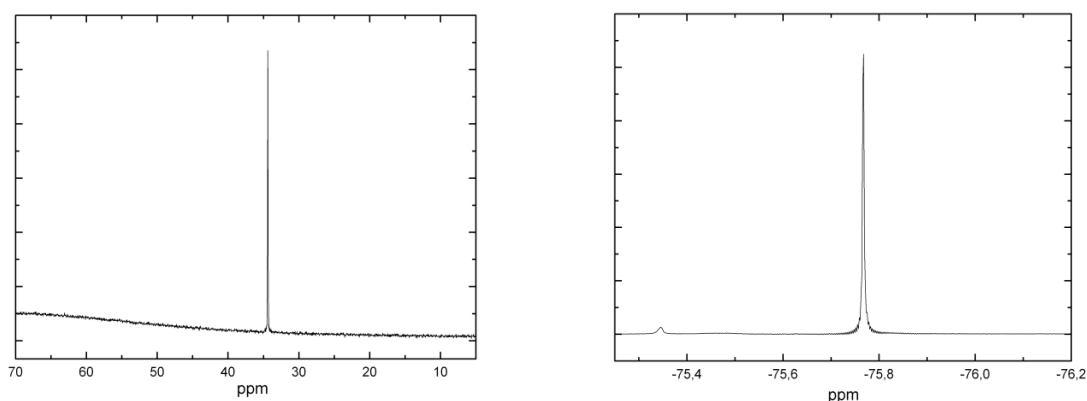


**Fig.82**  $^{27}\text{Al}$ -NMR(left) and  $^{19}\text{F}$ -NMR(right) of  $\text{bmimAl}(\text{nftb})_4$  after mixing it with water

### 5.2.2.2 IR/Raman spectroscopy

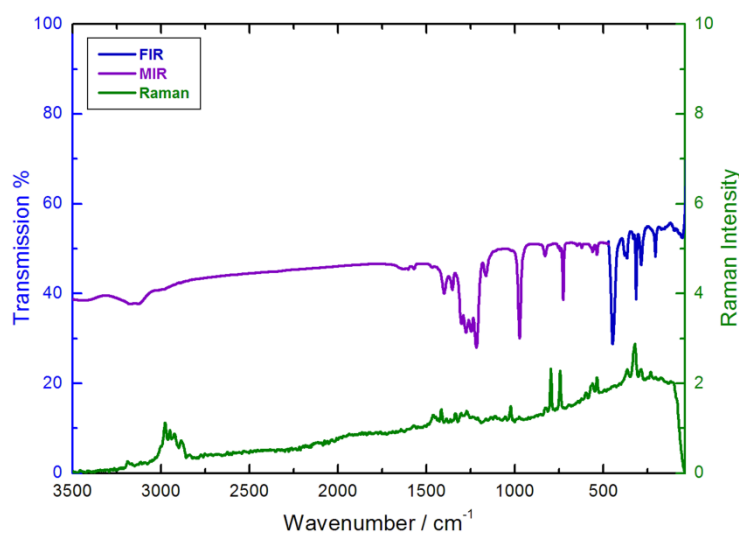


**Fig.83** FIR/MIR and Raman spectra of  $\text{bmimAl}(\text{nftb})_4$

The peaks from these spectra were assigned according to literature [2], and similar compounds containing either the anionic [1][3], or the cationic part [4]. The peaks from the

C-H stretching region are in the same range, as in the case of *bmimAl(hfip)*<sub>4</sub>, therefore can be concluded that hydrogen bonds in this compound are in the same strength level as for *bmimAl(hfip)*<sub>4</sub>.

**Tab.57** Assignment of IR/Raman vibrational frequencies for *bmimAl(nftb)*<sub>4</sub>

IR			Raman		
Wavenumber /cm <sup>-1</sup>	Intensity	Assignment	Wavenumber /cm <sup>-1</sup>	Intensity	
54	m		-		
99	m		-		
-			122	w	
170	w		-		
-			179	w	
206	m		-		
-			233	w	
287	m	ν Al-O	287	m	
315	s		-		
-			322	s	
332	w		-		
367	m		366	m	
448	s		-		
538	w		538	m	
559	w		-		
-			561	m	
-			598	w	
623	w		-		
650	w		N-C-C(chain)	-	
-			ν Al-O	692	w
727	s		-		
-			C-C(nftb)	744	s
-		ν Al-O	797	s	
-		-	825	w	
831	m	-CH <sub>2</sub> -	-		
974	s	C-C(nftb)	976	w	
-		C-C(chain)	1024	m	
-		ν C-O	-		
-		-	1055	w	
-		-	1111	w	
1165	m	-	-		
1217	s	-	1211	w	
1248	s	-CF <sub>3</sub> C-N-C(ring) C-C(ring)	-		
1277	s		1273	m	
1304	s		1306	m	
1354	m		1337	m	
1400	m		1416	m	
1471	w		1464	m	
1572	w	C-C(ring)	1574	w	
1628	w	-	-		
-		ν -CH <sub>2</sub> - ν -CH <sub>3</sub> ν =CH	2839	w	
-			2885	m	
-			2924	s	
-			2949	s	
2991	w		2976	s	
3159	m	3188	w		

\*w,m,s refer to the intensity of the peaks and are the abbreviations from w=weak; m=medium; s=strong

### 5.2.3 Physico-chemical properties

#### 5.2.3.1 Differential scanning calorimetry

The thermal behavior of  $bmimAl(nftb)_4$  was investigated in the range  $-30^\circ\text{C}$  to  $300^\circ\text{C}$ , with a heating/cooling rate of  $10^\circ\text{C}/\text{min}$ . The melting point is observed at  $149.1^\circ\text{C}$ . Crystallization starts at  $112.2^\circ\text{C}$ . The high melting point of this compound does not allow categorizing it as an ionic liquid; it will be classified as a molten salt. Supercooling takes place, with a difference between melting and crystallization point of  $36.9^\circ\text{C}$ . No further phase transitions and/or decomposition were observed in the analyzed thermal range.

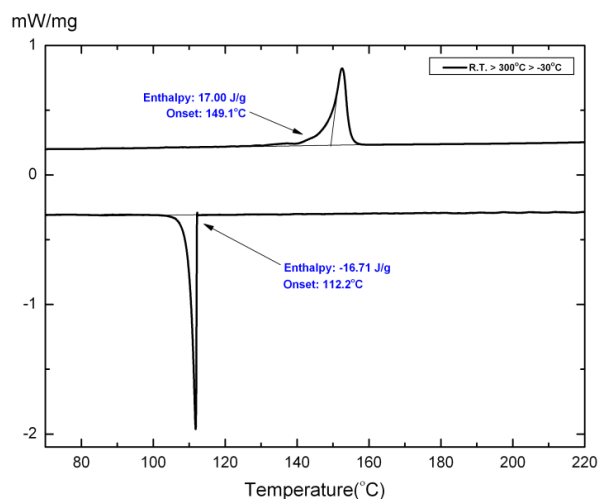


**Fig.84** DSC-thermogram of  $bmimAl(nftb)_4$

### 5.3 1-butyl-1-methylpyrrolidinium tetrakis(nonafluoro-tert-butyl)aluminate

#### 5.3.1 Preparation

$BmpyrrCl$  and  $LiAl(nftb)_4$  were mixed in a 1:1 molar ratio (1.536 mmol) under argon atmosphere, and placed together with 50 ml dry  $\text{CH}_2\text{Cl}_2$  in a Schlenk flask. The mixture was stirred at  $30^\circ\text{C}$  for 24h. Then the solution was decanted and filtered. The residual white solid was vacuum dried, with light heating. From the filtered solution, the solvent was removed under vacuum; whereas the yield is approximately 75.26%.

Combustion analysis (CHNS analysis) confirms the identity of the product: calculated 27.067% C, 1.815% H, 1.262% N; found 27.54% C, 2.13% H, 1.15% N.

The XRD-powder pattern confirmed by the presence of LiCl that metathesis had taken place (fig.85).

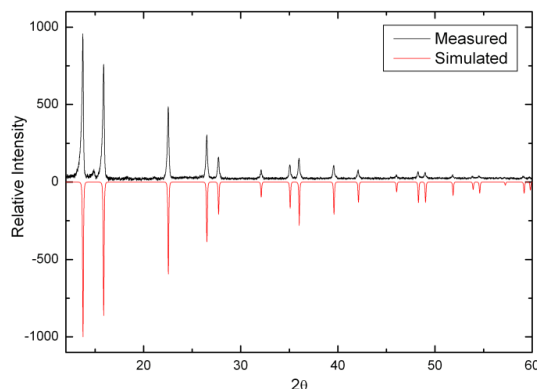


**Fig.85** XRD powder pattern of rest, compared with the simulated XRD-powder pattern of LiCl (measured on Stoe Stadi P diffractometer/ CuK $\alpha$  radiation)

### 5.3.2 Structural aspects

#### 5.3.2.1 $^{27}\text{Al}$ - and $^{19}\text{F}$ - NMR

$^{27}\text{Al}$ -NMR and  $^{19}\text{F}$ -NMR spectra were measured. For the measurements a mixture of deuterated chloroform and tetrahydrofuran (volumic ratio of 95:5) was used as a solvent.

The  $^{27}\text{Al}$ -NMR spectrum presents one singlet at 34.296 ppm, only 0.2 ppm slided compared to the spectrum of  $\text{LiAl}(\text{nftb})_4$  (fig.86).

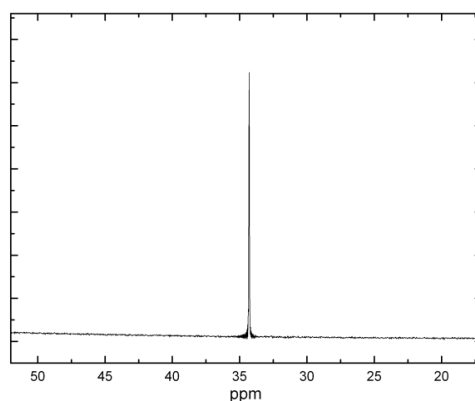


**Fig.86**  $^{27}\text{Al}$ -NMR spectrum of  $\text{bmpyrrAl}(\text{nftb})_4$

The  $^{19}\text{F}$ -NMR spectrum shows a singlet at -75.887 ppm (0.2 ppm shifted when compared with the  $^{19}\text{F}$ -NMR spectrum of the educt -  $\text{LiAl}(\text{nftb})_4$ ). In addition, a weak impurity doublet peak at -76.03 ppm is observed. The ratio between product and impurity peaks is 50:1. None of the two impurity peaks observed in the case of the educt  $\text{LiAl}(\text{nftb})_4$

are observed in the products  $^{19}\text{F}$ -NMR spectrum (fig. 87).

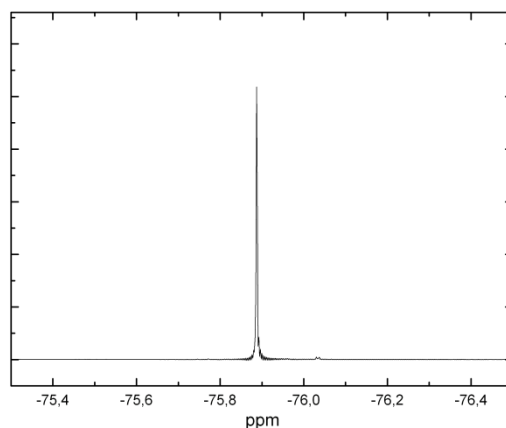


**Fig.87**  $^{19}\text{F}$ -NMR spectrum of  $\text{bmpvrrAl}(\text{nftb})_4$

### 5.3.2.2 IR/Raman spectroscopy

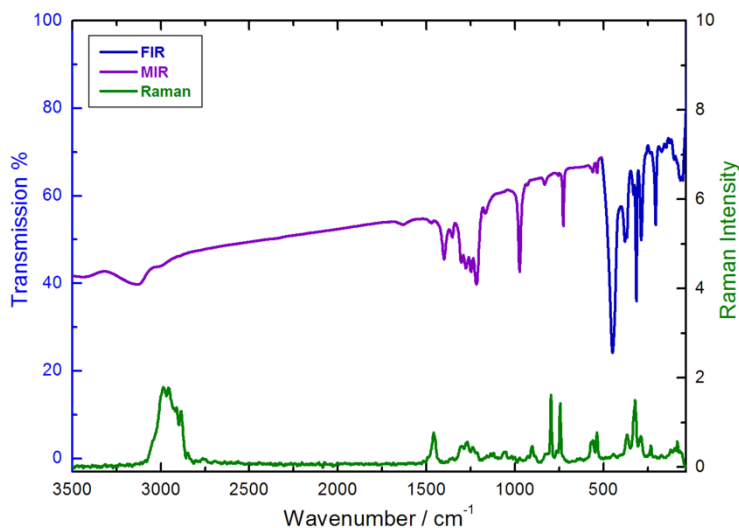


**Fig.88** FIR/MIR and Raman spectra of  $\text{bmpyrrAl}(\text{nftb})_4$

The spectra from figure 88 were analyzed using literature data [2] and similar compound IR/Raman data for the cationic part [5][6], as for the anionic part also [3]. Almost all the peaks were found to agree with the reported ones. By comparing it with the IR spectrum of  $\text{bmpyrrPF}_6$  [5], it can be observed that the C-H stretching vibrations range is (like for all compounds with weakly coordinating anions presented in this work) shifted to even higher wavenumbers (hence weaker hydrogen bonds).

**Tab.58** Assignment of the IR/Raman vibrational frequencies for bmpyrrAl(nftb)<sub>4</sub>

IR			Raman		
Wavenumber /cm <sup>-1</sup>	Intensity	Assignment	Wavenumber /cm <sup>-1</sup>	Intensity	
53	m		-		
65	m		-		
-			83	m	
-			98	m	
125	w		120	w	
146	w		-		
171	w		172	w	
206	s		-		
-			233	m	
287	s	ν Al-O	289	m	
315	s		322	s	
332	m		-		
368	s		366	m	
380	s		-		
449	s		446	w	
536	w		536	m	
561	w		561	m	
-			635	w	
727	s		-		
756	w		C-C(nftb)	744	s
-				797	s
831	w		-CH <sub>2</sub> -	829	w
-			903	m	
929	w	C-C(ring)	928	w	
974	s	C-C(nftb) C-C(chain) ν C-O	974	w	
-			1005	w	
-			1014	w	
-			1020	w	
-			1032	w	
-			1053	m	
-			1121	m	
-			1136	m	
1167	m		1159	w	
1217	s		-		
1248	s	-CF <sub>3</sub> C-N-C(ring) C-C(ring)	1238	m	
1277	s		1271	m	
1304	s		1298	m	
1354	m		1352	w	
1400	s	-			
1469	w	1460	s		
1631	w	C-C(ring)	-		
-			2764	w	
-			2849	w	
-		ν -CH <sub>3</sub> ν -CH <sub>2</sub> -	2885	s	
-			2910	s	
-			2957	s	
2995	w		2985	s	
3132	m		-		

\*w,m,s refer to the intensity of the peaks and are the abbreviations from w=weak; m=medium; s=strong

### 5.3.3 Physico-chemical properties

#### 5.3.3.1 Differential scanning calorimetry

The thermogram of  $bmpyrrAl(nftb)_4$  was recorded between  $-80^\circ\text{C}$  and  $300^\circ\text{C}$ , with a cooling/heating rate of  $5^\circ\text{C}/\text{min}$ . No solid-solid phase transition, or glass phase transition can be observed. Also, no decomposition takes place in this thermal range. Melting starts at  $201.7^\circ\text{C}$ , while supercooling occurs also, crystallization starting at  $186.2^\circ\text{C}$  (the difference between melting and crystallization is  $15.5^\circ\text{C}$ ). Due to its high melting point this compound is classified as a molten salt.

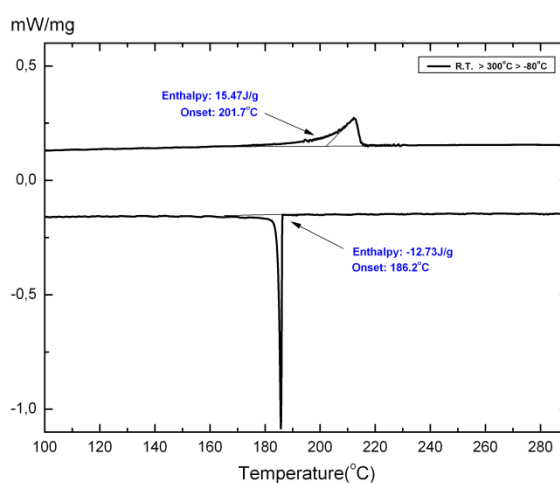


**Fig.89** DSC thermogram of  $bmpyrrAl(nftb)_4$

### 5.4 Summary

Two new molten salts,  $bmimAl(nftb)_4$  (75.24% yield) and  $bmpyrrAl(nftb)_4$  (75.26% yield) were synthesized, being categorized as molten salts because of their high melting points.

Despite the high melting point, these compounds have a high thermal stability (at least until  $300^\circ\text{C}$ ) and the advantage (comparing to their analogous ionic liquids from the previous chapter) of being stable towards hydrolysis, whereas the ionic liquids presented before are sensitive toward moisture (hydrolysis). These make them promising candidates as reaction media for numerous chemical systems.

The high melting points are a surprise, since  $[Al(nftb)_4]^-$  anion is larger than  $[Al(hfip)_4]^-$ , and the expected trend in this class of compounds would be a lowering of the melting point with increased anion size [7]. A better packing in the crystal lattice is assumed to cause these high melting points. That these molten salts possess less vibrational freedom degrees as the previously presented ionic liquids, is shown first through IR/Raman spectra, where less peaks appear, by comparing with the same spectra of  $bmimAl(hfip)_4$  and  $bmpyrrAl(hfip)_4$ . Also no other phase transitions were observed. In the Raman spectra, the stretching regions of C-H bonds suggest the existence of very weak hydrogen bonds, as in the case of the previously presented ionic liquids.

The  $[Al(nftb)_4]^-$  anion should render even weaker coordinating abilities in these compounds [1]. Due to their high melting points, viscosity and voltammetric measurements are difficult to determine. However the potential window should be in the same range as in the case of the previously presented ionic liquids. High electrochemical stability, air stability, and in the same time high thermal stability (at least up to 300°C) make these molten salts ideal candidates (as electrolytes) for thermal batteries (and also for other electrochemical applications).

## 5.5 Literature

- [1] I. Krossing, *Chem.--Eur. J.* **2001**, 7(2), 490-502.
- [2] J. Weidlein, U. Müller, K. Dehnicke, *Schwingungsfrequenzen I-Hauptgruppenelemente*, Georg Thieme, Stuttgart, **1981**.
- [3] A. Bihlmeier, M. Gonsior, I. Raabe, N. Trapp, I. Krossing, *Chem.--Eur. J.* **2004**, 10, 5041-5051.
- [4] R. W. Berg, M. Deetlefs, K. R. Seddon, I. Shim, J. M. Thompson, *J. Phys. Chem. B*, **2005**, 109, 19018-19025.
- [5] J. Golding, N. Hamid, D. R. MacFarlane, M. Forsyth *et al.*, *Chem. Mater.* **2001**, 13, 558-564.
- [6] O. B. Babushkina, S. Ekres, G. E. Nauer, *J. Phys. Chem. A* **2008**, 112, 8288-8294.
- [7] P. Wasserscheid, T. Welton, *Ionic Liquids in Synthesis-2<sup>nd</sup> Edition*, VCH, Weinheim, **2008**.

## 6. Appendix

### 6.1 General methods

#### 6.1.1 Synthesis techniques

All the reagents were weighed and filled in reaction vessels or ampoules in the glove box (Unilab Series, MBraun, Germany) under argon atmosphere.

For the synthesis of the tetrahalogenidometallates, only borosilicate glass ampoules were used for the reactions. The ampoules were closed under dynamic vacuum. The syntheses were carried out by using high temperature cylindrical ovens with a ceramic inner tube (Horst GmbH, Lorsch, Germany), and a temperature controller fitted to these ovens (Horst GmbH, Type HT MC1, Lorsch, Germany).

For the synthesis of the ionic liquids and molten salts the Schlenk technique was used.

All the manipulations outside the glove box were made using vacuum/ inert gas lines with Teflon screw-valves and septum technique.

Crystals for XRD analysis were isolated in a glove box (MBraun) with a built-in stereo microscope (MZ6, Leica Microsystems, Wetzlar, Germany). The polarizing filters adapted to this microscope contributed to the qualitative evaluation of the crystals. Glass capillaries were purchased at Glas W. Müller, Schönwalde, Germany.

#### 6.1.2 XRD-powder analysis

The samples for the powder diffraction measurements were prepared in the glove box, by filling a finely ground amount of substance in glass capillaries, which were sealed.

The diffraction data were recorded on a Huber G670 powder diffractometer (Huber, Rimsting, Germany) –with Mo  $K_{\alpha}$  radiation, and on a STOE Stadi P powder diffractometer (Stoe & Cie, Darmstadt, Germany) –with Cu  $K_{\alpha}$  radiation (both at the University of Cologne).

The peaks were evaluated with the help of the included database PDF-2 in WinXPow XRD powder spectra processing software [Powder Diffraction File, PDF-2 Database Sets 1-5: International Centre for Diffraction Data, The Newtown Square, PA (USA) **1995**], or by comparing the measured powder diffractograms with the simulated ones (from the crystal structure data base – see section 6.2, ICSD).

### 6.1.3 XRD single crystal analysis

Suitable crystals were fixed in glass capillaries and sealed under argon atmosphere in the glove box.

The data were recorded with the following devices:

- Imaging-Plate-Diffraction-System, IPDS I-graphite monochromator Mo K<sub>α</sub> radiation- (Stoe & Cie, Darmstadt, Germany) at the University of Cologne (Institute of Inorganic Chemistry)
- Imaging-Plate-Diffraction-System, IPDS II-graphite monochromator Mo K<sub>α</sub> radiation - (Stoe & Cie, Darmstadt, Germany) at University of Cologne (Institute of Inorganic Chemistry)
- Bruker AXS Smart-graphite monochromator Mo K<sub>α</sub> radiation- (Karlsruhe, Germany), at the University of Bochum (Faculty of Chemistry and Biochemistry)
- Sapphire2-CCD, Oxford Diffraction-graphite monochromator Mo K<sub>α</sub>- (Oxford Diffraction, Abingdon-Oxfordshire, UK) at the University of Bochum (Faculty of Chemistry and Biochemistry)

The refinement parameters which test the conformity of the structure are as follows:

- residual index R (also noted R<sub>1</sub>), gives, when multiplied by 100, the mean percentage deviation between observed and calculated structural amplitudes.

$$R = \frac{\sum_{hkl} ||F_o| - |F_c||}{\sum_{hkl} |F_o|}$$

F<sub>o</sub> = observed structure factors / F<sub>c</sub> = calculated structure factors

The value of R should be below 0.1, whereas values smaller than 0.25 indicate that the structure is correct [1].

- weighted residual index  $wR_2$ , shows through its variation, if a change in the calculated structural model fits with the registered reflections; this term contains the weight functions multiplied with the minimized error squared sums from refinement.

$$\omega R_2 = \sqrt{\frac{\sum_{hkl} \omega (F_o^2 - F_c^2)^2}{\sum_{hkl} \omega (F_o^2)^2}}$$

$\omega$  = the weight function

This parameter should be below 0.15 [2].

- goodness of fit GooF, indicates to what extent the found distribution of differences ( $|F_o| - |F_c|$ ), matches the distribution expected from the weights used by the refinement step. Theoretically, the value of GooF should be 1.0 [1].

$$GooF = \sqrt{\frac{\sum_{hkl} \omega (F_o^2 - F_c^2)^2}{m - n}}$$

m = number of reflections / n = number of parameters

#### 6.1.4 Nuclear magnetic resonance

For the NMR measurements screw-capped NMR tubes with Teflon seal (Norell Inc., Landisville, USA) were used, in order to ensure an inert atmosphere for the air sensitive compounds. The NMR tubes were filled and closed in the glove box.

The probes were measured at 25°C on a Bruker Avance II 300 NMR System (Oxford/SpectroSpin narrow bore magnet, 7.0 Tesla), equipped with an automatic sample changer (at the University of Cologne, Institute of Inorganic Chemistry).

#### 6.1.5 IR/Raman spectroscopy

For infrared spectroscopy the samples were pressed in tablets under inert conditions. In the case of far range infrared (FIR=200-10 cm<sup>-1</sup>/ practically the FIR measurement was run

in the range 500-50  $\text{cm}^{-1}$ ) polyethylene was used as filling material. In the middle infrared range (MIR=4000-200  $\text{cm}^{-1}$ / practically MIR measurements were run in the range 4000-500  $\text{cm}^{-1}$ ) potassium bromide was used to encapsulate the probes.

The samples for Raman spectroscopy were filled as powders in glass tubes with a diameter of 1 mm and sealed under argon atmosphere.

The devices used to measure these spectra are:

- Bruker IR-Spectrometer IFS/66v/S (with microscope)  
(at the University of Cologne, Institut für Anorganische Chemie)
- Bruker Raman-Spectrometer FRA106/S  
(at the University of Cologne, Institut für Anorganische Chemie)

#### **6.1.6 Differential scanning calorimetry**

The thermograms were recorded on a DSC204 F1 Phoenix device (Netzsch GmbH, Selb, Germany); the measuring unit is a  $\tau$ -sensor and the cooling was ensured through liquid/gaseous nitrogen flow. All samples were weighed and closed in aluminum crucibles under argon atmosphere. As reference served an empty aluminum crucible with a pierced lid. All measurements were run under argon, which was calibrated at 20 ml/min (purge gass) and 70 ml/min (protection gass) flow rates.

#### **6.1.7 Cyclic voltammetry**

The measurements were run under argon atmosphere, due to the sensitivity of the probes toward hydrolysis. The measurement system consisted of a potentiostat Autolab PGStat-12 (Eco Chemie B.V., Utrecht, Netherlands) and a measuring cell unit made of glass (Deutsche Metrohm, Filderstadt, Germany), a platinum working electrode with an active surface of 2 mm diameter (Deutsche Metrohm, Filderstadt, Germany), a counter electrode-wire made of platinum (Deutsche Metrohm, Filderstadt, Germany) and a silver rod (Deutsche Metrohm, Filderstadt, Germany) as quasi reference electrode.

### 6.1.8 Combustion analysis (CHNS)

The quantitative elemental analysis was made through combustion of the probes at approximately 1010 °C in oxygen stream. Carbon, hydrogen, nitrogen and sulphur are evaporated or oxydized; the resulted CO<sub>2</sub>, H<sub>2</sub>O, N<sub>2</sub> and SO<sub>2</sub> are separated and detected chromatographically.

For the measurements a Euro Vektor CHNS-O-Elementaranalysator EuroEA 3000 (HEKAtech GmbH, Wegberg, Germany) was used.

### 6.1.9 Viscosity

For the viscosity measurements a glass Micro-Ubbelohde viscosimeter type 537 30/ capillary no. III (Schott Instruments, Mainz, Germany) was used. Because the samples were moisture sensitive, and because the samples melt above 25°C, the measurements were run in the glove box, under inert atmosphere, and at a temperature of 60°C (in order to keep the measuring system at this constant temperature an oil bath adapted for this purpose was used as thermostate). These type of viscosimeters are suitable to determine the kinematic viscosity. The viscosimeter have an instrument constant K ( $K=1.020 \text{ mm}^2/\text{s}^2$ ), which is used to calculate the kinematic viscosity using the following formula:  $\nu = K \cdot t$ , whereby  $\nu$  is the kinematic viscosity and  $t$  is the time interval needed for the sample to reach the second gradation. The arithmetic mean of the three measurements conducted for each sample, gives the final viscosity value.

### 6.1.10 Literature

- [1] G. H. Stout, L. H. Jensen, *X-Ray Structure Determination-A Practical Guide*, John Wiley&Sons, **1989**.
- [2] W. Massa, *Kristallstrukturbestimmung*, B.G. Teubner, Stuttgart, **1994**.

## 6.2 Software

The following software products were used during this PhD work:

- crystal structure solution
  1. WinGX package [1]
  2. SHELXS-97(direct method) [2]; SirWare SIR-92 [3]
  3. SHELXL-97 [2] (differential Fourier synthesis/least square method refinement)
- crystallographic data reduction
  1. X-Red (Stoe & Cie **2002**, Darmstadt, Germany)
  2. CrysAlis RED, version 1.171.32.11 (Oxford Diffraction Ltd., **2007**)
  3. SAINT Plus package 2004/1 (Bruker)
- numerical absorption correction
  1. X-Shape (Stoe & Cie **2002**, Darmstadt, Germany)
  2. CrysAlis RED, version 1.171.32.11 (Oxford Diffraction Ltd., **2007**)
  3. SAINT Plus package/ SADABS 2004/1(Bruker)
- crystal structure visualization
  1. Diamond 3.0 (Crystal Impact GbR, Bonn, Germany)
  2. Ortep 3, version 2.01 (Farrugia L.G., University of Glasgow, UK)
- XRD-powder analysis
  1. STOE WinXPow (Stoe & Cie, Version 1.07, Darmstadt, Germany)
- NMR spectra processing
  1. TopSpin 1.3 (Bruker BioSpin)
  2. MestReC Lite 4.7.0.0 (Mestrelab Research SL, Santiago de Compostela, Spain)
- DSC data processing

1. Proteus, version 4.7.0 (Netzsch GmbH, Selb, Germany)
- cyclic voltammetry data processing
  1. GPES, version 4.9 (Eco Chemie B.V., Utrecht, Netherlands)
- for literature search and structural database
  1. SciFinder search engine, version **2006** (American Chemical Society)
  2. Inorganic Crystal Structure Database, version 1.4.4, **2008-1** (Fachinformationszentrum, Karlsruhe, Germany)
- for spectra processing
  1. Origin 7 (OriginLab Corp., Nothampton, USA)
- for graphical processing
  1. Corel Draw X3, version 13 (Corel Corp., Ottawa, Canada)
  2. ChemBioOffice **2008** (Cambridge Soft, UK)

### References

- [1] L. J. Farrugia, *J. Appl. Cryst.* **1999**, *32*, 837.
- [2] SHELXS-97, G. M. Sheldrick, *Acta Crystallogr. Sect. A: Found. Crystallogr.* **2008**, *64*, 112.
- [3] SIR-92, A. Altomare, G. Cascarano, C. Giacovazzo, A. Guagliardi, *J. Appl. Cryst.* **1993**, *26*, 343.

### 6.3 Chemicals

In powder (100 mesh), 99.99%, Aldrich

InCl<sub>3</sub>, 98%, Aldrich

InI<sub>3</sub>, 99.99%, Aldrich

TlCl, 99%, Acros Organics

TlBr, 99.9%, Acros Organics

TlI, 99.999%, Aldrich

CsI, 99.9%, Chempur

NH<sub>4</sub>Cl, 99+%, Acros Organics

NH<sub>4</sub>I, 99+%, Acros Organics

AlI<sub>3</sub>, ≥ 95%, Merck

AlCl<sub>3</sub>, ≥ 98%, Merck

AlBr<sub>3</sub>, ≥ 98%, Merck

GaCl<sub>3</sub>, ≥ 95%, Knapsack

GaBr<sub>3</sub>, 99.999%, Aldrich

GaI<sub>3</sub>, 99%, ABCR

LiAlH<sub>4</sub>, 95%, Acros Organics

1-Chlorobutane, 99+%, Acros Organics

1-Methylpyrrolidine, 98%, Acros Organics

1-Methylimidazole, 99%, Acros Organics

1,1,1,3,3,3-Hexafluoroisopropanol, 99.5%, Acros Organics

Perfluoro-tert-butyl alcohol, 99%, Apollo Scientific

Isopropanol, 99.5%, Acros Organics

Ethyl acetate, 99.5%, Acros Organics

Toluene, 99.5%, Acros Organics

CDCl<sub>3</sub>, 99.8%, Deutero

## 6.4 Abbreviation list

X - halogen atom

R - organic rest

mmol - millimole

pm - picometer

h - hour

min - minute

s - second

°C - degree Celsius

K - Kelvin

J - Joule

V - volt

cSt - centistokes

mPa - millipascal

tab - table

fig - figure

HOMO - highest occupied molecular orbital

IR - infrared

DSC - differential scanning calorimetry

NMR - nuclear magnetic resonance

XRD - X-ray diffraction

S.O.F. - Site Occupation Factor

IL - ionic liquid

RTIL - room temperature ionic liquid

WCA - weakly coordinating anion

hfip - hexafluoro-isopropyl rest

nftb - nonafluoro-tert-butyl rest

bmim - 1-butyl-1-methylimidazolium

bmpyrr - 1-butyl-1-methylpyrrolidinium

bmimAl(hfip)<sub>4</sub> - 1-butyl-3-methylimidazolium tetrakis(hexafluoroisopropyl)aluminate

bmimAl(nftb)<sub>4</sub> - 1-butyl-3-methylimidazolium tetrakis(nonafluoro-tert-butyl)aluminate

bmpyrrAl(hfip)<sub>4</sub> - 1-butyl-1-methylpyrrolidinium tetrakis(hexafluoroisopropyl)aluminate

bmpyrrAl(nftb)<sub>4</sub> - 1-butyl-1-methylpyrrolidinium tetrakis(nonafluoro-tert-butyl)aluminate

bmimBF<sub>4</sub> - 1-butyl-3-methylimidazolium tetrafluoroborate

bmimPF<sub>6</sub> - 1-butyl-3-methylimidazolium hexafluorophosphate

bmimTFSI - 1-butyl-3-methylimidazolium bis(trifluoromethane-sulphonyl) imide

## 6.5 Publication list

- [1] T. Timofte, A.-V. Mudring, Indium(I) tetrachloroaluminate, *Acta Crystallogr., Sect. E: Struct. Rep. Online* **2005**, *E61(9)*, i199.
- [2] T. Timofte, S. Pitula, A.-V. Mudring, Ionic Liquids with Perfluorinated Alkoxyaluminates, *Inorg. Chem. (Washington, DC, U. S.)*, **2007**, *46(26)*, 10938.
- [3] T. Timofte, A.-V. Mudring, Indium(I) tetraiodoaluminate, *Z. Anorg. Allg. Chem.* **2008**, *634(4)*, 622.
- [4] T. Timofte, A.-V. Mudring, Indium(I) heptachlorodigallate(III), *Z. Anorg. Allg. Chem.* **2008**, *634(4)*, 624.

# Curriculum Vitae

## Persönliche Daten

Name	Timofte
Vorname	Tudor Lucian
Anschrift	Marktstr. 8, PLZ 44866, Bochum, Deutschland
Geb.-Datum	13.09.1980
Geb.-Ort	Iasi, Rumänien
Staatsangehörigkeit	rumänisch
Familienstand	verheiratet

## Schulbildung und Studium

Seit 10/2005.....	Promotion, Universität zu Köln
2006.....	Master Abschluss , „Al.I.Cuza“ Universität-Iasi, Rumänien
2004-2006.....	„Al.I.Cuza“ Universität-Iasi, Rumänien Fakultät für Chemie-Fach Dynamik und Analyse in den chemischen Systemen
2004-2005.....	„Socrates-Erasmus“ Stipendium, Universität zu Köln
2004.....	Bachelor Abschluss, „Al.I.Cuza“ Universität-Iasi, Rumänien
1999-2003.....	„Al. I. Cuza“ Universität – Iasi, Rumänien Fakultät für Chemie – Fach Chemie Abschluss Diplom Chemiker
1999.....	Erwerb des Abiturdiploms
1995-1999.....	Schulgruppe „M. Sturdza“, Iasi, Rumänien
1991-1995.....	Gymnasium „M. Eminescu“, Iasi, Rumänien
1987-1991.....	Grundschule „Carol I“, Iasi, Rumänien

## Sprachkenntnisse

Rumänisch.....	Muttersprache
Englisch.....	in Wort und Schrift
Deutsch.....	in Wort und Schrift

## Aktivitäten an der Universität

Seit 02/2007-03.2009	Wissenschaftlicher Mitarbeiter, Ruhr-Universität, Bochum
Seit 10/2005-01.2007	Wissenschaftlicher Mitarbeiter, Universität zu Köln
2004-2005	Studentische Hilfskraft, Universität zu Köln

**Datum:** 04.11.2008

Ich versichere, dass ich die von mir vorgelegte Dissertation selbstständig angefertigt, die benutzten Quellen und Hilfsmittel vollständig angegeben und die Stellen der Arbeit - einschließlich Tabellen, Karten und Abbildungen -, die anderen Werken in Wortlaut oder dem Sinn nach entnommen sind, in jedem Einzelfall als Entlehnung kenntlich gemacht habe; dass diese Dissertation noch keiner anderen Fakultät oder Universität zur Prüfung vorgelegen hat; dass sie noch nicht veröffentlicht worden ist; dass ich eine solche Veröffentlichung vor Abschluss des Promotionsverfahrens nicht vornehmen werde.

Die Bestimmungen der geltenden Promotionsordnung sind mir bekannt. Die von mir vorgelegte Dissertation ist von Frau Prof. Dr. Anja-Verena Mudring betreut worden.

Köln, den 04 November 2008,

Tudor Lucian Timofte